West Virginia Department of Transportation
Division of Highways

Nondestructive Evaluation of Pavement Layers Using Combined Dynamic and Acoustic Testing Technique

Research Team

Samir N. Shoukry, Ph. D.
Department of Mechanical and Aerospace Engineering

David Martinelli, Ph. D.
Olga Selezneva, M.S.C.E.
Department of Civil and Environmental Engineering

West Virginia University
Harley O. Staggers National Transportation Center
P.O. Box 6103, Morgantown, WV 26506-6103

Sponsored by West Virginia Department of Transportation, Division Highways of and Mid Atlantic Universities Transportation Center.

Technical Report Documentation Page

1 PB99-134546	2. Government Accession No.	3. Recipient's Catalog No.
4. Title and Subtitle Nondestructive Evaluation of Pavement Layers Using Combined Dynamic and Acoustic Testing Technique		5. Report Date October 1996 6. Performing Organization Code III-9807
7. Author(s) Samir N. Shoukry, David R. Martinelli. Olga Selezneva		8. Performing Organization Report No.
9. Performing Organization Name and Address West Virginia University Harley O. Staggers Transportation Center PO Box 6106 Morgantown, WV 26505-6106		10. Work Unit No. (TRAIS) 11. Contract or Grant No.
12. Sponsoring Agency Name and Address West Virginia Department of Transportation Mid Atlantic Universities Transportation Center		13. Type of Report and Period Covered Final November 1995 - February 1997 14. Sponsoring Agency Code

15. Supplementary Notes

Sponsored by a grant from West Virginia Department of Transportation, Division of Highways, and Mid Atlantic Universities Transportation Center.

16. Abstract

Rational evaluation of the pavement condition depends on the availability of insitu material properties of pavement layers. These data are crucial for a correct evaluation of the pavement structural capacity and its remaining service life. The most acceptable nondestructive testing technique for pavement structural capacity evaluation is the Falling Weight Deflectometer test (FWD). The FWD test results are influenced by loading, climate, and pavement condition. Alternatively, acoustic testing techniques that are based on the mechanism of stress wave propagation in structural materials have been applied for the evaluation of material properties. The Spectral Analysis of Surface Waves (SASW) is typically used for the nondestructive moduli profiling of pavements and soil sites. In this study the development of a combined dynamic and acoustic nondestructive testing technique for the evaluation of pavement layers moduli is explored.

Explicit dynamic finite element analysis was used to investigate the mechanisms of displacement propagation through pavement layers under the action of an impact load. The study focuses on developing an understanding of the effect of layers interface bond on the accuracy of the FWD deflection basins for different types of pavement structures. The accuracy of the finite element models developed in this investigation was experimentally verified by comparing the theoretical results with those measured during an actual FWD test. Additionally, the flexible model results were compared with the published results obtained using several theoretical methods. The theoretical deflections predicted by the dynamic finite element models developed in this study were in close agreement with the experimentally measured deflections.

For unbonded pavement structures with a flexible top layer, the displacements measured on the top surface carried little correlation to the deformation in subsequent layers. In these cases, complicated patterns of behavior occurred between the AC layer and the rest of the pavement structure. Care should be taken to ensure the existence of an interface bond when testing "black-top" pavements using FWD. The accuracy of FWD results will also be influenced by the condition of bonds between the layers of rigid pavements. The work presented in this study demonstrates that many structural problems in pavements can be studied by examining their behavior under dynamic loads.

17. Key Words Nondestructive testing, Falling Weight Deflectometer, Pavement Modeling.		18. Distribution Statement	
19. Security Classification (of this report). Unclassified	20. Security Classification (of this page). Unclassified	21. No. of Pages	22. Price

III-9807

ACKNOWLEDGMENT

The authors wish to extend thanks to West Virginia Division of Highways and Mid-Atlantic-Universities-Transportation-Center for sponsoring the work, and to WVDOH project monitor Mr. Rodney Welder.

TABLE OF CONTENTS

LIST OF TABLES

LIST OF FIGURES

CHAPTER 1

NONDESTRUCTIVE EVALUATION OF PAVEMENT LAYERS MODULI

1.1. INTRODUCTION

Pavements deteriorate with time. The reasons for the deterioration may be excessive traffic load, environmental effects, or material disintegration. If the pavement shows signs of structural deficiency, rehabilitation will be required to strengthen the present pavement condition. In order to choose appropriate rehabilitation procedures, the structural capacity of the existing pavement should be evaluated first. Considerable savings in rehabilitation costs can be made by accurate prediction of the strength of the existing pavement. The magnitude of stresses and strains in pavement layers are the indicators of the structural capacity of a pavement system. To evaluate the stress-strain parameters, the pavement layers moduli should be measured. This job can be done in two ways:

1. Using destructive testing and laboratory material evaluation.

2. Using nondestructive testing.

Because of material disturbance during sampling, destructive testing using core samples produce results which under estimate the material properties especially in case of anisotropic materials like soil or gravel.

Nondestructive testing (NDT) of pavements has gained much recognition in recent years due to its economical advantages compared to the destructive techniques. NDT based on surface deflection measurements has been accepted by most highway agencies as a standard practice for the evaluation of pavements structural capacity. The new AASHTO Guide for Design of Pavement

Structures 1993 recommends the use of "dynamic" NDT deflection measuring devices for surface deflection measurements. The surface deflections measured by the NDT are used to predict the moduli of pavement layers through a theoretical procedure called backcalculation.

Over the years, many nondestructive testing techniques of pavement structures were developed. However, in recent years two categories of nondestructive testing emerged. The first is based on the measurment of the structural vibrations of the top top layer. In this category, the falling weight deflectometer is the most popular device. The second category of non destructive testing techniques is based on the propagation of elastic waves in the different pavement layers. This wave propagation approach forms the basis of the theory of spectral analysis of surface waves.

According to a comparative study by Hoffman and Thompson *(1)* for the available nondestructive pavement testing devices, the Falling Weight Deflectometer (FWD) is the best commercially available device for the nondestructive evaluation of pavement structural capacity. A number of procedures are currently available for the FWD data analysis and backcalculation of pavement layer moduli; though, each of them has limitations. The problems of reaching a better understanding of the mechanism of pavement deflections induced by a dynamic impact and developing more accurate methods of surface deflection data analysis have been under continuous research for the past three decades. In this study, we will examine the two major categories of nondestructive testing techniques.

1.2. FALLING WEIGHT DEFLECTOMETER

The Falling Weight Deflectometer (FWD) is a nondestructive testing device employed by many highway agencies for the evaluation of the structural capacity of existing pavements and in-situ evaluation of the material properties of pavement layers. The FWD induces surface pavement deflections that are in a close match with those induced by traffic loading *(1)*. The understanding of pavement behavior and correct interpretation of data obtained from a FWD test are key factors for

correct rehabilitation procedures.

1.2.1. Falling Weight Deflectometer Testing Technique

The FWD method is listed in the ASTM standards under a fixed destination D 4694. The scope of the method was stated as follows:

This test method describes the measurement of vertical deflection response of the surface to an impulse load applied to the pavement surface. Vertical deflections are measured on the load axis and at the points spaced radially outward from the load axis. An impulse load more nearly represents the moving vehicle load-pulse applied to prototype pavements than does a static load (2).

During the test, a force pulse generated by a weight dropped on a spring system is transmitted through a steel plate resting on the pavement surface. Standard loading plates are 300 and 450 mm (12 and 18 in.) in diameter. The loading plate has an opening in the center to allow a deflection-measuring sensor to be installed. The weight is lifted to a known height by the guided system so that, when dropped, it will impart the desired force on the pavement. When the weight is dropped, the resulting vertical movement of the pavement surface is measured at the specified locations using deflection sensors. A schematic drawing of the FWD setup is shown in Figure 1.1. By varying the mass or the drop height, the impact on the pavement surface can be varied to account for different loading conditions, i.e., vehicle weights. For nondestructive evaluation of highway pavements, a load equal to the single axle load is frequently used. The FWD equipment induces a small static preload on the pavement surface of the range 3 to 14% of the maximum dynamic load *(3)*. Due to the small magnitude of the preload compared with the maximum dynamic amplitude, weight of the equipment is excluded during the evaluation of the results. The impact load pulse has an approximate shape of a half-sine wave and duration of 20 to 60 ms. The rise time, as a time from the beginning of the loading till the peak value, varies between 10 and 30 ms *(2)*.

The surface deflections are measured by up to seven transducers mounted on a holding bar lowered automatically with the loading plate. The transducers are usually spaced one foot apart and placed on the pavement surface in the direction of traffic. Transducers may be of several types such as geophones (absolute measurement transducers), velocity transducers, or accelerometers. A load cell is used to measure the applied load on each impact. During each test, variations in the load and surface deflections with the time are recorded and stored for future evaluations. To evaluate the pavement moduli of different layers, peak deflections values are extracted and used in the construction of the deflection basin presented in Figure 1.2.

Based on the results of the test, decisions are made about rehabilitation procedures and overlay design for highway and airfield pavements. Errors made during interpretation of test data may result in making inappropriate rehabilitation decisions and great economical losses. Therefore, the correct evaluation of the test results is very important from an economical point of view.

1.2.2. Backcalculation of Pavement Moduli

The deflection data collected during a FWD test is later used in an analytical procedure called backcalculation of pavement moduli. The backcalculation procedure involves theoretical calculations of the deflections produced under a known applied load using an assumed set of layers' moduli. The theoretical deflections are then compared with those measured during the test. In case of differences between the theoretical and measured deflections, the assumed pavement layer moduli are then adjusted and the process is repeated until the difference between the theoretical and measured values falls within acceptable limits. Techniques like iteration, database searching, regression analysis, and artificial intelligence (neural networks) have been used as backcalculation tools*(4, 5)*.

Most of the existing backcalculation algorithms use iterative analysis. In this case, the solution for the theoretical deflections is initiated at the distant sensor locations assuming that the surface deflections at the distant sensor positions are due to strains or deflections in the subgrade layer only and independent of the overlying layers *(6 - 8)*. As shown in Figure 1.1, the stress zone

intersects the interface between the subbase and subgrade layers at the radial distance $r = a_e$. This means that any surface deflection value obtained from the deflection basin at or beyond the distance $r = a_e$ is due only to the deformations (stresses) within the subgrade layer. Thus, from the known values of the measured deflections at the outer geophone positions, in-situ modulus of the subgrade can be evaluated. From the above discussion, a_e value is obviously very important. The AASHTO guide for design of pavement structures (1993) suggests the following formula for the determination of a_e *(8)*:

$$a_e = \sqrt{a^2 + (D_3\sqrt{\frac{E_p}{M_R}})^2}$$

where a_e = radius of a stress bulb at the subgrade-pavement interface, inches;
a = FWD load plate radius, inches;
D = total thickness of pavement layers above the subgrade, inches;
E_P = effective modulus of all pavement layers above the subgrade, psi;
M_R = subgrade resilient modulus, psi.

The AASHTO guide gives a graph for the determination of E_P over M_R ratio for a 150mm (6 inches) radius loading plate, known total thickness of pavement layers above the subgrade, known maximum deflection under the center of the loading plate, and known load magnitude *(8)*.

In the backcalculation procedure, the modulus of the lowest subgrade layer is changed in the repetitive iterative procedure until such value is found that will produce surface deflection at a distant geophone tolerable with the measured one. Once the value for the lowest layer is found, it is assumed to be the "true" value and is used as a constant in the evaluation of moduli for the more shallow layers. The solution progresses from the distant geophone locations to the center of load application and layer moduli are evaluated from the bottom to the top layers, as shown in Figure 1.2. Knowledge of existing pavement layer thicknesses, Poisson's ratios, and load magnitude are necessary conditions for backcalculation procedure. The pavement layer moduli derived in the above process

are further used for the stress and strain analysis of the pavement structure.

The major assumption used in backcalculation algorithms is that the amount of surface deflection at any point is dependent on the stress-strain state in the subsequent layers. This assumption is true for static or monotonous loading but may be violated if the load is dynamic. One of the objectives of the present research is to investigate the validity of this assumption for different conditions of bond strength between layers.

1.2.3. Available Backcalculation Programs

In 1991 a comprehensive review of existing software for backcalculation procedures was published as a result of project SHRP-90-P-001B sponsored by the Strategic Highway Research Program *(9)*. A list of the most commonly used backcalculation programs from that report modified and updated for present day information is shown in Table 1.1.

1.2.4. Problems with Backcalculation Algorithms

As indicated in the above review, most of the backcalculation programs are based on the static multilayered elastic theory, although FWD loading is dynamic by nature *(10 - 12)*. Major limitations of the elastostatic analysis is that it does not count for such factors as material inertia and damping. As noted by Hoffman and Thompson *(13)*, inertial effects in the pavement layers subjected to FWD impact may be significant and therefore need to be considered in the theoretical analysis.

As pointed by Lytton et al. in 1989, none of the programs based on the static layered elastic theory could guaranty the accurate results for every test section *(14)*. Lytton and Chou stated that two independent agencies who used the same backcalculation software to determine moduli for the same pavement section, ended with different results. Therefore, engineering judgement plays an

important role in the evaluation of the test results.

Irwin, et al. reported that most errors occur during the evaluation of the surface layer modulus *(15)* and Huang stated that this is especially true in case of the thin asphalt layers *(16)*. One reason may be the mismatch in the pattern of dynamic static deformations of the surface layer.

Sebaaly *(17)* observed that during FWD test a physical phenomenon of surface wave propagation from the source of impact takes place affecting the pattern of surface deformations recorded by the set of transducers. The surface waves propagate outward in a manner similar to the waves on the surface of water initiated by a dropped object. Consequently, the pattern of surface deformation due to an impact load would differ from that induced by the stationary load assumed in static analysis. Therefore, a study of dynamic deflection propagation through different pavement systems under the action of different impacts simulating the range of FWD loads is necessary for the accurate evaluation of FWD results.

1.3. ACOUSTIC TECHNIQUES FOR MODULI EVALUATION

The basic idea behind Acoustic testing techniques is to generate a stress wave and record the velocity of the stress wave during its propagation from one point to another. The velocity of wave propagation is related to the layer shear modulus. Acoustic techniques are generally known as wave propagation testing techniques. In the past, two wave propagation approaches were developed. The first is a destructive testing approach known as the crosshole method. The second is a nondestructive testing method based on the surface wave theory and known as the Spectral Analysis of Surface Waves.

1.4. CROSSHOLE TESTING METHOD

The crosshole testing technique *(18)* is considered an accurate method for layers moduli evaluation using destructive testing. On the other hand, it is time consuming and expensive. In order to perform a crosshole test, two or more boreholes are drilled to the desired depth then a source capable of generating stress waves is lowered to the measurement depth in one of the boreholes. One or two receivers are lowered to the same depth in the other borehole. The measurement of the travel time depends on how many receivers are being used. If one receiver is used, the travel time is measured from source to receiver (direct travel time measurement) as illustrated in Figure 1.3. If two receivers are used, the travel time is measured between the two receivers (interval travel time measurements). The distance between the two boreholes equals to the distance from the source to the first receiver (10 ft). The wave velocity at the measurement depth is simply calculated by dividing the travel distance by the measured travel time. Typically the receiver consists of a three-component geophone. The vertical geophone is used to capture the vertical component of the shear wave velocity (β). The radial geophone senses the propagating compression waves (α) and the tangential geophone senses the horizontally propagating shear wave (υ). By knowing the depth and assuming a proper Poissons' ratio the shear modulus could be calculated from:

$$\alpha = \sqrt{\frac{L + 2 * G}{\rho}} \qquad \beta = \sqrt{\frac{G}{\rho}}$$

Where :

L (Lames'constant) = $2*G*\nu/(1-2*\nu)$

ν = Poissons' ratio

G = shear modulus

ρ = density

Variations to the crosshole method include downhole, uphole and in-hole methods. A complete description of those methods could be found in reference *(18)*.

1.5. SPECTRAL ANALYSIS OF SURFACE WAVES

The spectral analysis of surface waves (SASW) is a nondestructive technique based on the theory of wave propagation in an infinite elastic half space. Unlike shear and compression waves which propagate along a spherical wave front, surface waves propagate along a cylindrical wave front as they spread out from the source. A plane surface wave has two components of motion: a vertical component and a radial component. The two components are combined to form an elliptical path for the material particles. The important feature in surface waves is that the particle displacement decays exponentially with depth, and as the wave length increases the particle displacements extend to a greater depth. Surface waves in a layered medium are dispersive waves whose velocity of propagation (often called phase velocity) vary with frequency.

Pavement moduli evaluation using surface waves is based on the dispersive nature of surface waves propagating in a layered elastic half space. The SASW testing technique was developed in the eighties *(19 - 25)*. The methodology of the technique can be divided into two phases. The first phase is experimental in which an impulse is applied to the pavement surface and the dispersion of surface wave velocities at various frequencies is measured. The resulting curve is reduced to a relation between the phase velocity and the wave length and is called the dispersion curve. In the second phase, the dispersion curve is used to compute the pavement shear moduli at various depths *(26)* using an inversion algorithm.

1.5.1 Spectral Analysis of Surface Waves Experimental Phase

Although the theoretical basis of the SASW testing was known since the early 1950's *(27 -29)*, the technique required the use of high speed computers and real time signal processing. The availability of digital frequency spectrum analyzers during the 1980's simplified the experimental part of the technique and enabled its use in pavement testing.

The general instrumentation setup typically used in SASW testing is illustrated in Figure 1.4. The setup consists of two receivers, a digital frequency spectrum analyzer with digital storage

capability and an impulse source. The impulse source should be capable of generating surface wave energy over the desired frequency range. A 4 oz. impact hammer is used to generate the high frequency range and another 8 lb. hammer is used to generate the low frequency waves *(30)*. The receivers used in SASW testing of pavements are either geophones or accelerometers. Piezoelectric accelerometers are more suitable for testing pavement sites. The frequency range of the receivers vary according to the depth at which the modulus is required. In pavement sites where the interest is to find the layers moduli at relatively shallow depths, it is recommended to use piezoelectric accelerometers of having high frequency range (1 k Hz to 50 k Hz according to reference *31*).

The digital frequency spectrum analyzer performs a fast Fourier transformation on the signals from the two receivers and compute the phase shift at different frequencies. If the analyzer is not fitted with a digital storage device (floppy disk), it should be connected to a digital computer that is used to store the phase versus frequency data and dispersion curve calculations.

There are two test configurations for the source and receivers as shown in Figure 1.5. In the common receivers mid point configuration, the receivers at different distances have a common mid point while the impact is applied on both sides of the receivers and an average is taken for every distance between receivers. This test configuration is reported *(30, 32)* to reduce the scatter in the measured dispersion curve. In the common source geometry the source is placed at a fixed location while the distance between the receivers is varied. During testing, the distance between the source and the nearest receiver should be kept equal to the distance between the two receivers to minimize the interference from body waves.

To construct the experimental dispersion curve the two receivers are first placed at a distance "X" from each other. An impact is applied and the analyzer is triggered to measure the phase shift between the two signals at various frequencies. Once the phase shift Φ between the signals recorded by the two receivers at a particular frequency f is known, the wave length is calculated as follows:

$t = \Phi * f / 2 * \pi$ sec.

$V_{phase} = X/t$ ft/sec

$L = V_{phase}/f$ ft

where:

t = travel time

V_{phase} = phase velocity

f = frequency

X = distance between the sensors

L = wave length

The distance X between the two receivers is varied and the phase velocities at various wave lengths are calculated again until the phase velocities at all wave lengths of interest are found. The phase velocities are then avaeraged for every wave length to produce the experimental dispersion curve illustrated in Figure 1.4.

1.5.2. Evaluation of Shear Moduli From the Dispersion Curve

The process of evaluation of the shear moduli profile from the experimental dispersion curve is called inversion. The theoretical approach of the inversion technique is based on the work of Haskel *(26)*. This work was later adapted for testing pavements by Nazarian *(19)*. The inversion procedures could be simply described as follows:

1. The site is modeled as multi layers overlaying a half space. Each layer is assumed a thickness, Poissons' ratio, and density.

2. Shear moduli values are assumed for all layers.

3. A theoretical dispersion curve is calculated using Haskel's equations.

4. The resulting theoretical dispersion curve is compared with the measured one. If the two curves are close to each other, then the shear moduli profile assumed in step number three is correct. If the two curves are away from each other, a new shear moduli profile is assumed and the calculations are repeated. During the iteration procedures the layer depths, densities, and Poisson's ratios are kept constant to simplify the caculations.

1.6. CONCLUSION

The techniques of nondestructive evaluation of pavement moduli are dependent on the propagation of stress waves through pavement layers. Both the falling weight deflectometer approach and SASW require an understanding of the mechanisms of propagation of the dynamic impact through pavement structures. This may lead to a better interpretation of the nondestructive testing results results.

Table 1.1. Available backcalculation programs (9).

Program Name	*Subroutine Name*	*Theory*	*Backcalculation method*	*Source*
BISDEF	BISAR	Multi-layer elastic	Iterative	USACE-WES
CHEVDEF	CHEVRON	Multi-layer elastic	Iterative	USACE-WES
CLEVERCALC	CHEVRON	Multi-layer elastic	Iterative	Royal Institute of Technology, Sweden
COMDEF	BISAR	Multi-layer elastic	Data Base	M. Anderson
ELSDEF	ELSYM5	Multi-layer elastic	Iterative	Texas A&M University, USACE-WES
EMOD	CHEVRON	Multi-layer elastic	Iterative	PCS/LAW
EVERCALC	CHEVRON	Multi-layer elastic	Iterative	J. Mahoney
FPEDDI	BASINPT	Multi-layer elastic	Iterative	W. Uddin
ILLIBACK	ILLIBACK	Plate on elastic foundation theory	Closed form solution	University of Illinois
ILLI-CALC	ILLIPAVE	Nonlinear elasto-static finite element modeling	Iterative	University of Illinois
ISSEM4	ELSYM5	Multi-layer elastic	Iterative	R. Stubstud
MODCOMP	CHEVRON	Multi-layer elastic	Iterative	L. Irwing, Szebenyi
MODULUS	WESLEA	Multi-layer elastic	Data Base	Texas Transportation Institute
PADAL	PADAL	Multi-layer elastic	Iterative	S.F.Brown, et.al.
WESDEF	WESLEA	Multi-layer elastic	Iterative	USACE-WES
MICHBACK	CHEVRON	Multi-layer elastic	Iterative	Michigan State University

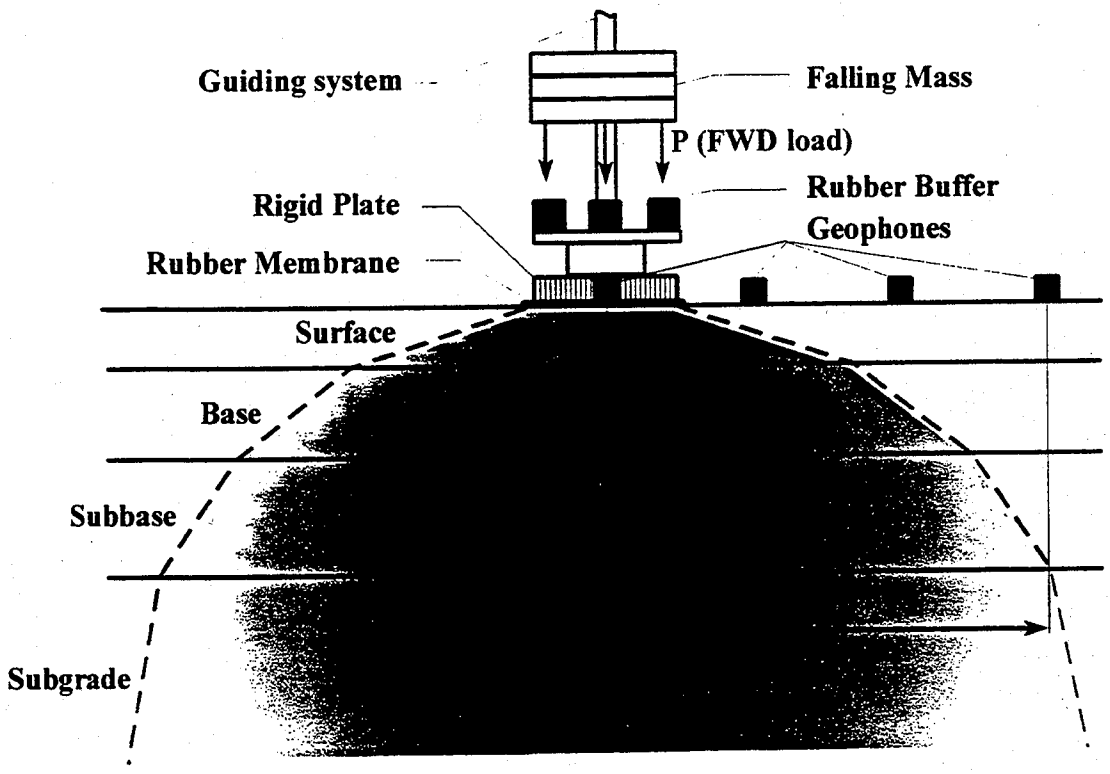

FIGURE 1.1. FWD setup and schematic presentation of the stress bulb.

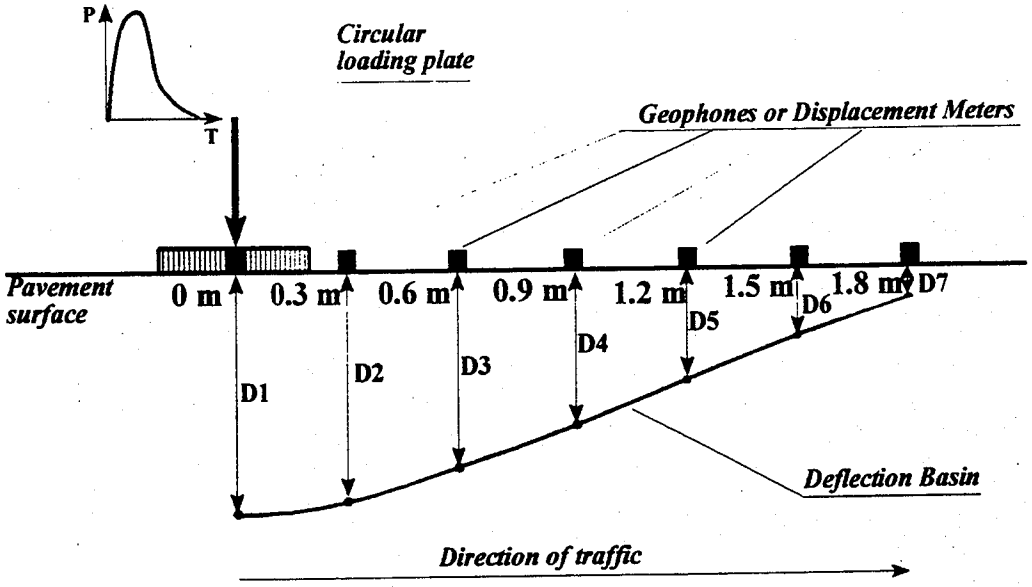

D1, D2, ... D7 are maximum surface deflections measured at geophone locations

FIGURE 1.2 Schematic presentation of a deflection basin obtained from FWD results.

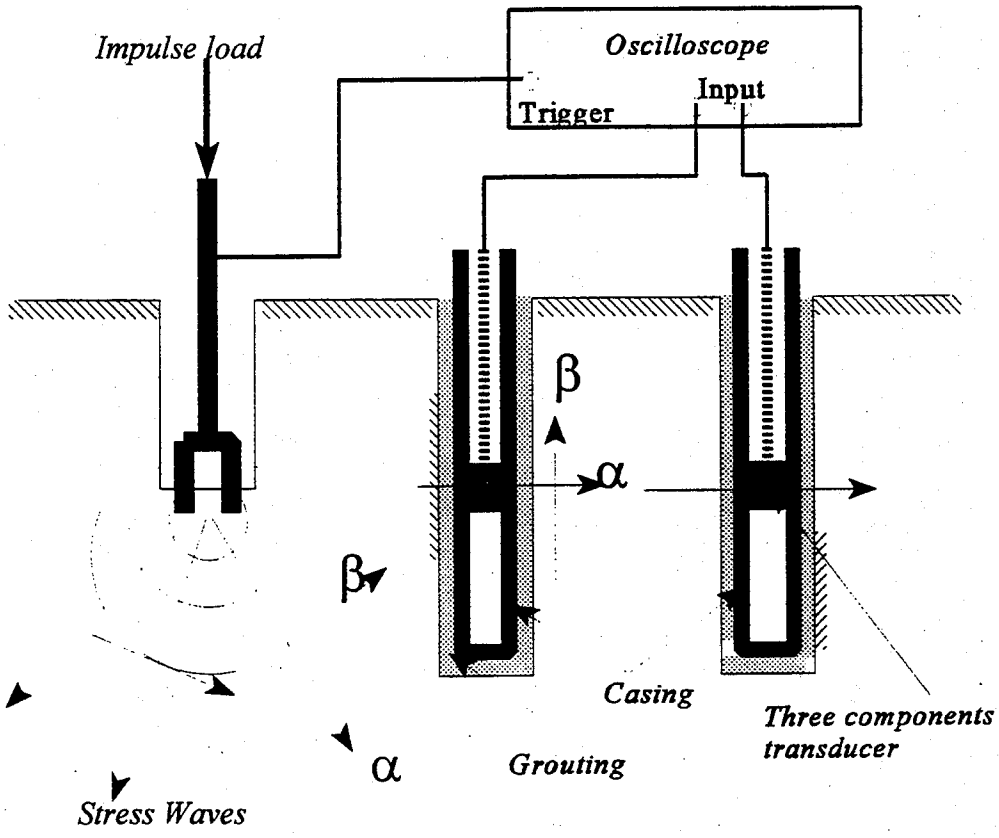

FIGURE 1.3 Crosshole Testing Configuration.

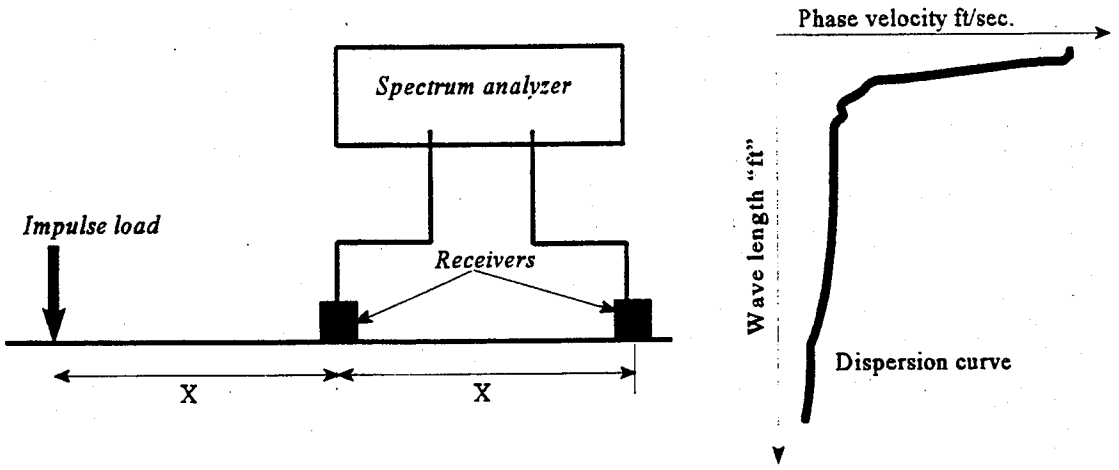

FIGURE 1.4 Schematic Representation of SASW Testing Setup and the Dispersion Curve.

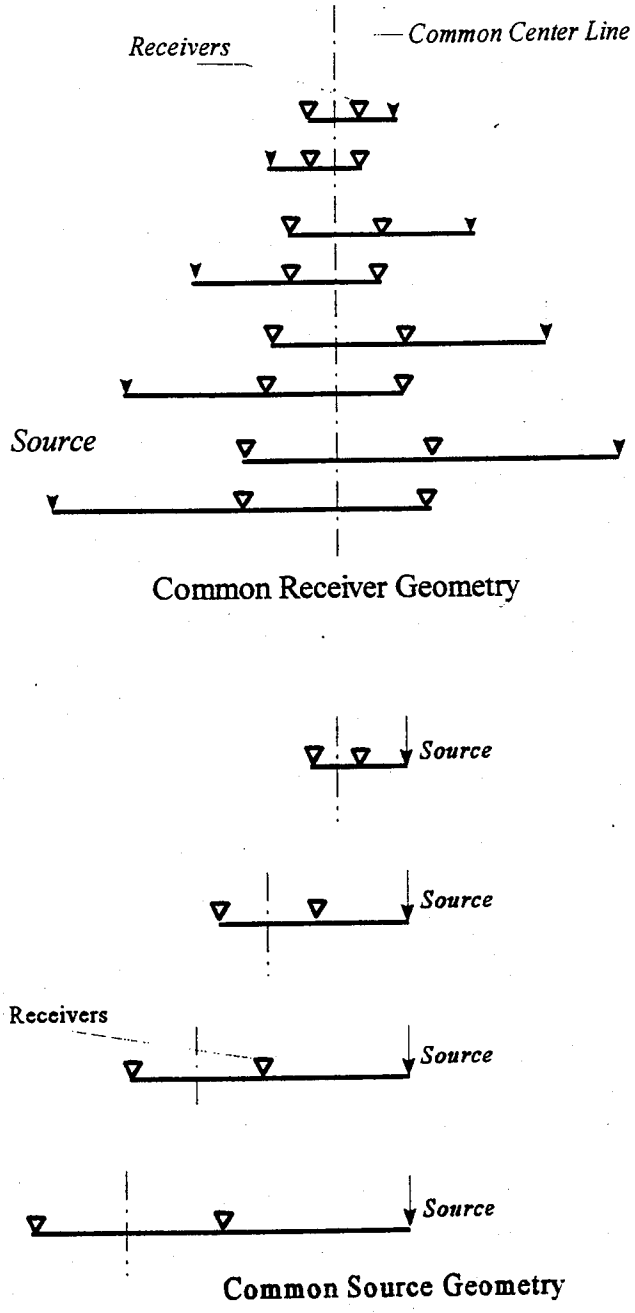

FIGURE 1.5 Source and Receivers Configurations *(32)*.

CHAPTER 2

DEVELOPMENT OF DYNAMIC FINITE ELEMENT MODELS

2.1. INTRODUCTION

The objective of the finite element simulations presented in the following chapters is to investigate the response of different pavement structures to impact loads. The practical purpose of such investigation is to examine the validity of the assumptions used in the evaluation of the data obtained from the FWD test and to find ways to improve the test results and enhance the overall understanding of the pavement response to impact loads. Due to the complex nature of the problem, no closed form solution is available that simulates the response of a multilayered pavement structure to impact loading without major simplifications. However, a numerical technique with discrete formulation of the problem, such as the finite element method, can serve as an alternative solution that produces theoretical simulations close to the real life conditions. From the review of finite element codes, DYNA3D code was found to be the most suitable for the solution of the pavement-impact problem. DYNA3D is a public domain finite element software developed by Lawrence Livermore National Laboratory for the analysis of differnt types of structures subjected to the dynamic loads. As a result of the analysis, deflections and stresses can be evaluated at any point in the structure.

In the development of the pavement models, two guidelines were followed:

(a) the model should be as much realistic and accurate as possible,

(b) model size and complexity should be computationally efficient.

The development of the finite element model consisted of the following steps:

1. Model configuration and choice of elements
2. Material models
3. Load model
4. Choice of the analysis procedure

2.2. MODEL CONFIGURATION

The FWD test setup, recommended by ASTM standard D 4694-87, was used in the development of the model configurations *(1)*. In this study, three different types of pavement structures were modeled: flexible, rigid, and composite. The pavement response to a single impact load applied over a circular plate was studied. According to the standard D 4694-87, the loading plate was positioned at 900 mm (3 feet) from the outer edge of the pavement and in the middle of the slab in the longitudinal direction.

2.2.1. Dimensions for Flexible Pavement Model

Flexible AC pavements are continuous in the direction of traffic and jointless in the transverse direction. Also, asphaltic material is softer than concrete material, so the response of flexible pavements to the impact load would be more localized than the response of rigid concrete pavements. Flexible pavements frequently have shoulders made of the same material as the surface course. This creates the continuity condition for the propagation of the stress waves generated by the impact load. The above observations led to the development of the 3D flexible pavement model with the dimensions of 6 x 6 x 8 feet. To create the effect of continuity of the model beyond the specified dimensions, nonreflective boundary conditions were used along the sides and the bottom of the model. In the case of an uncracked pavement without structural irregularities, the response of the pavement is symmetric and only a quarter of the model can be analyzed. The finite element mesh for the flexible pavement model with dimensions and boundary conditions is presented in the next chapter in Figure 2.1.

2.2.2 Dimensions for Rigid and Composite Pavement Models

The principal difference between the flexible AC model and the models that include a rigid concrete layer is the finite dimensions of concrete slabs. The mechanism of the stress wave propagation through the finite concrete slabs is different from the propagation through the continuous layer such as AC. Each time a stress wave reaches the slab edge, some energy is reflected back and some propagates away. Reflected waves can change the pattern of the slab response to the applied impact load. Another consideration in the modeling of concrete slabs is the position of the loading plate. As was stated above, for the current study the loading plate position was chosen to be 900 mm

(3 feet) from the outer edge and at the middle of the slab in the direction of traffic. Taking into consideration the slab size, being on average 3.6x9.0 m (12x30 feet), the loading plate position is clearly much closer to the outer longitudinal edge than to any other. Therefore, the time required for the stress wave to reach this edge is much less than that required to reach any of the other three edges. In this study of pavement response to FWD load, only the reflection from the outer edge of the pavement was considered during the time of investigation. For all the other sides of the model, non-reflective boundary conditions were prescribed. Figure 5.2 shows the finite element mesh for the composite pavement model with dimensions and boundary conditions and Figure 6.2 shows the rigid pavement model.

2.2.3. Element Type

Review of finite element modeling of pavement structures reveals that pavements were modeled using either structural plate elements *(33 - 37)* or solid brick elements*(38 - 47)*. The solid brick element approach, used for the three-dimensional analysis, gives a better opportunity to account for the variation in the displacements through the element thickness. Therefore, the solid element approach was used in this study in preference to the structural element approach. Each pavement layer was modeled using 8-node solid hexahedron elements. To assure accuracy of the results, a finer mesh was used in the layers that experience higher stresses.

2.2.4. Boundary Conditions

The effect of finite model dimensions was compensated by the selection of the proper boundary conditions. The following boundary conditions were prescribed along the models boundaries:

1. The bottom of the model is fully fixed.
2. Rollers on the sides of the model allow free vertical deformation.
3. Symmetry plane boundary conditions were prescribed along the transverse plane to perform calculations only for one half of the model.

The non-reflective boundaries feature allows radiating waves to be absorbed when they reach

this boundary, giving the effect of a continuous layer. Non-reflective boundary conditions were used to simulate a semi-infinite extension for the soil media laying under the pavement structure when bedrock was assumed to be at the depths exceeding the model depth. Similarly, non-reflective boundaries were used to simulate an infinite extension of the pavement structure in the longitudinal direction.

2.2.5. Modeling of Pavement Interfaces

Thoughtful consideration was given to the aspect of the interaction between subsequent layers in the pavement structure. As a result, two types of pavement layers interface were used in the study: fully bonded and fully unbounded. These two cases represent two extremes, and therefore should give a clear picture of the difference in pavement response with regard to layer bonding. Two DYNA3D formulations of interface types were chosen for analysis:

1. Interface with a possibility of separation that allows two bodies to be separated or be in contact. This option permits relative motion between any two layers and simulates the case of a broken bond between layers.

2. The tied interface option permits tying two parts with different element sizes. In this formulation, the surface with the finer mesh is used as a "slave" and the surface with a coarse mesh is used as a "master." "Slave" nodes are restricted from penetration of "master" surfaces.

To avoid interpenetration of the pavement layers with untied interfaces, a penetration penalty method was used in the specification of interfaces between different pavement layers. In the DYNA3D formulation of the penalty method, normal interface springs are placed between all penetrating nodes and contact surfaces. A spring stiffness matrix is then incorporated into the global stiffness matrix. The interface stiffness is chosen to be approximately of the same order of magnitude as the stiffness of the element perpendicular to the interface. In the case of high pressures at the interfaces, penetration can be avoided by scaling up the spring stiffness or reducing integration time

steps. When penetrations are indicated during the solution process, a restoring force is placed on a penetrating node to return it to the surfaces. The force is proportional to the depth of penetration, the bulk modulus of penetrated material, the dimensions of the penetrated element, and the penalty scale factor.

2.3. MATERIAL MODELS

A broad range of constitutive models for pavement materials is available in practice. The literature review of previous studies on the behavior of pavement materials shows that stresses induced in pavement structures under the FWD, with the maximum pressure of 640 kPa (92.8 psi) used in this study, are likely to be within the elastic range*(3, 40)*. Therefore, linear elastic material models were used to characterize the response of all layers.

2.3.1. Linear Elastic Models

It is a known fact that AC and geologic materials are not elastic but experience some permanent deformation after each load application. However, as the number of load repetitions increases, the amount of plastic strain due to each load repetition decreases. If the load is repeated for a large number of times, the deformation under any new load below the load that caused plastic deformation will be almost all recoverable. In this case, the recoverable strain is proportional to the load and can be treated as elastic. The elastic modulus derived from the recoverable strain is called the resilient modulus. This modulus is widely used to characterize the elastic response of the pavement materials. Linear elastic properties of the pavement materials used in this study are presented in Table 2.1.

2.3.2. Linear Viscoelastic Models

AC response to the load is time and temperature-dependent. At temperatures above 60°F

such factors as loading time, loading rate, and the rate of load repetitions have a significant effect on the response of AC material. Hopman, et al. *(48)* pointed out that AC response to a short duration loading is similar to that of a linear elastic solid. During the current study, the influence of the viscous properties on AC response, due to the impact load, was studied and results are presented in Chapter 3.

The viscoelastic model in DYNA3D is based on Key's formulation for deviatoric or distortional viscoelasticity *(49)*:

$$s_{ij}=2\int_0^t G(t-\tau)\dot{e}_{ij}d\tau$$

where s_{ij} -- deviatoric stress,

$\dot{e}_{ij}$ -- deviatoric strain rate,

G -- shear relaxation modulus,

t -- reduced time (represents a shift in time dependent on temperature),

τ -- actual time.

The time-dependent shear relaxation modulus was presented as

$$G(t)=G_\infty+(G_0-G_\infty)e^{-\beta t}$$

where G_∞ -- long-time shear modulus,

G_0 -- short-time shear modulus,

β -- decay constant dependent (inverse of the shear relaxation time),

t -- actual time.

Short-term viscous material properties are used in this formulation to characterize the instantaneous material response and viscous strain rate. Long-term viscous material properties are used to define the behavior of the fully retarded material and the rate of the retarded strain.

The definitions of instantaneous material properties come from the formulation of the Maxwell viscoelastic model Figure 2.1(a). According to the Maxwell formulation, if the strain in the material is kept constant, the stress will gradually relax and, after a long period of time, will become zero. The time required for the stress to be reduced to 36.8 percent of its original value is used as a relaxation time according to Maxwell formulation.

Long-term viscous material properties related to the Kelvin viscoelastic model are illustrated in Figure 2.1(b). According to the Kelvin formulation, under the constant applied pressure, the strain will increase with the time until it reaches its fully retarded value as the time approaches infinity.

The standard linear solid model used in the current study contains attributes of both Maxwell and Kelvin models. The change of strain with time is presented in Figure 2.1(c). The volumetric response in the current material model formulation was assumed to be elastic. Linear viscoelastic material model constants are given in Chapter 3.

2.4. LOADING CONDITIONS

A circular loading plate (LP) was added to the model for more accurate simulation of the FWD setup. The plate was 300 mm (12 in) in diameter and fabricated from steel. The semi-rigid behavior of the plate permits more even load distribution under the plate. The plate mesh is shown in Figure 2.2 and the plate properties are given in Table 2.1. The loading plate serves as a load transferring device for the pavement structure. Because of the loading and geometrical symmetry around a transverse plane passing through the center of the loading plate, only one half of the pavement and loading plate was used in the analysis. The load pressure was evenly distributed over the plate surface. An integration time step for the analysis was chosen equal to the time required for the stress wave to propagate through the least dimension of the smallest element in order to assure the accuracy of the explicit solution.

2.4.1. Gravitational Loads

It was considered important to incorporate the effect of gravity as an initial condition in the model. The gravity option allows to include the initial downward compressive stress in the pavement layers. The magnitude of the stress due to gravity near the surface is not large, but it does increase with depth and cannot be neglected in studies of stress-strain states of the lower layers. The amount of upward deflection in the layers due to impact is also affected by the gravity loads. Acting downwards, gravity would reduce the magnitude of rebound in pavement layers. Loads due to gravity are included in the formulation of the governing equation of equilibrium as a part of body forces.

2.5. EXPLICIT DYNAMIC ANALYSIS IN DYNA3D SOFTWARE PACKAGE

To perform a dynamic analysis of a pavement system under impact, system equilibrium equations should be solved first. To solve the equilibrium equations in a time domain, numerical integration is needed. Two integration schemes are popular for the solution of dynamic problems *(50, 51)*:

1. The first is an explicit integration, in which displacements at time $t+\Delta t$ are solved directly in terms of previous displacements and dynamic equilibrium conditions established at time t. This formulation allows the use of a diagonal mass matrix that is a very advantageous feature leading to substantial savings in time for the models with a large number of nodes. However, small time steps are required to obtain a stable solution. This method is valuable for the solution of large problems with short loading times, such as impact problems.

2. The second is an implicit integration, in which displacements at time $t+\Delta t$ are expressed as a function of velocity and acceleration vectors evaluated at time $t+\Delta t$; in this case, the equation of dynamic equilibrium is solved for the time $t+\Delta t$. In this formulation, an effective stiffness matrix can no longer be diagonal; therefore, solution of the dynamic equilibrium equation becomes time consuming. The advantage is that the solution is unconditionally

stable and larger time integration steps can be used. This method is very useful for the solution of smaller problems with minor dynamic effects.

The finite element package DYNA3D uses explicit time integration by means of a central difference formula according to which

$$\Delta t^{n+1/2} = \tfrac{1}{2}(\Delta t^{n} + \Delta t^{n+1})\, u^{n+1} = u^{n} + v^{n+1/2}\Delta t^{n+1/2}$$

$$v^{n+1/2} = v^{n-1/2} + a^{n}\Delta t^{n}$$

where Δt -- integration time step,

u -- global displacement vector,

v -- global nodal velocity vector,

a -- acceleration vector obtained from the direct solution of the equation of motion established in the previous time step.

TABLE 2.1. Properties of Pavement Layers and Loading Plate

Type of material	Layer thickness (mm)	Young's modulus (kPa)	Poisson's ratio	Mass density (kg/m^3)
		Flexible Pavement *(55)*		
Asphalt concrete	100	3.430E+06	0.35	2320.5
Crushed stone	350	2.400E+05	0.4	2240.5
Subgrade A-4(6)	1950*	6.859E+04	0.45	1840.4
		Rigid Pavement *(41)*		
Concrete	200	3.210E+07	0.18	2400.0
Base	150	1.170E+07	0.4	2240.5
Subgrade	2050	8.170E+04	0.4	2080.5
		Composite Pavement		
Asphalt-concrete	150	2.743E+06	0.3	2400.0
Concrete	200	2.743E+07	0.18	2400.0
Gravel	150	2.058E+05	0.4	2160.6
Sandy soil	1800	8.230E+04	0.3	2080.5
		Steel Plate		
Steel plate	25	2.067E+08	0.3	7826.0

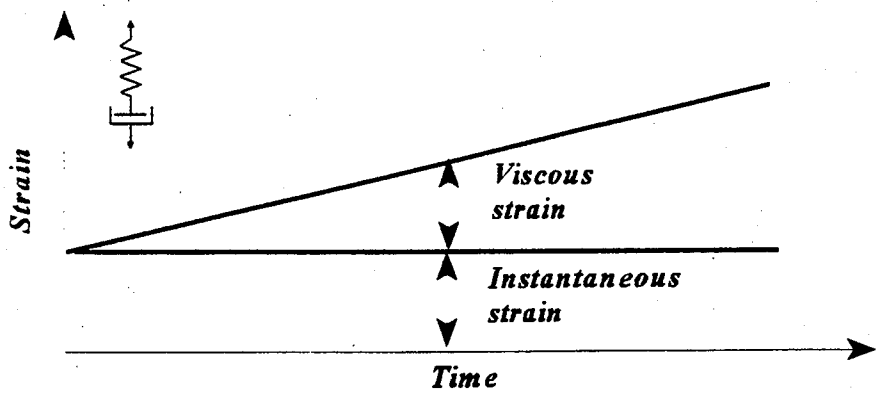

(a) Maxwell model

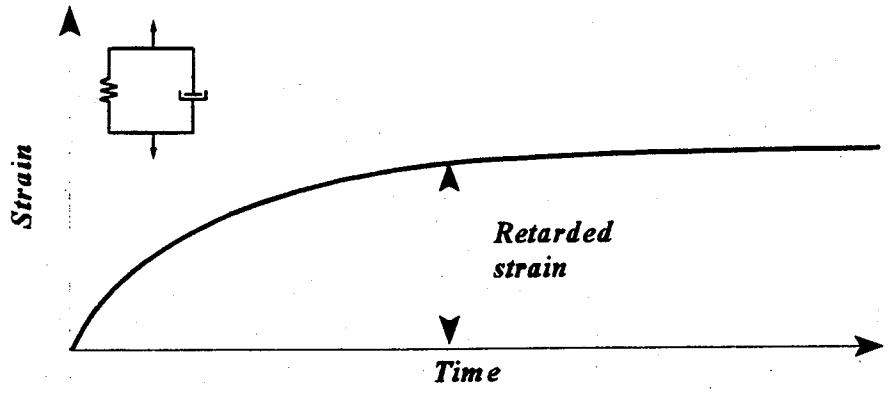

(b) Kelvin model

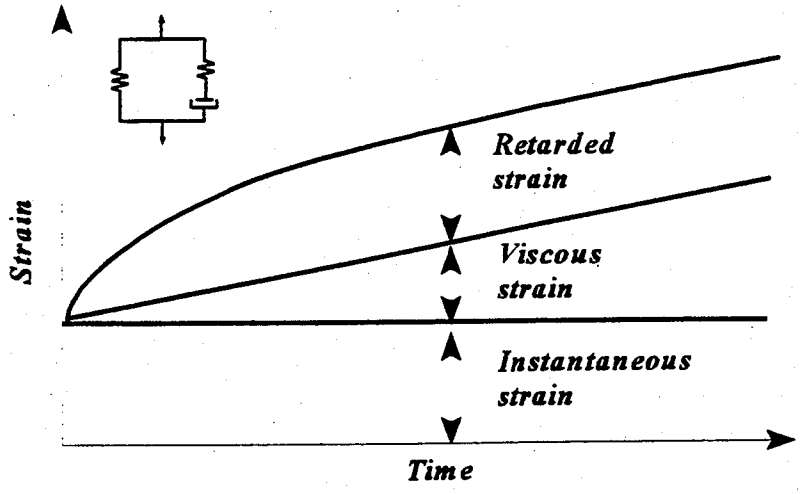

(c) Generalized model

FIGURE 2.1 Mechanical models for the viscoelastic materials.

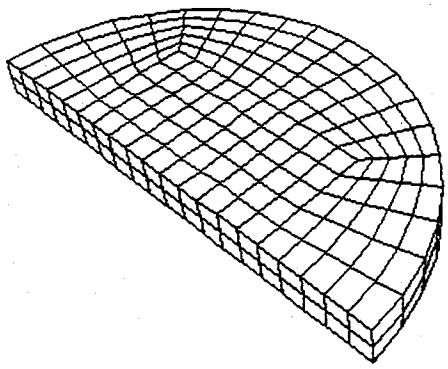

FIGURE 2.2 Model of the half of the loading plate.

CHAPTER 3

EXPERIMENTAL VERIFICATION OF FINITE ELEMENT MODEL

3.1. VERIFICATION STRATEGIES

One way of investigating the accuracy of the theoretical model is to compare the theoretical results with the field measurements for the same structure under identical loading conditions. The important precaution in this procedure is to make sure that the properties of modeled and tested materials are the same. In the case of multilayered pavement structure, this task is very difficult due to the nature of the geologic materials. The mechanical properties of soils are highly dependent on the moisture content, density, confined pressure, and stress path. The condition of a soil sample extracted from the pavement structure and then transported to the laboratory for the testing is unlikely to be identical to the condition of the soil during the time of the experiment. Therefore, there is no guarantee of an exact match between field and theoretical results, although, they should be within the reasonable tolerance. Some researchers ignore laboratory evaluation of pavement properties in verification studies, as was demonstrated in the work done by Zagloul et.al *(39)*. Their verification analysis was based solely on matching the measured and computed displacements. However, the literature review has shown that many different moduli combinations can be backcalculated based on the same deflection data.

To overcome the limitations of the above approach, the following guidelines were followed:

1. The values of the material properties used in the theoretical model should be consistent with the laboratory test results for the materials of the tested pavement section.
2. If the comparison is made between several different theoretical solutions, the same set of material properties should be used in any other pavement analysis programs or backcalculation algorithms.
3. Deflection basins obtained from the different theoretical analyses should be compared with

the measured ones.

Following the above guidelines, the material data for this verification study were obtained from the laboratory test results published by Hoffman and Thompson for the Sherrard section *(52)*. This section consisted of a 4 inch AC layer over 14 inches of crushed stone base. The subgrade was presented by AASHTO soil type A-4 that corresponds to fine grained silt-clay materials. The resilient modulus of the subgrade soil was determined by subjecting soil samples to repetitive loading of different magnitudes. The resilient modulus of AC layer was determined by the repetitive indirect tensile test at 77°F. Properties of crushed stone base were obtained from Traylor *(53)*. Hoffman and Thompson compared the laboratory measured moduli with backcalculated moduli and concluded that the correlation was reasonable and followed a logical trend with surface pavement temperature. A summary of pavement layer properties used for the current verification study is given in Table 3.1.

The FWD used in field testing for the determination of backcalculated pavement moduli had the following characteristics: (a) the diameter of the loading plate was 30 cm (12 in); (b) the load impulse had a uniform distribution over the plate; (c) the magnitude of the load impulse was 35.5 kN (8 kip); (d) the load duration was 40 ms; (e) the loading plate was positioned 900 mm (3 ft) from the edge of the pavement. Surface deflections were recorded by velocity transducers at 0, 300, 600, and 900 mm (0, 1, 2, 3 feet) from the center of the loading plate.

No information was found related to the state of the bond between different layers. Therefore, a decision was made to analyze two cases: one with fully bonded interfaces and one with fully unbonded interfaces. Based on the Sherrard section data, two finite element models for the flexible pavement were built following the guidelines outlined in Chapter 2. The two models are identical except for the interface bonds. Each model has dimensions of 1800x1800x2400 mm (6x6x8 feet) and consists of three layers, as shown in Figure 3.1. The models were meshed using 8-node solid brick elements. The impulse load is applied through the steel plate. Figure 3.2 presents the curve of the pressure-time relation used in the verification analysis.

The same Sherrard section data were also used by Sebaaly et al. to verify the elastodynamic solution using multi-layer computer program DYNAMIC2 *(3)* and later by J. Mallela, et al. to verify the pavement model created using the ABAQUS general finite element code *(41)*. In the verification procedures, the above researchers compared results obtained using their theoretical models with the measured ones and the one obtained by static solution using the DYNAMIC2 program with the zero frequency.

3.2. RESULTS OF THE VERIFICATION MODEL

In the current investigation, the results of the new theoretical model created using DYNA3D were compared with the measured results and with the results of the above verification studies. To construct the deflection basins from the model results, first the deflection versus time records for the specified surface points were extracted from the solution database, as shown in Table 3.2. Then, maximum vertical deflections were obtained from the record to create a deflection basin. The deflection basins constructed from the maximum measured and calculated vertical deflections obtained by different methods are compared in Figure 3.3.

The deflections predicted by DYNA3D model show a good agreement with the measured deflections. The deviations of theoretically predicted deflections from the measured ones are 0.5, 5, 9.5, and 38 percent increasing with the distance from the center of the loading plate.

All the theoretical models gave a higher error in the vertical deflection value at the distant position. As known from the principle of backcalculation presented in the literature review, deflections at distant positions are mostly affected by the modulus of the subgrade layer. Therefore, the difficulty in obtaining very accurate predictions of soil modulus may be the reason for a higher deviation in the measured and computed results at distant positions.

3.2.1. Effect of Viscoelasticity of Asphalt-Concrete Material

AC material is known to show viscous behavior especially at high temperatures and long load durations. To study the effect of viscosity in the material behavior in the case of a short impulse load, linear viscoelastic properties were prescribed to the AC layer and used with the same model of Sherrard section. To characterize viscoelastic properties, the following material constants were derived from existing linear elastic data where possible or appropriate values were taken from the literature.

G_0 =	1.326e+06 kPa (1.923e+05 psi)	short-time shear modulus,
G_∞ =	2.653e+05 kPa (3.8450e+04 psi)	long-time shear modulus,
β =	1.015	decay constant (inverse of the shear relaxation time).

The relaxation time value of 0.985 seconds for asphalt material was obtained from the work of Mikhail *(54)*. The loading duration used in this study is about 44 percent of the relaxation time. This means that, during the time of interest, the material will not have enough time to show its viscoelastic behavior fully; thus, the material response to such short loading duration will be mostly affected by the short-term properties.

The analysis was repeated for the case of bonded and unbonded interfaces. A small difference of 8 percent was found between the elastic and viscoelastic results. Therefore, linear elastic characterization of the AC is appropriate for modeling of the AC response to the short time impact loads. The comparison of deflection basins from all the models created by DYNA3D for the verification study with the measured results is presented in Figure 3.4.

TABLE 3.1. Material Properties for the Verification Model

Pavement Layer	Type	Thickness (mm)	Moduli (kPa)	Poisson's Ratio	Mass Density (kg/m^3)
Surface	Asphalt concrete	100	3.430E+06	0.35	2320.5
Base	Crushed stone	350	2.400E+05	0.4	2240.5
Subgrade	A-4	1950*	6.859E+04	0.45	1840.4

* The depth to bedrock was not reported. In the verification study, nonreflective boundary was used at the bottom of the model.

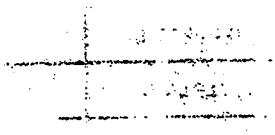

Table 3.2. Vertical Deflections at the Specified Surface Locations Vs. Time.

Time, sec	Vertical deflections at the specified offsets from the center of the loading plate, inches			
	0"	12"	24"	36"
1.716731E-41	4.000000E+00	3.200000E+01	4.400001E+01	5.600000E+01
9.997138E-04	-1.165175E-05	-1.788825E-06	1.785205E-07	1.314987E-09
1.999639E-03	-6.822820E-05	-1.767844E-05	2.715442E-06	1.123786E-07
2.999458E-03	-1.912520E-04	-6.304473E-05	6.483358E-06	3.480371E-06
3.999277E-03	-3.916192E-04	-1.500086E-04	4.262882E-06	1.312676E-05
4.999297E-03	-6.729032E-04	-2.861859E-04	-1.204004E-05	2.817378E-05
5.999972E-03	-1.032754E-03	-4.738419E-04	-5.011587E-05	4.437894E-05
6.999839E-03	-1.473533E-03	-7.145645E-04	-1.153127E-04	5.445241E-05
7.999862E-03	-2.011973E-03	-1.014614E-03	-2.101760E-04	5.215177E-05
8.999670E-03	-2.670659E-03	-1.384096E-03	-3.352569E-04	3.484770E-05
9.999581E-03	-3.467918E-03	-1.834739E-03	-4.914663E-04	3.162202E-06
1.099938E-02	-4.414356E-03	-2.376097E-03	-6.824264E-04	-4.322207E-05
1.199999E-02	-5.501878E-03	-3.012012E-03	-9.161875E-04	-1.075280E-04
1.299978E-02	-6.690003E-03	-3.732227E-03	-1.202577E-03	-1.943733E-04
1.399984E-02	-7.926320E-03	-4.514992E-03	-1.545286E-03	-3.156002E-04
1.499972E-02	-9.168413E-03	-5.330603E-03	-1.946902E-03	-4.677535E-04
1.599938E-02	-1.038857E-02	-6.157016E-03	-2.380056E-03	-6.468606E-04
1.699930E-02	-1.156692E-02	-6.970938E-03	-2.822784E-03	-8.517038E-04
1.799954E-02	-1.267900E-02	-7.751403E-03	-3.264402E-03	-1.074904E-03
1.899983E-02	-1.369890E-02	-8.478143E-03	-3.691569E-03	-1.304005E-03
1.999921E-02	-1.460692E-02	-9.134886E-03	-4.092652E-03	-1.528322E-03
2.099927E-02	-1.539557E-02	-9.714601E-03	-4.458792E-03	-1.740228E-03
2.199954E-02	-1.605706E-02	-1.021181E-02	-4.778998E-03	-1.932742E-03
2.299917E-02	-1.657766E-02	-1.061656E-02	-5.046471E-03	-2.098434E-03
2.399976E-02	-1.694171E-02	-1.091821E-02	-5.264796E-03	-2.234527E-03
2.499991E-02	-1.713517E-02	-1.110741E-02	-5.422833E-03	-2.338760E-03

2.599948E-02	-1.715098E-02 *	-1.117835E-02	-5.517810E-03	-2.408147E-03
2.699958E-02	-1.698082E-02	-1.112668E-02	-5.544590E-03	-2.440013E-03
2.799979E-02	-1.660542E-02	-1.094604E-02	-5.503780E-03	-2.434111E-03
2.899989E-02	-1.601314E-02	-1.062756E-02	-5.395497E-03	-2.395083E-03
2.999963E-02	-1.522021E-02	-1.017139E-02	-5.219046E-03	-2.326924E-03
3.099942E-02	-1.427223E-02	-9.593923E-03	-4.974740E-03	-2.232131E-03
3.199954E-02	-1.322786E-02	-8.923694E-03	-4.666203E-03	-2.110597E-03
3.299972E-02	-1.212696E-02	-8.193231E-03	-4.304353E-03	-1.961744E-03
3.399968E-02	-1.101019E-02	-7.431755E-03	-3.904040E-03	-1.788726E-03
3.499915E-02	-9.901242E-03	-6.663188E-03	-3.482579E-03	-1.595935E-03
3.599977E-02	-8.807724E-03	-5.903158E-03	-3.056319E-03	-1.389068E-03
3.699995E-02	-7.739757E-03	-5.165225E-03	-2.641405E-03	-1.175827E-03
3.799992E-02	-6.714081E-03	-4.459400E-03	-2.247110E-03	-9.647553E-04
3.899946E-02	-5.750909E-03	-3.795855E-03	-1.878872E-03	-7.667175E-04
3.999966E-02	-4.874372E-03	-3.184180E-03	-1.534990E-03	-5.794955E-04
4.099986E-02	-4.108859E-03	-2.636210E-03	-1.216095E-03	-4.052340E-04
4.199970E-02	-3.447015E-03	-2.163617E-03	-9.363268E-04	-2.532360E-04
4.299970E-02	-2.877354E-03	-1.768075E-03	-7.068511E-04	-1.284575E-04
4.399953E-02	-2.388192E-03	-1.434665E-03	-5.282945E-04	-4.157040E-05
4.499968E-02	-1.970592E-03	-1.162120E-03	-4.006132E-04	7.855244E-06
4.599940E-02	-1.623491E-03	-9.545168E-04	-3.204723E-04	2.548949E-05
4.699998E-02	-1.338865E-03	-7.946130E-04	-2.787397E-04	1.671476E-05
4.799939E-02	-1.108391E-03	-6.736592E-04	-2.674431E-04	-9.778712E-06
4.899986E-02	-9.239370E-04	-5.840330E-04	-2.672116E-04	-4.573061E-05
4.999953E-02	-7.775503E-04	-5.128615E-04	-2.746889E-04	-8.961945E-05

*Maximum values defined in the heavy lined boxes.

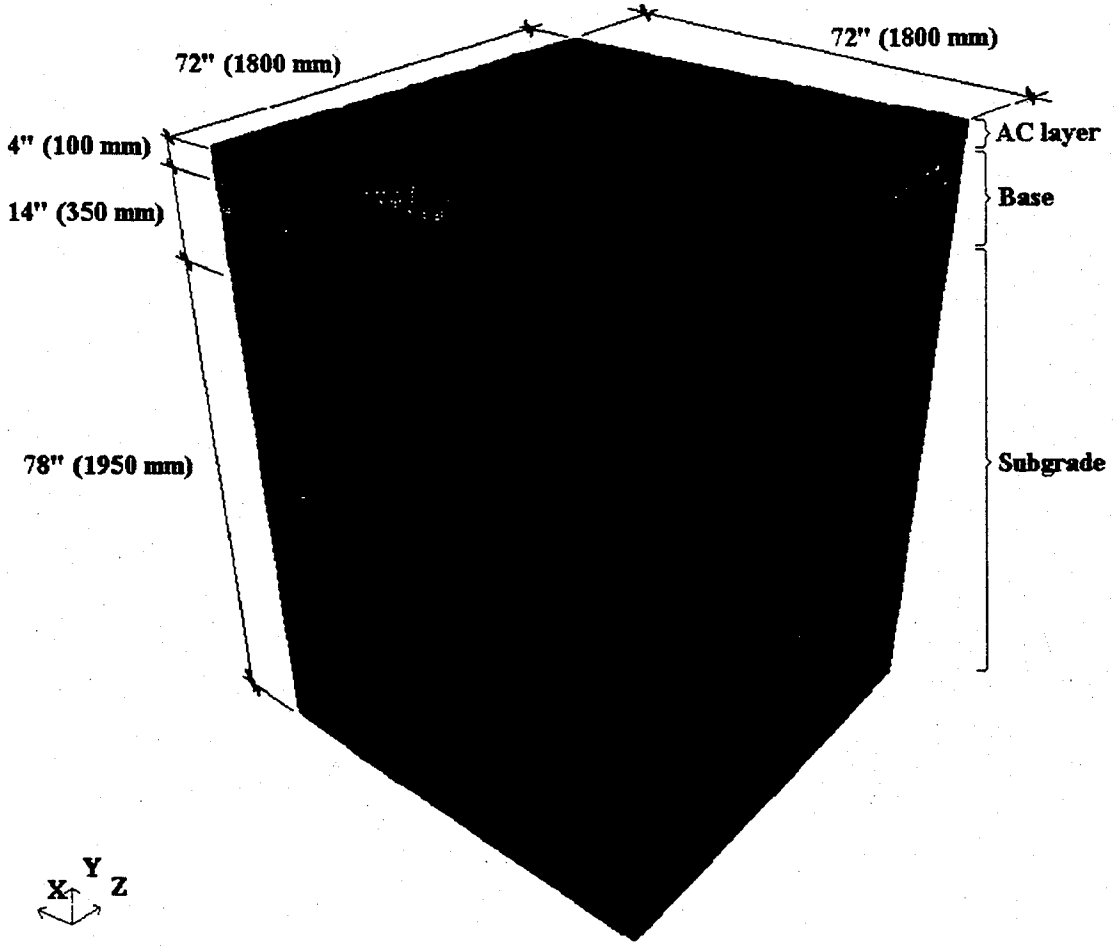

FIGURE 3.1 Finite element mesh of the flexible pavement for the verification study.

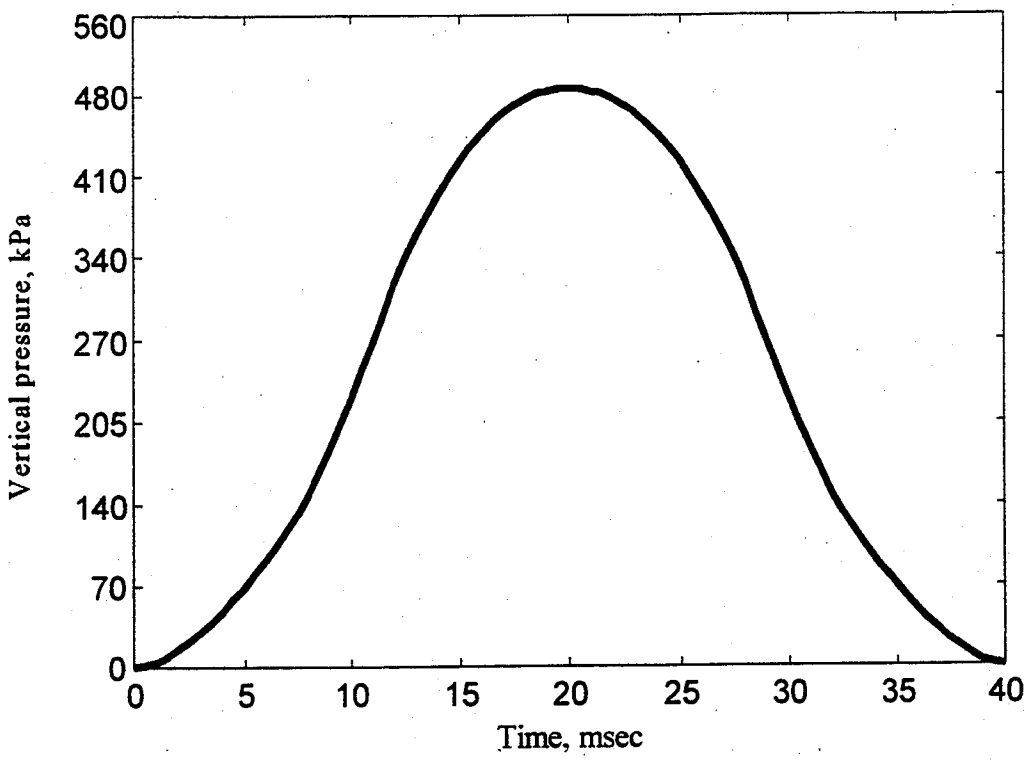

FIGURE 3.2 Curve of vertical pressure change with time *(3)*.

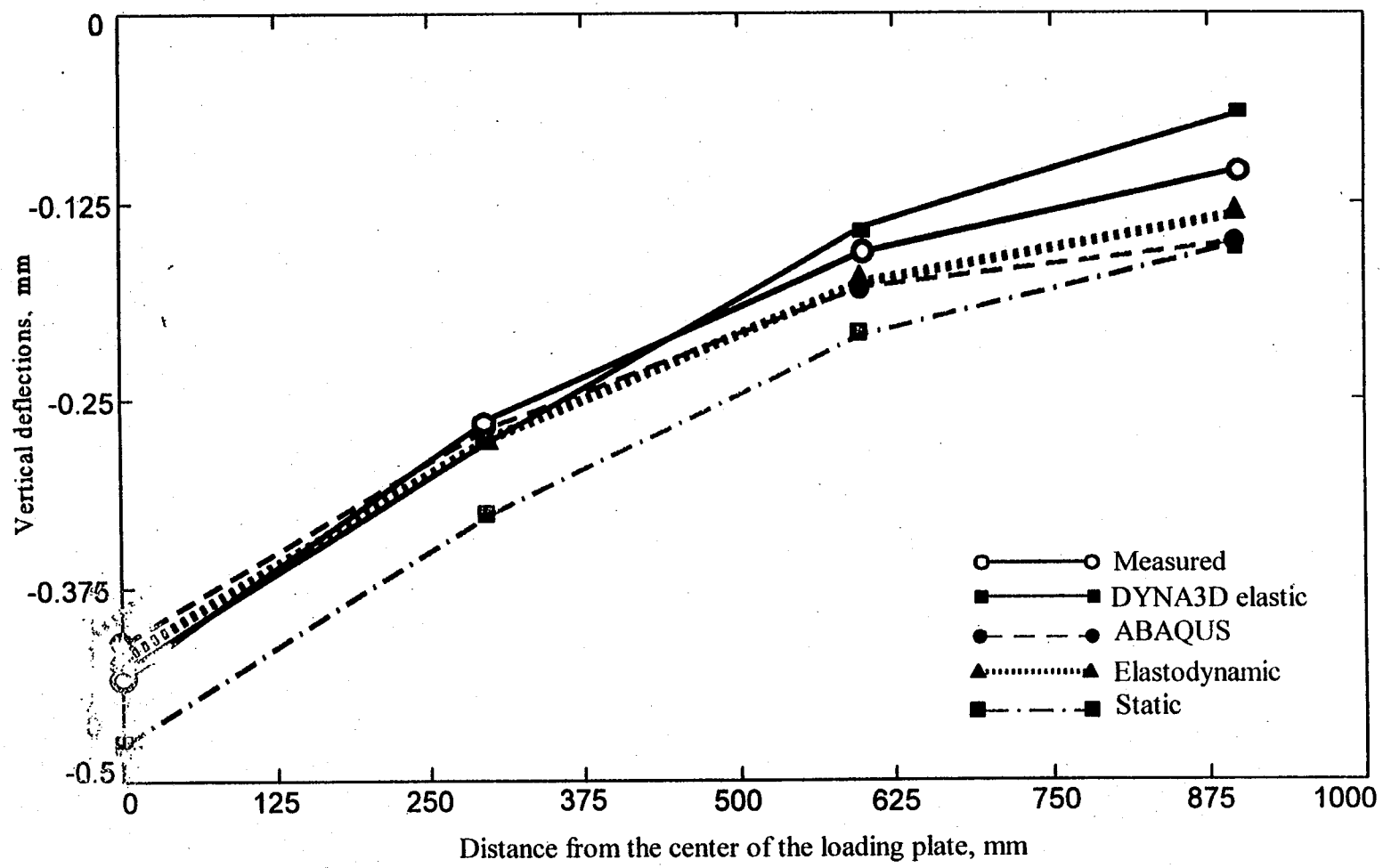

FIGURE 3.3 Comparison of the deflection basins obtained by different methods.

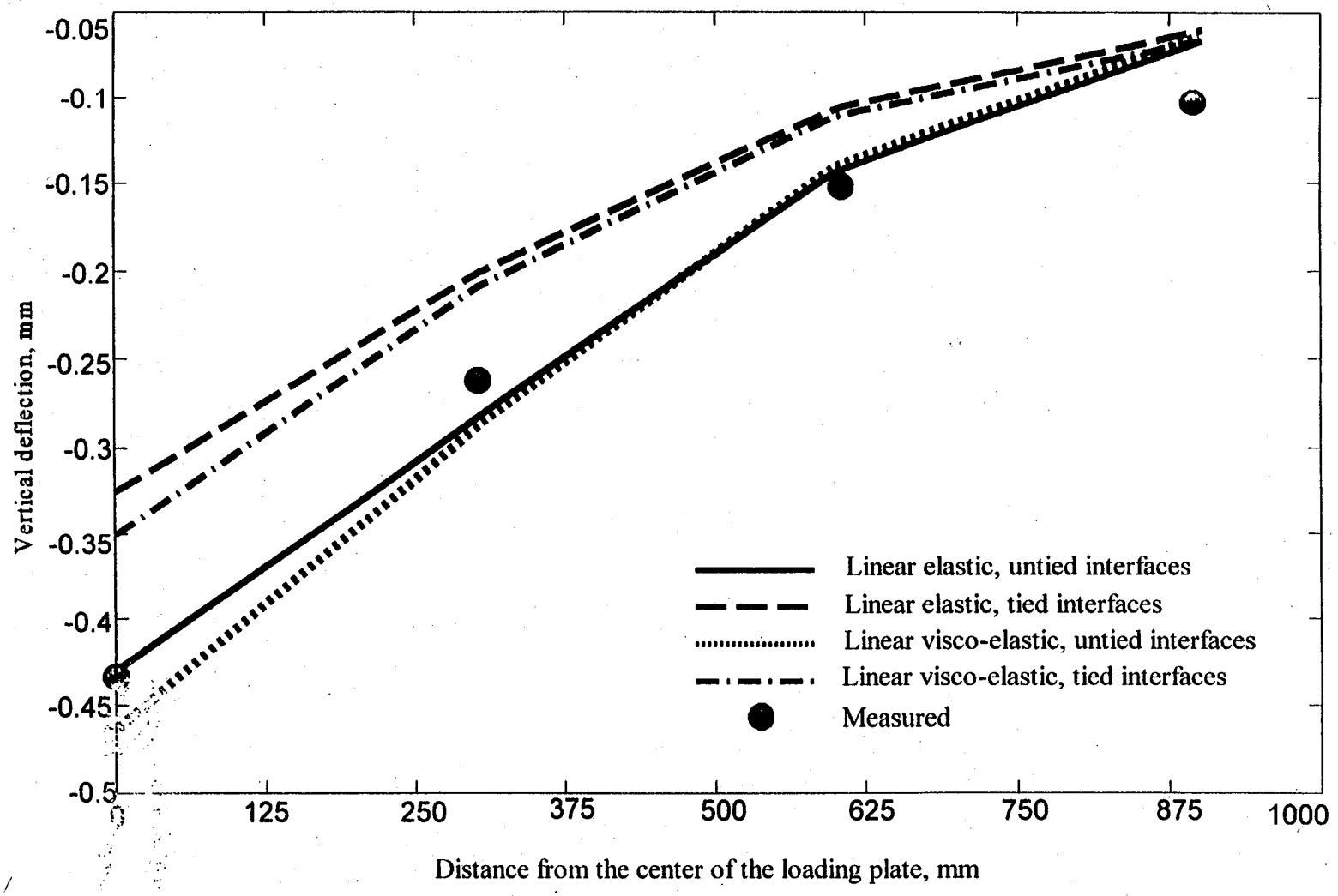

FIGURE 3.4 Deflection basins with different state of bond between the pavement layers.

CHAPTER 4

THEORETICAL ANALYSIS OF FLEXIBLE PAVEMENTS UNDER FWD LOAD

4.1. INTRODUCTION

The theoretical analysis presented in this chapter simulates the response of the flexible pavements to the FWD. The loading conditions, material properties, and model dimensions were taken from the verification model in Chapter 3. Two cases of fully bonded and fully unbonded interfaces were considered in this study. Created finite element models allow the user to study the pavement response at any point in the model and at any instance of time.

4.2. VERTICAL DEFORMATION VERSUS TIME

To analyze the contribution of different layers to surface deflections, record of vertical deformation change with time for several points were extracted from the analysis database. Unlike the conventional method of surface deflection measurement, deflections were obtained not only for the surface geophone locations but also through the depth of the pavement. This deflection data enables quantitative analysis of the dynamic deformation propagation through the pavement structure. The deflection vs. time graphs reveal that for the haversine impact load with a peak at 20 milliseconds, all the substantial vertical deflection will be eliminated after 50 milliseconds from the beginning of the load application. Therefore, the 50 milliseconds period was used in the current study. The above time period includes the time of load application of about 40 milliseconds followed by a free system response of 10 milliseconds.

For each pavement model, points for the deflection vs. time study were chosen so that the surface points would coincide with the geophone locations used in the FWD test. Those locations are at 0(0"), 300(12"), 600(24"), 900(36"), and 1200(48"), millimeters from the center

of the loading plate. In-depth points were located on the top and bottom of each pavement layer along the vertical line passing through the surface point of geophone location. The positions of the points are shown in Figure 4.1.

The vertical deformations versus time plots of for different offsets from the loading plate are presented in Figures 4.2 to 4.6. Each figure contains two different plots; the upper plot represents the case of bonded interfaces and the lower plot represents the case of unbonded interfaces. Each plot contains five deflection versus time curves for the points on the top and bottom of each layer along the same vertical section.

In the case of bonded interfaces, graphs for any set of points lying along the same vertical line appear to have similar patterns of vertical deformation, with only a difference in magnitude of the maximum response and a slight time delay in the response of the lower points. This delay increases with the depth. Therefore, in this case, the surface deflections are highly correlated to the deflections in the subsequent layers and reveal the pavement response through its depth.

In the model with unbonded interfaces, the patterns of deformation for different layers are all similar in the vicinity of the load, but show some deviation with the distance from the load. For example, at the 900 mm (36") offset from the center of the loading plate at the beginning of the load application, the AC layer experiences upheaval resulting in the initial upward vertical deformation, as shown in Figure 4.5. Simultaneously, the lower layers experience downward deformations. This behavior results in the separation of the AC layer from the rest of the pavement structure. The separation increases even more at the offset of 1200 mm (48"), as shown in the bottom graph of Figure 4.6.

The magnitude of the maximum upward deformation of the pavement surface is 45 times less than the magnitude of the maximum downward surface deformation. It is likely that such small vertical deformations will be ignored during the evaluation of FWD results, due to

limitations of the sensors sensitivity. However, this behavior can be used as an indicator of the loss of the bond between the pavement layers, if more sensitive equipment would be used. The knowledge of the state of the bond between pavement layers is very important for the accurate evaluation of pavement structural capacity.

The condition of the bond between pavement layers is reflected in the rate of the displacement rebound. Layers of the flexible pavement models with unbonded interfaces rebound faster than layers of the model with bonded interfaces, as can be seen in the Figure 4.4 and Figure 4.5.

Comparison of the results for the models with bonded and unbonded interfaces shows that the main backcalculation assumption of the surface deformation representing the deformation in the subsequent layers is valid if the existing pavement has well-bonded interfaces. The FWD serves in this case as a reliable tool for the evaluation of the pavements structural capacity. However, for the case of unbonded interfaces, the FWD readings from the distant geophones may not represent the deformations in the lower layers. That is, the deformation of the surface layer is independent of deformation at the top of the soil layer. Real pavements seem to behave as unbonded layers. Support for this observation comes from Figure 3.4, where unbonded models produced deflection results that are more consistent with experimentally measured ones.

4.3. EFFECT OF LAYERS BONDING ON DEFLECTION BASIN

In the backcalculation algorithms, surface deflection basins are used to evaluate the moduli of different layers in the pavement structure. Therefore, the accuracy of construction and interpretation of the deflection basins are essential for the reliability of the FWD results.

The deflection basins for the flexible model with bonded and unbonded interfaces were

constructed from the finite element analysis results, as shown in Figure 4.7. In each case, the maximum downward vertical deflections were used to build the deflection basin. The deflection basins for the cases of bonded and unbonded interfaces show up to 32 percent difference in the values of the maximum surface deflections.

The deflection basin for the bonded model is not as sharp (absolute difference between maximum and minimum deflection is less than that for unbonded interfaces) as the one for the unbonded model and all the deflection basin points remain below zero coordinate.

4.4. DYNAMIC DISPLACEMENT DISTRIBUTIONS

Fringes of vertical displacement distribution for the several instances of time are presented in Figures 4.8 to 4.10. To get a better insight on the displacement propagation, two mutually perpendicular cuts were made through the center of the loading plate to reveal the displacement distribution on the quarter of the pavement model. Each figure contains two plots: one for the unbonded model and another for the bonded one. Both models show similar displacement distributions in the form of a spherical bowl spreading away from the center, as the time of load application increases. However, there are two differences in the models behavior. First, the model with no bond between layers shows separation of the AC layer and formation of a temporary void on the model side adjacent to the shoulder. Second, there is a difference in the magnitude of the vertical deflection. Results for the bonded model show consistently smaller deformation than those for the unbonded model. Therefore, the pavement with bonded interfaces appears to be stiffer and capable of carrying higher structural capacity.

The fringes of the vertical deformation reveal the contribution of different layers to the surface deflection. In Figure 4.11, obtained for the time of maximum center deformation, the surface deformation under the center of the loading plate is higher than the deformation of the top of the base layer. The deformation of the top of the base layer is higher than the

deformation of the top of the soil layer. Therefore, all three layers contribute to the surface deformation. At 600 mm (24") offset from the center of the loading plate, the vertical deformations of AC layer and base layer are of the same magnitude but larger than the deformation of the soil layer. In this case, the surface deflection reading reveals the amount of deformation in the base layer that, in its own turn, is affected by the deformation in the soil layer. Going further from the center of the loading plate, at the offset of 900 mm (36") fringes of vertical deformation show that the surface deflection is of the same magnitude as deflection on the top of the base layer and on the top of the subgrade layer. This means that surface deflection reading at 900 mm (36") offset geophone location represents the deformation of the top of the subgrade.

4.5. CONCLUSIONS

The results of dynamic 3D finite element analysis of the flexible pavement structure under the action of a FWD load led to the conclusion that backcalculation results may be affected by the condition of the bond between the layers of the flexible pavement. The dynamic deflection patterns are significantly different in the cases of bonded and unbonded interfaces. Once the bonds between layers are broken, the top layer has more freedom of vibration and the pavement structure no longer behaves as a solid, but behaves rather as a set of plates of different stiffness. Backcalculation procedure that could account for the condition of the bond between pavement layers would result in higher accuracy of moduli evaluation for flexible pavements. If during the evaluation of FWD data, some sections consistently show higher deformation under the center of the loading plate and lesser deformation at the distant geophone locations, compared with other tested sections of the same pavement structure, then there is a strong possibility of delamination of the pavement layers.

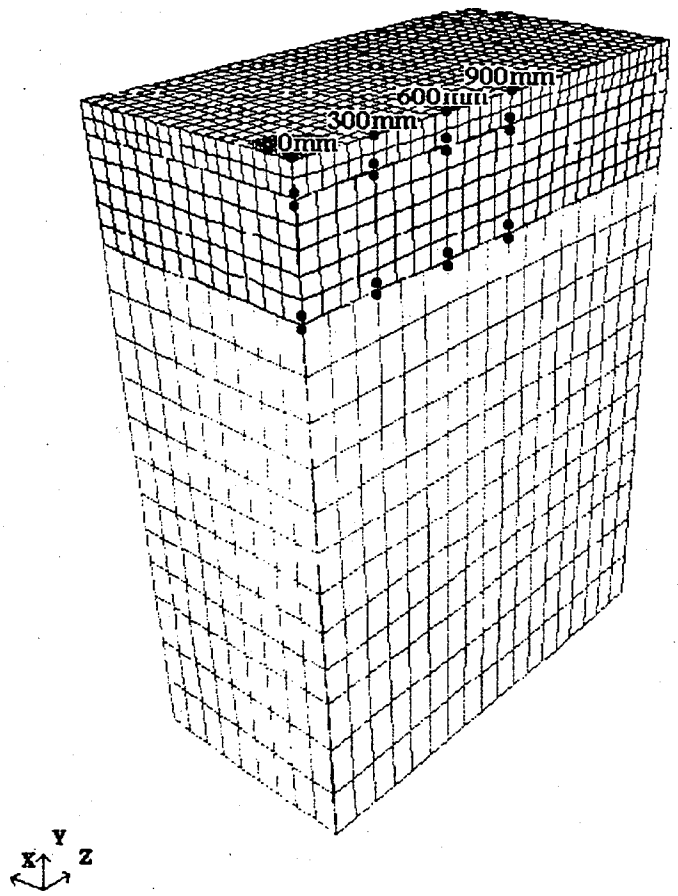

FIGURE 4.1 Positions of the points selected for recording the displacement time-histories.

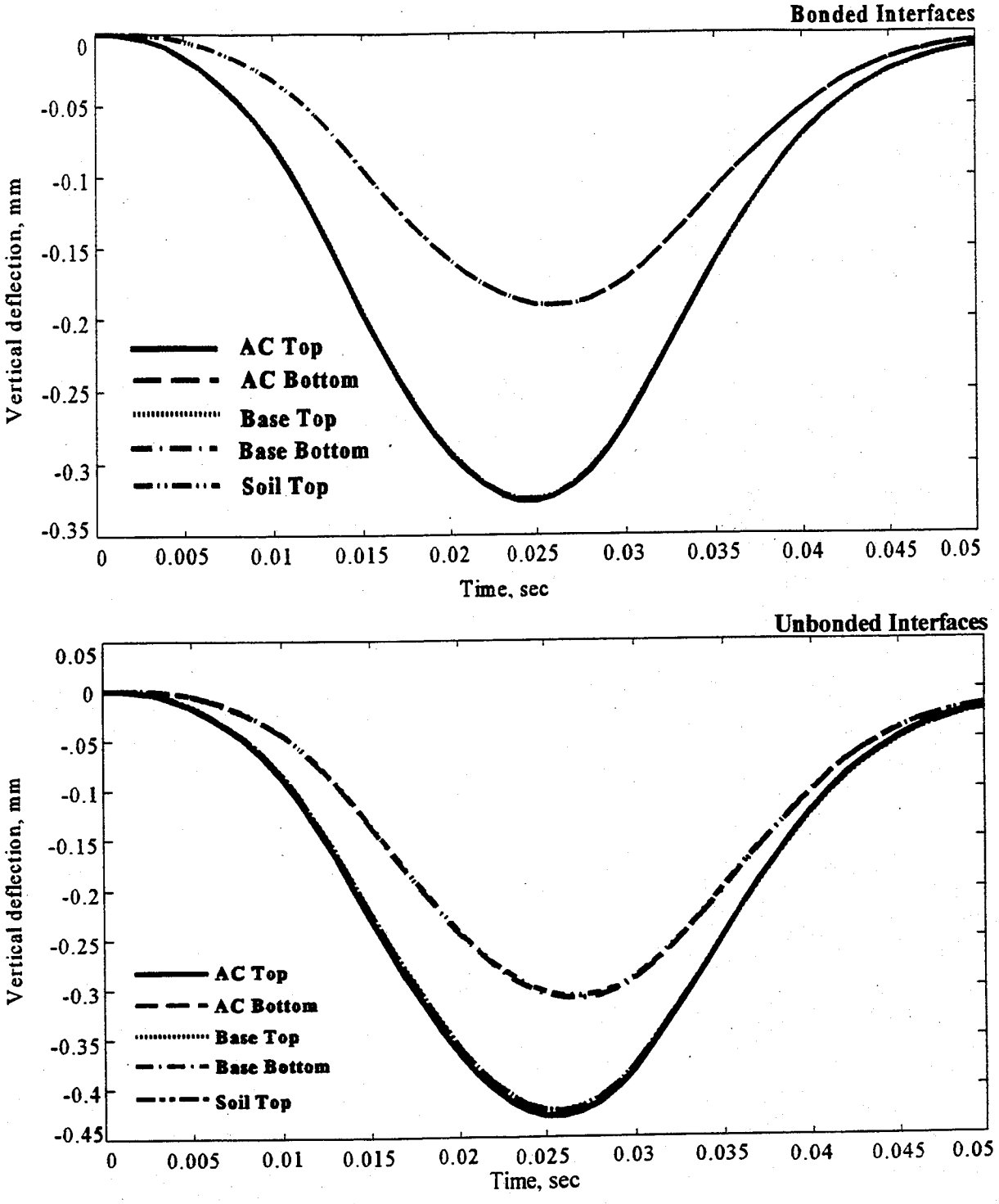

FIGURE 4.2 Deflection vs. time curves for flexible pavement models at 0 mm offset.

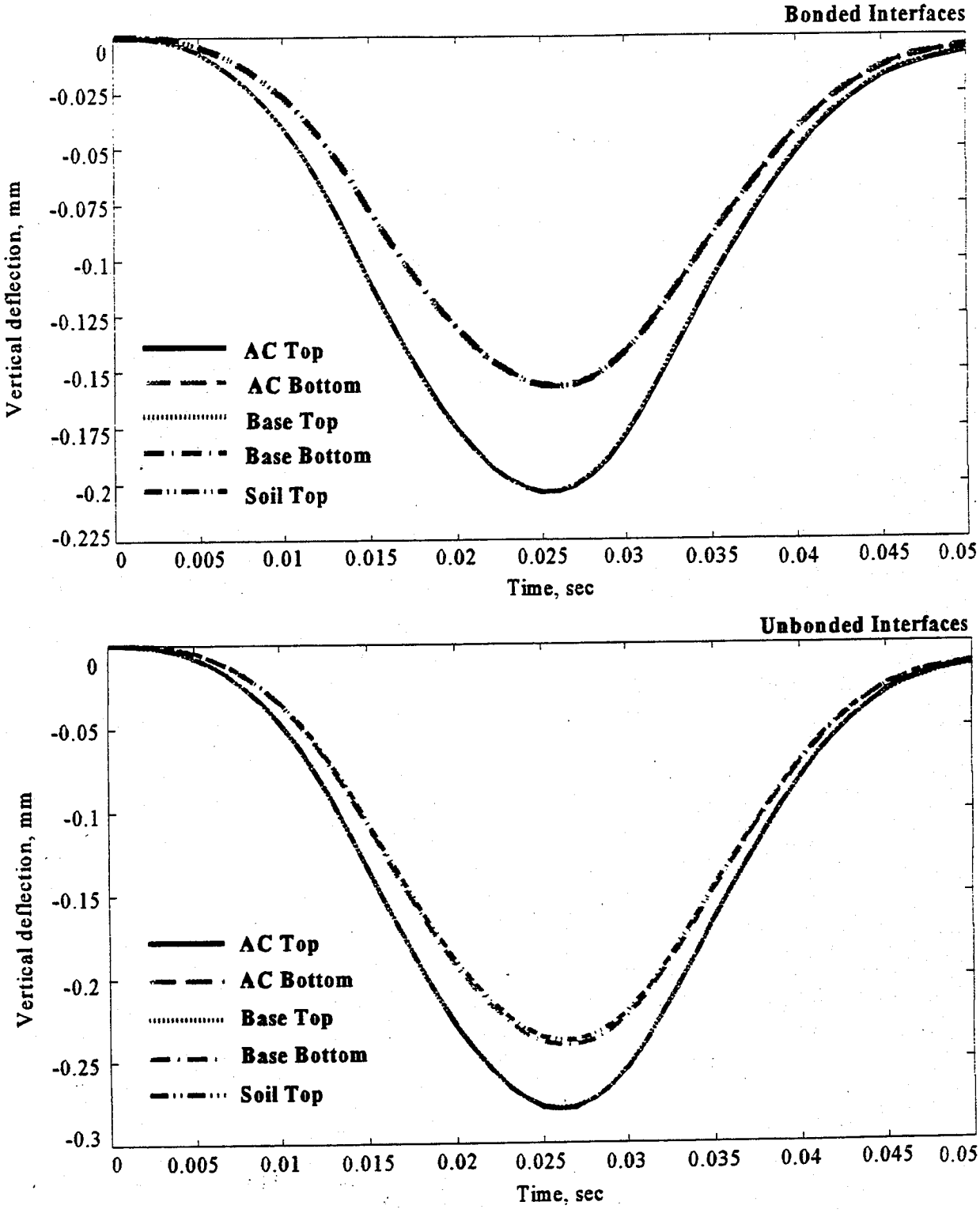

FIGURE 4.3 Delection vs. time curves for flexible pavement models at 300 mm offset.

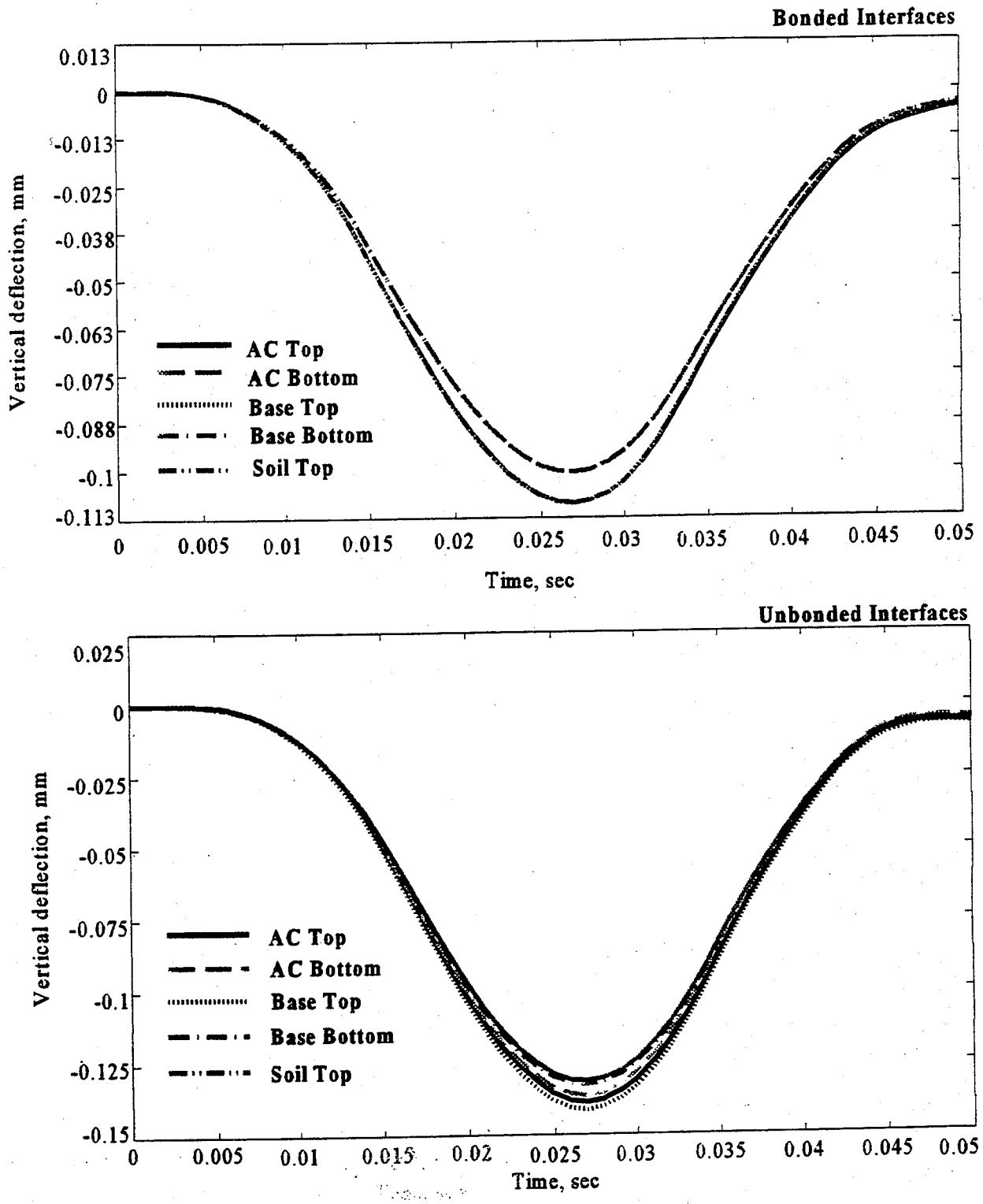

FIGURE 4.4 Deflection vs. time curves for flexible pavement models at 600 mm offset.

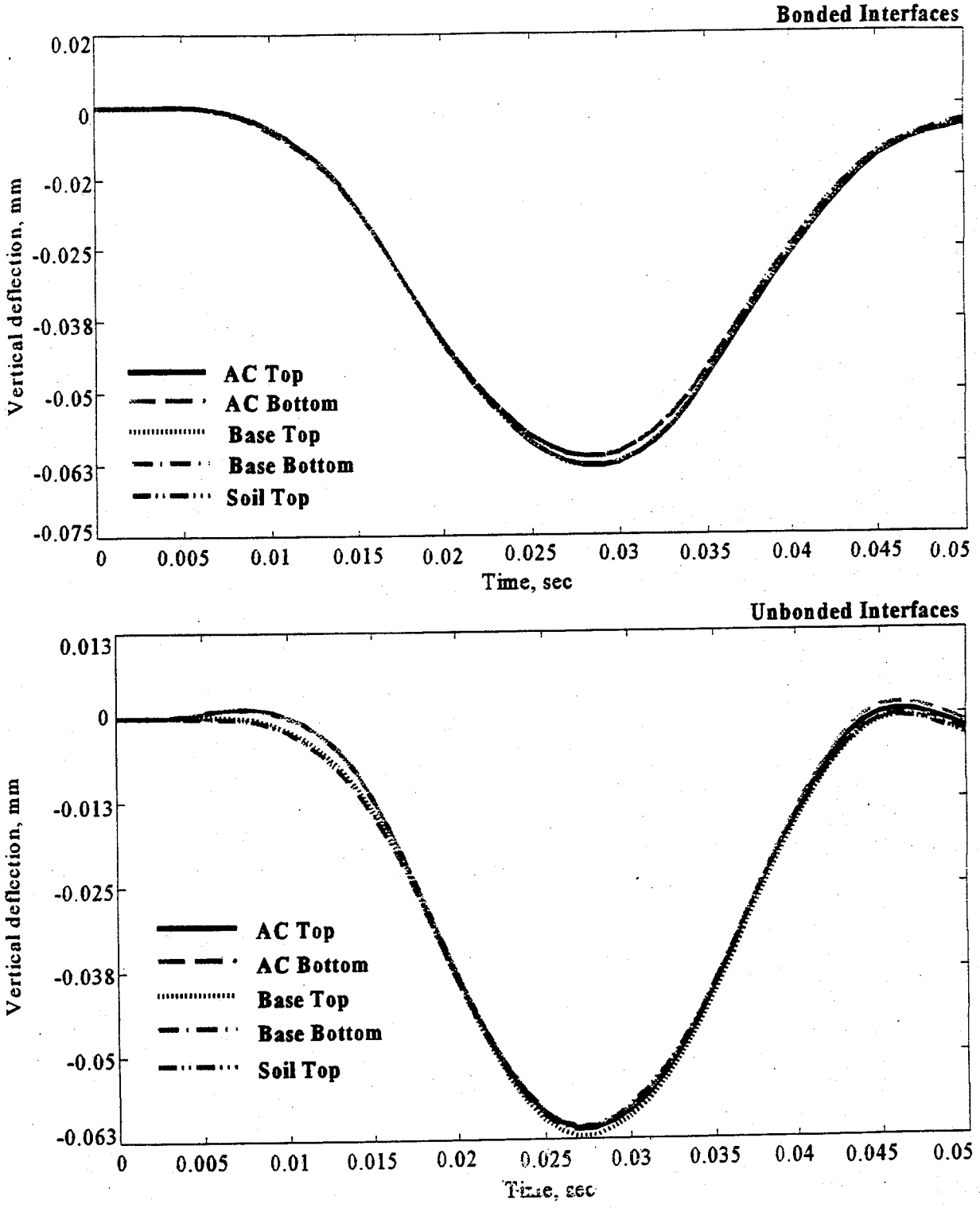

FIGURE 4.5 Deflection vs. time curves for flexible pavement models at 900 mm offset.

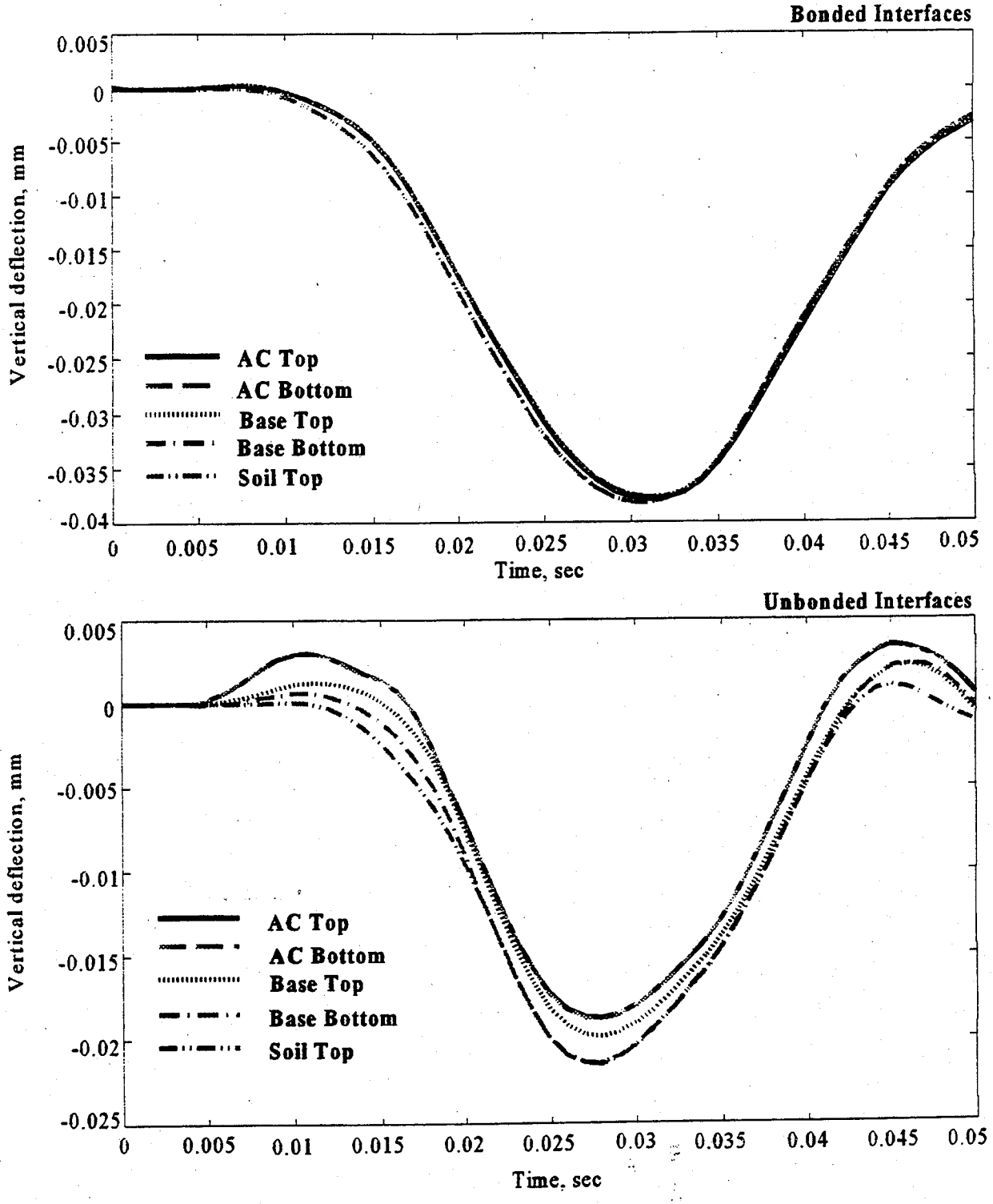

FIGURE 4.6 Deflection vs. time curves for flexible pavement models at 1200 mm offset.

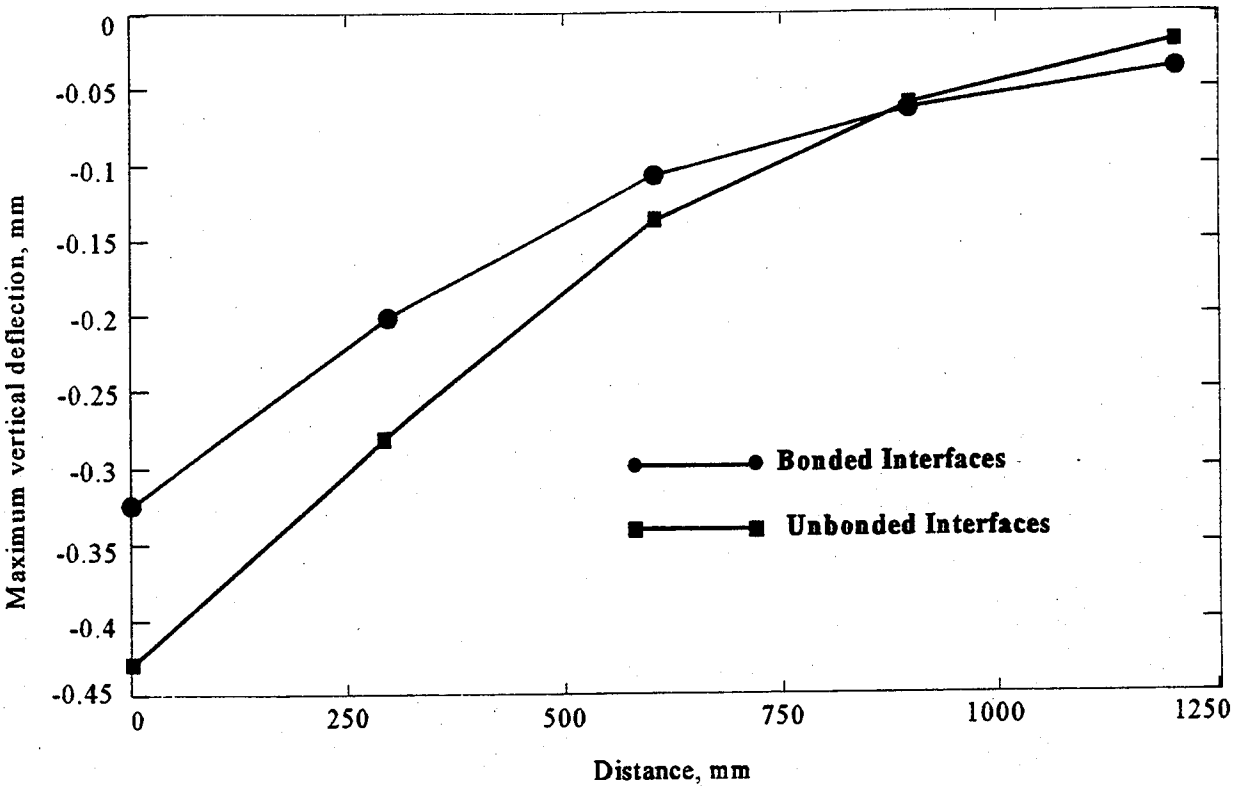

FIGURE 4.7 **Deflection basins for the flexible pavement models with bonded and unbonded interfaces.**

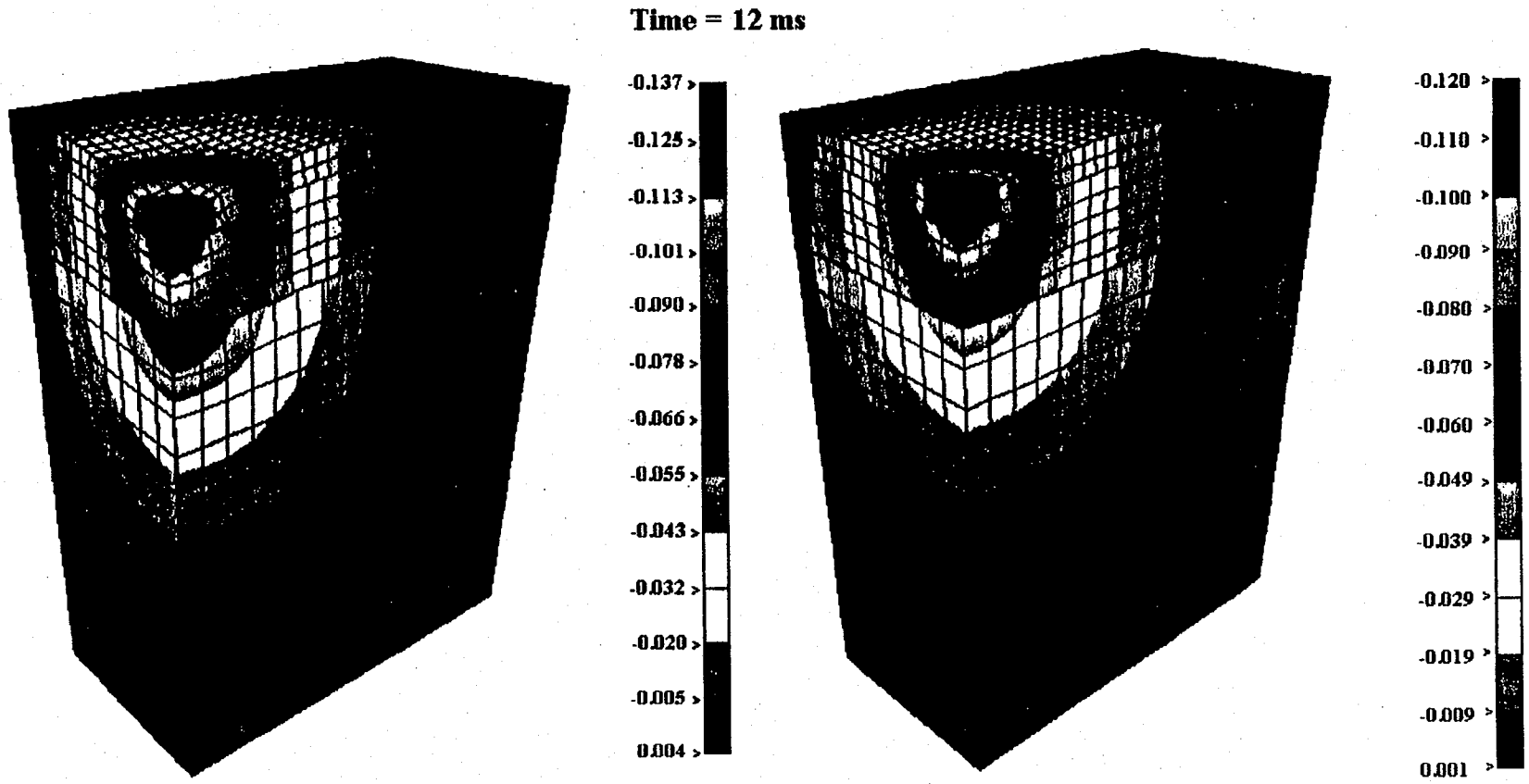

FIGURE 4.8 **Fringes of vertical deformation in flexible pavement in mm. (a) unbonded interfaces, (b) bonded interfaces.**

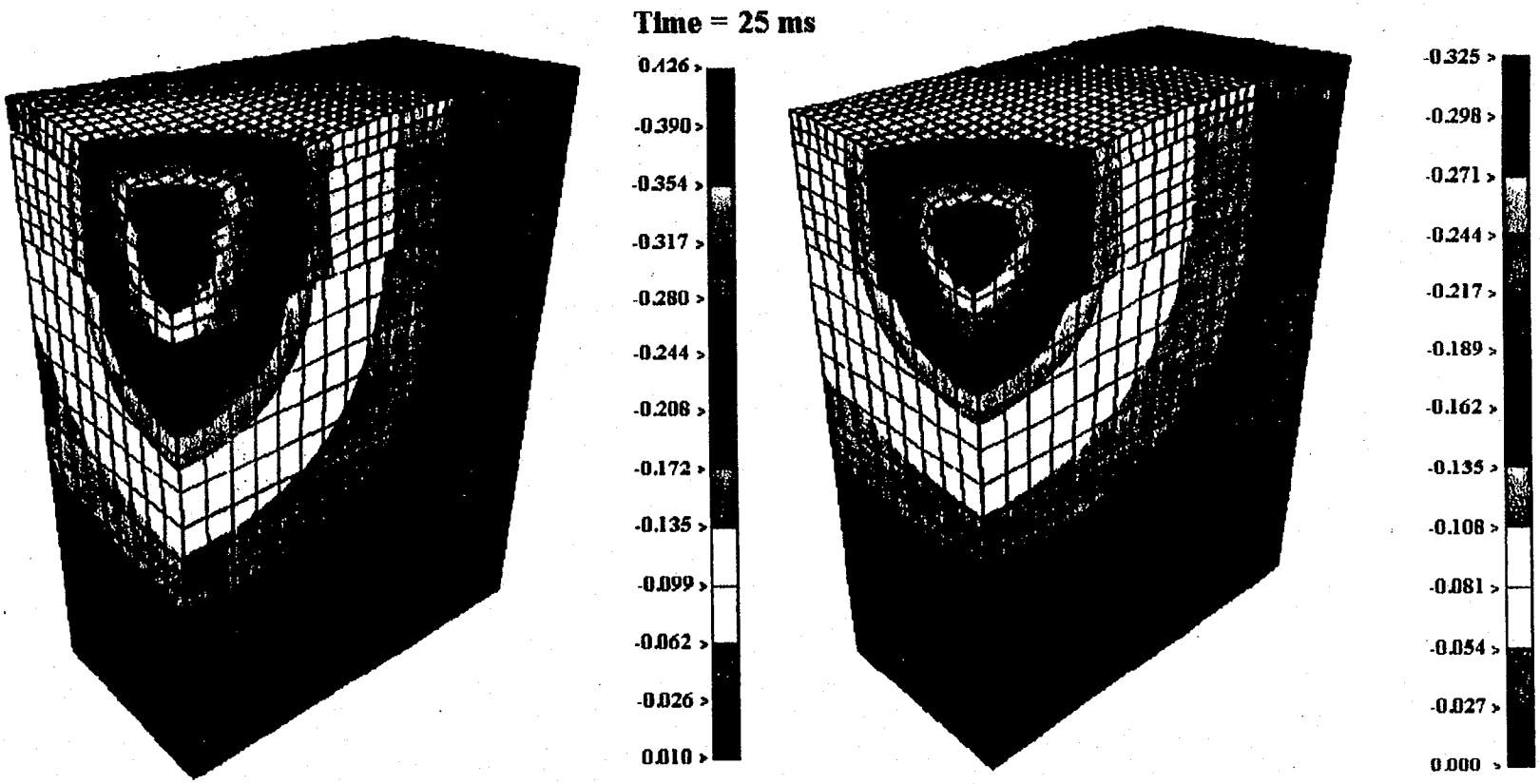

FIGURE 4.9 Fringes of vertical deformation in flexible pavement in mm. (a) unbonded interfaces, (b) bonded interfaces.

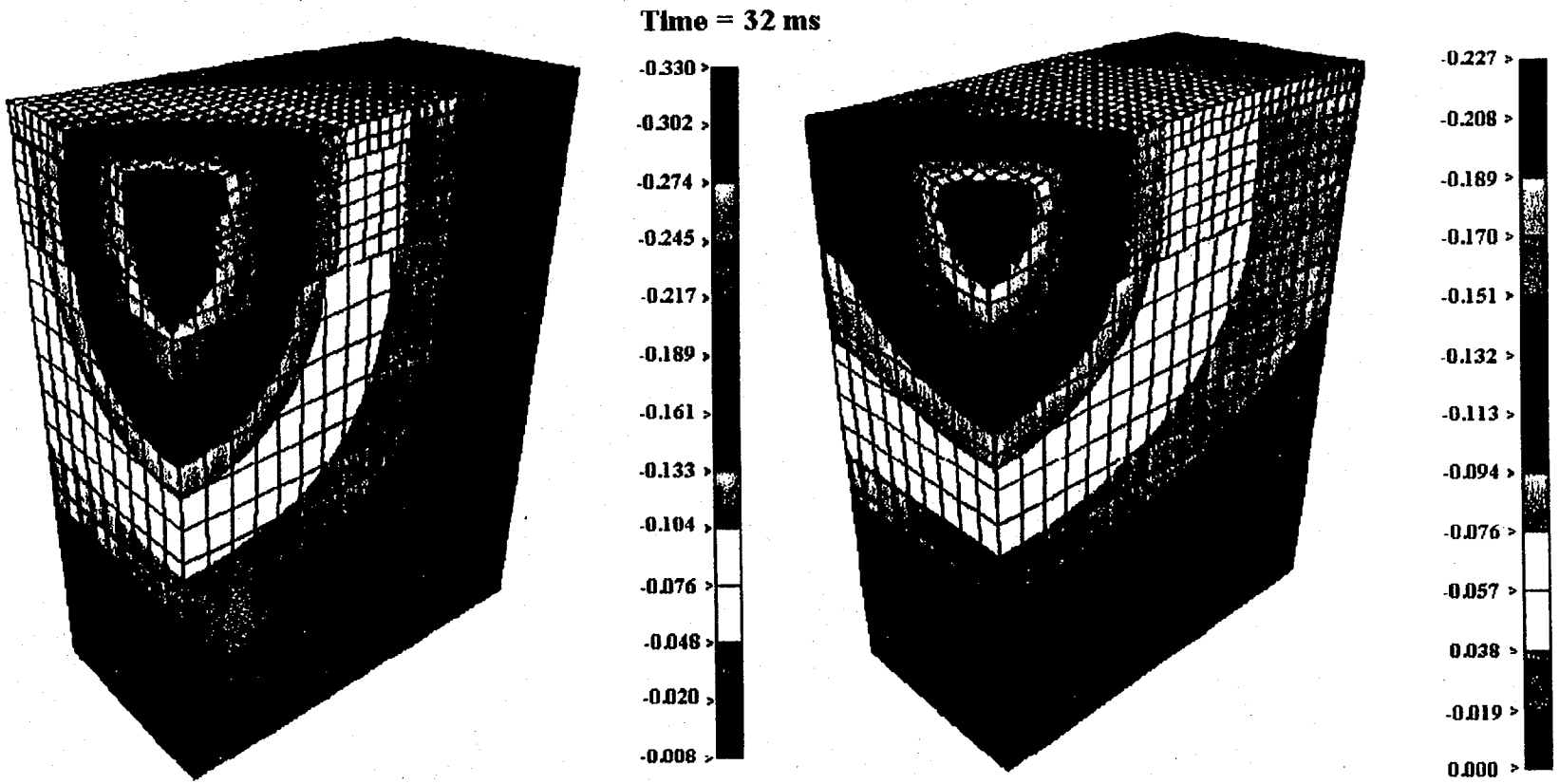

FIGURE 4.10 Fringes of vertical deformation in flexible pavement in mm.

(a) unbonded interfaces, (b) bonded interfaces.

CHAPTER 5

THEORETICAL ANALYSIS OF COMPOSITE PAVEMENTS UNDER FWD LOAD[1]

5.1. INTRODUCTION

This chapter focuses on developing an understanding of the dynamic behavior of a rigid pavements with a straight asphalt-concrete overlay when subjected to impact loads. Figure 5.1 shows a section of the pavement used in this investigation. Pavement layer properties are given in Table 2.1. While the impact load used in this paper is typical of that encountered in FWD test, the observations reached may be valid when the loads are imposed by truck tires moving on a rough pavement surface (assuming the applicability of the principal of superposition and that the pavement materials are elastic which is a common assumption in pavement design).

The finite element model of the composite pavement with the proper boundary conditions and a loading plate similar to the one used in the FWD tests was modeled, as shown in Figure 5.2. An impact pressure-time curve was obtained from a study by J. Mallela, et al. *(47)*, was digitized over increments of 1 millisecond, and used in the analysis. The impact pressure was assumed to be evenly distributed over the top plate surface. The pressure-time relation is shown in Figure 5.3. The integration time step chosen for the analysis was 1 milliseconds for a total time duration of 100 milliseconds. The dynamic analysis was carried out for the composite pavement model twice for the cases of fully bonded and fully unbonded interfaces.

1 Part of the material presented in this chapter was accepted for publication in the Transportation Research Board for 1997

5.2. VERTICAL DEFORMATION VERSUS TIME

Records of dynamic deflection change with time were obtained at seven vertical sections. Each section contains seven vertically aligned points, as shown in Figure 5.4. The positions of surface points were chosen to coincide with seven geophone positions typically used in an FWD test, at offsets of 0(0"), 300(12"), 600(24"), 900(36"), and 1200(48") millimeters from the center of the loading plate. Figures 5.5 to 5.9 show the deflection versus time plots obtained for two cases of the same composite pavement. Top graphs show results for the model with fully bonded interfaces and bottom graphs for the model with unbonded interfaces. Each individual graph contains seven curves for the points located on the top and bottom of each layer.

The Figure 5.5 to 5.9 show time shifts in maximum response of different layers that can be attributed to the dynamic behavior of the material. Therefore, the maximum surface deflection recorded by a geophone during an FWD test does not necessarily correspond to the maximum dynamic displacements of underlying layers. The existence of these time shifts may lead to errors in estimation of the pavement moduli profile based on the Falling Weight Deflectometer (FWD) test results. Most of the existing backcalculation algorithms use the maximum deflection records at several surface points to backcalculate the moduli profile of the pavement. This calculation approach is valid for statically applied loads. Since the FWD load is an impact load, pavement layers respond in a different manner due to inertia effects and the stress wave propagation phenomenon. Maximum surface deflection data may be insufficient for the evaluation of the pavement layer moduli.

In Figure 5.5, both bonded and unbonded pavement models show that the shift in time between the maximum deformation of the top of the asphalt or concrete layer and the maximum deformation of the top of the gravel layer is negligible. On the other hand, the time shift between the maximum deformation of the top of the gravel layer and maximum deformation of the top of the soil layer is very well defined. The reason for that is the difference in the speeds of stress wave propagation through different materials and the layer thicknesses. The speed of stress waves propagation is dependent on the elastic properties of the material. For example, for the primary

compression wave this relation will be in the form:

$$E=(koef)v_p^2$$

where

$$koef=\frac{(1+\mu)(1-2\mu)\rho}{(1-\mu)}$$

μ -- Poisson's ratio;

ρ -- material density;

v_p-- velocity of a primary compression wave;

E -- Young's modulus.

The above relations show that the speed of the compression wave is proportional to the square root of the Young's modulus of the material. For the material with a higher modulus of elasticity, a stress wave propagates through the layer and reaches the next layer faster than for the material with a lower modulus. Table 2.1 shows that the moduli of elasticity of concrete and asphalt layers are respectively 133 and 13.3 times higher than that of the gravel layer. Therefore, gravel acts as a buffer that delays the arrival of the compressive stress wave to the top of the soil layer.

One of the objectives of the current investigation is to study the effect of a bond between layers on pavement response to impact. In practice, rigid pavements are constructed by overlaying a highly compacted gravel layer over soil and then overlaying concrete over gravel. Later this pavement can be overlaid by several AC layers forming a composite pavement structure. Due to the differences in the layers compressibility and material inertia, the layers interfaces experience tensile stresses with each vehicle pass. These tensile stresses are responsible for weakening the bond between layers. As a result of a broken bond, pavement layers may vibrate under dynamic loading in a way that resembles plate vibrations. This kind of pavement can be represented as a series of thick

plates resting on a solid elastic media.

Deflection versus time graphs for the bonded model show that all pavement layers have a similar pattern of deformation, as shown in Figures 5.5 to 5.9. Therefore, the pattern of surface deformation of the composite pavement with fully bonded interfaces represents well the pattern of deformation of each layer in the structure.

In the pavement with unbonded interfaces, the pattern of vertical deformation of the delaminated AC overlay starts to deviate from the deformation of the rest of the structure starting from the 600 mm (24") offset from the center of the loading plate. The pattern of deformation of the structure below the overlay is governed by the deformation of the most rigid concrete layer. The AC layer experiences a plate vibration motion on the top of the vibrating concrete layer. During vibration the two layers separate and then come back together. At such instances, the recorded surface deformations become uncorrelated to the deformation of subsequent layers as shown in Figures 5.7 to 5.9. Another interesting observation of the model behavior starts from the offset of 900 mm (36") where the AC layer experiences an initial upheaval that is absent in the case of bonded interfaces.

5.3. EFFECT OF LAYERS BONDING ON DEFLECTION BASIN

Deflection basins constructed for two cases of the composite pavement show a 30 percent maximum absolute difference in the results. Figure 5.10 shows that the model with unbonded interfaces has higher deformation under the center of the loading plate and lower at the distant geophone locations as compared to the model with bonded interfaces. Therefore, steep deflection basins obtained from the tests of the composite pavements may indicate a loss of bond between layers.

5.4. DYNAMIC DISPLACEMENT DISTRIBUTIONS

Figure 5.11 shows the propagation of vertical displacements captured at several instances of time. A vertical transverse cut through the center of the loading plate makes visible the deflection propagation through the different pavement layers. The deformation results shown in Figure 5.11 indicate that pavement response to FWD load is highly affected by the type of bond between layers. A pavement structure with bonded interfaces deforms as a three-dimensional solid composed of several layers with varying stiffness. The deformation field has a spherical bowl form that propagates away from the center of load application.

For unbonded interfaces, shown in Figures 5.11a, b, and c, the deformation of an asphalt-concrete overlay is a combination of a solid material response with the vibration of a plate on an elastic foundation. Upon the load application, the asphalt-concrete layer experiences compression against the stiffer layer of concrete. The asphalt-concrete material squeezed between the loading plate and the concrete surface attempts to relieve its compressive stress by trying to flow away radially from the loading plate region. This results in a material upheaval around the loading plate. In the case of the unbonded Asphalt-concrete/Concrete interface, the asphalt-concrete layer rises against its own weight outside the loading plate. This leads to the formation of the annulus of void observed in Figures 5.11a and b and a subsequent plate vibration behavior. The void is temporal in nature and closes with time.

If the Asphalt-concrete/Concrete interface has a strong bond that does not fail, the upheaval forces in the asphalt-concrete layer outside the loading plate try to push the free surface upward causing an additional tensile stress at the interface and through the thickness of the asphalt-concrete layer. Similar additional tensile stresses are likely to be observed under the repeated traffic load leading to the bond failure due to fatigue.

Figures 5.11c and 5.11f demonstrate that, regardless of the bond between layers, both models show a reflection of the displacement from the bottom of the subgrade resting on a stiff bedrock. This behavior can be observed at the time of 24 msec from the beginning of the load application.

Peaks of the surface deflections have occurred before this instance of time at all the geophone locations, as can be seeing in the Figures 5.5 to 5.9. Therefore, maximum surface deflections in the discussed models are not affected by the reflective waves. However, in the practical use of an FWD test on shallow pavement section, deflection records may not reveal a true story due to reflective wave interference.

5.5. CONCLUSIONS

The results presented in this chapter led to the conclusion that a FWD test may result in incorrect evaluation of the overlaid pavements that suffered delamination or, in general, pavements whose layer interfaces have deteriorated. In this case, the only way to estimate pavement moduli would be to lower the applied dynamic load to a small level that would not cause any separation at the interfaces. This may be achieved by using a stress wave propagation technique such as spectral analysis of surface waves, if the interfaces are free of voids.

The model with unbonded interfaces has shown more flexibility by having higher deformation under the center of the loading plate and lower at the distant geophone locations compared to the model with bonded interfaces. Therefore, steep deflection basins obtained from the tests of the composite pavements may indicate loss of bonds between layers. Delamination of the asphalt-concrete layer may be detected by observing a positive reading of the displacement sensors (FWD sensors should be DC coupled in order to observe this trend).

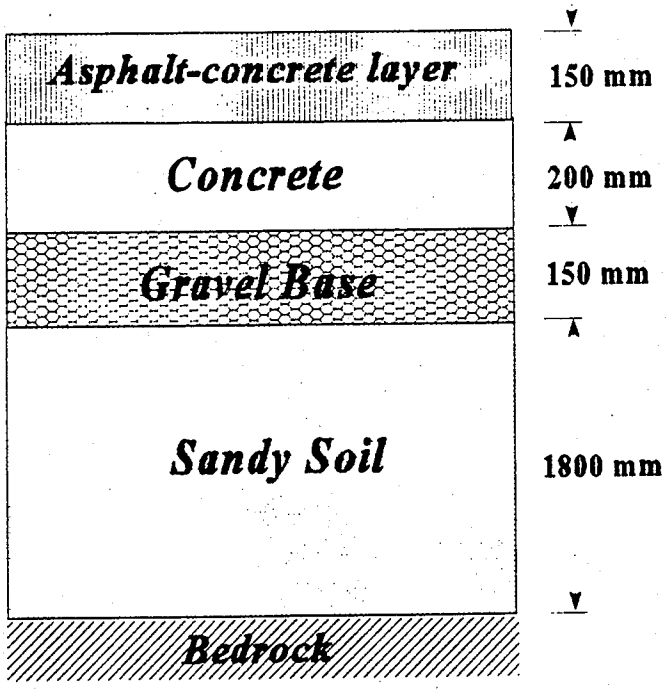

FIGURE 5.1 Composite pavement layers.
1 mm = 0.0394 in.

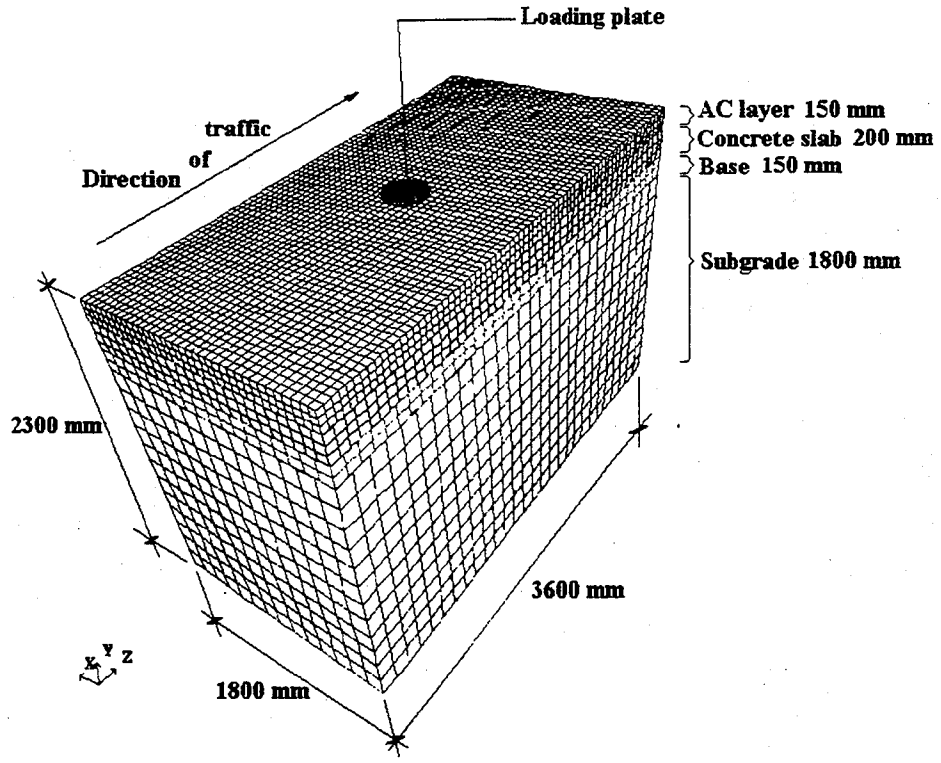

(a) Full model

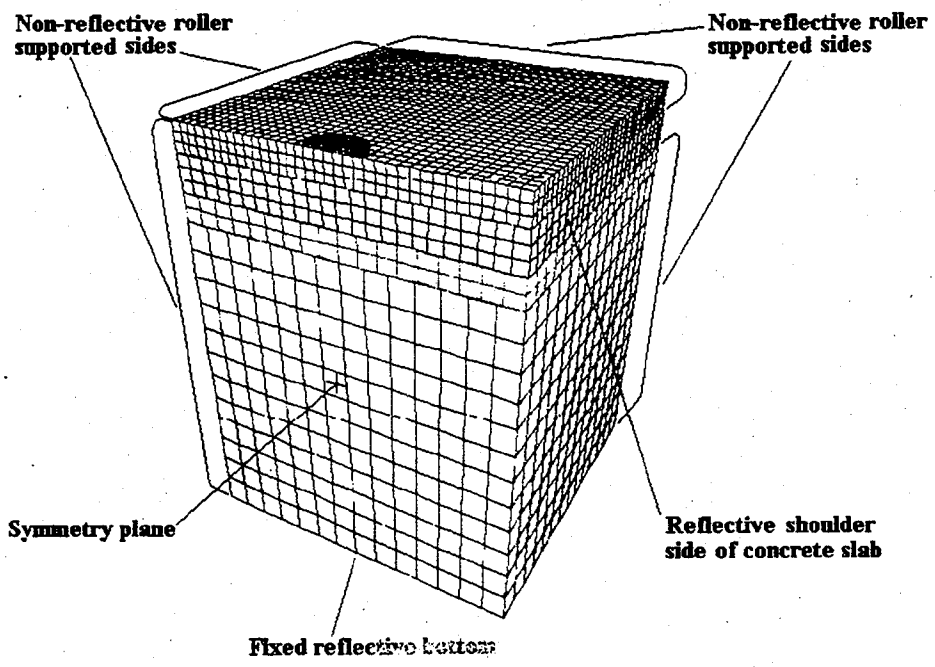

(b) Half model

FIGURE 5.2 Finite element mesh of the composite pavement.

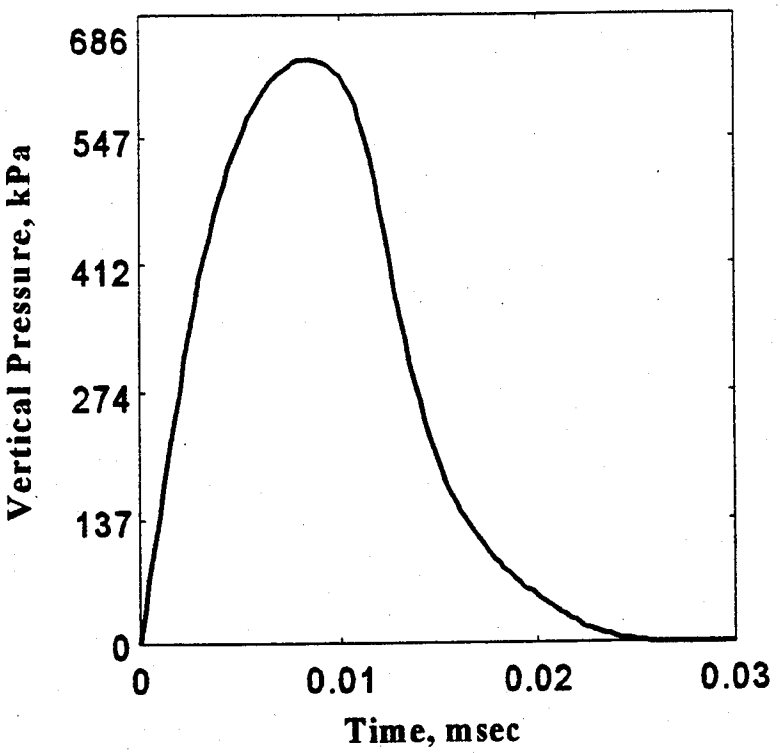

FIGURE 5.3 Loading curve used with the composite pavement model.

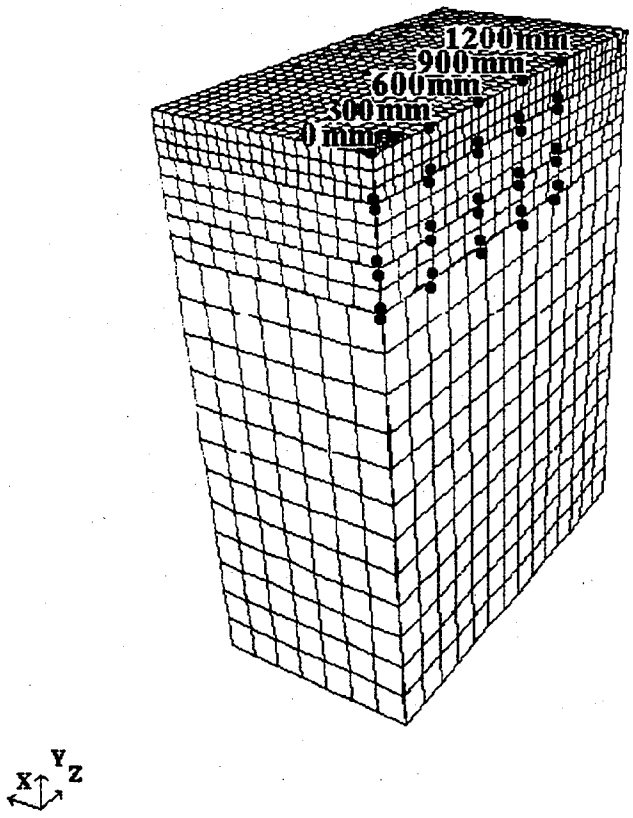

FIGURE 5.4 Positions of the points selected for recording the displacement time-histories.

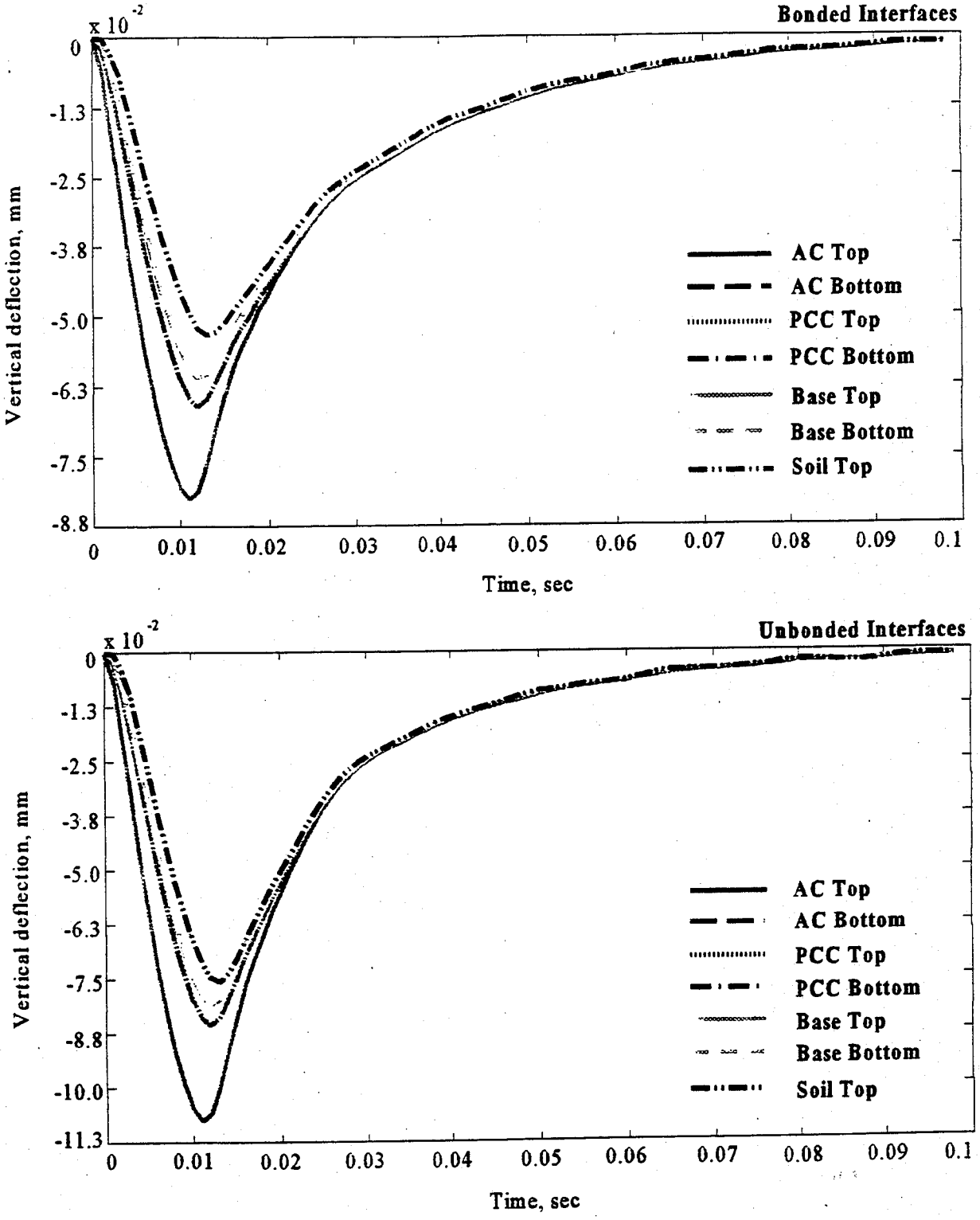

FIGURE 5.5 Deflection vs. time curves for composite pavement models at 0 mm offset.

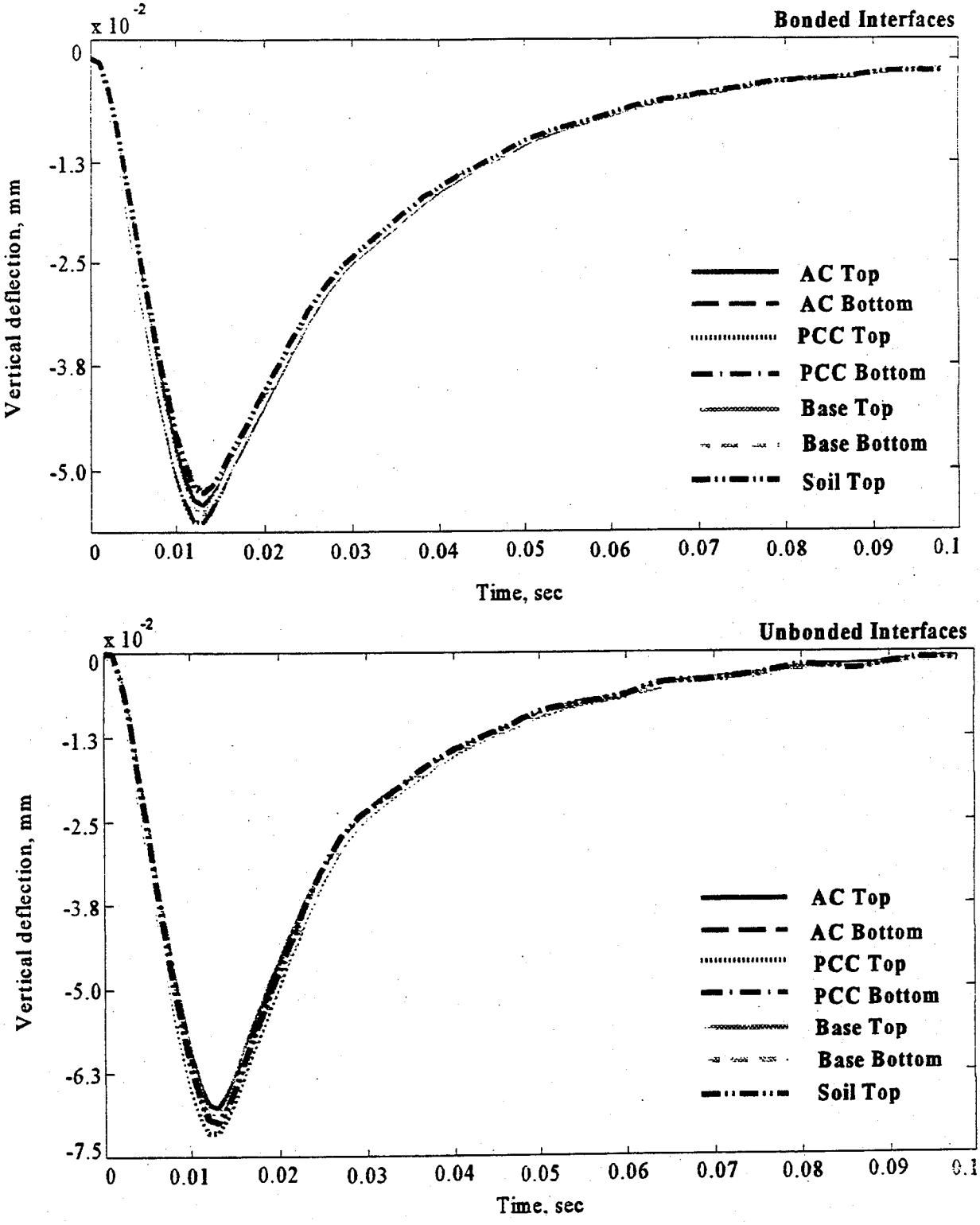

FIGURE 5.6 Deflection vs. time curves for composite pavement models at 300 mm offset.

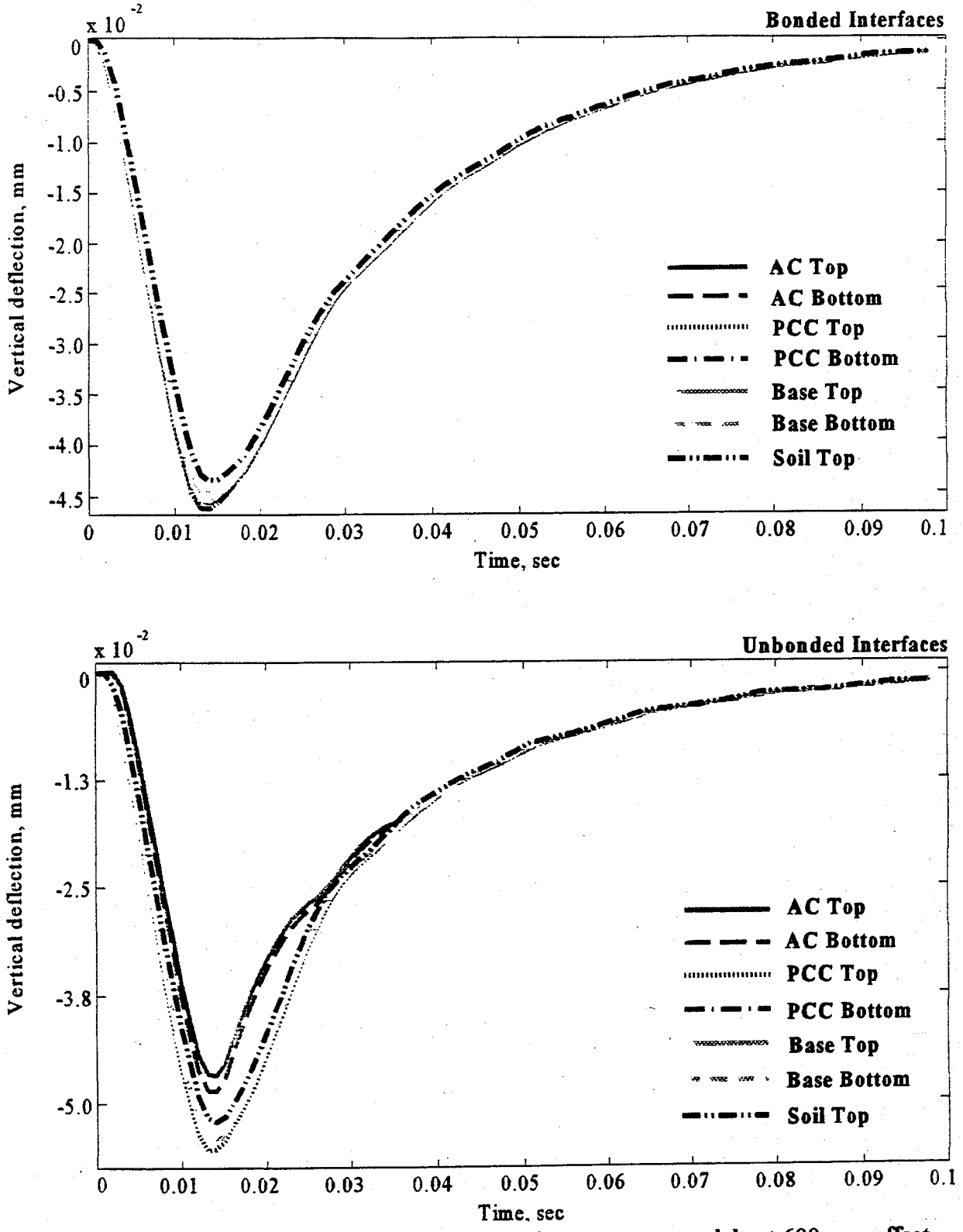

FIGURE 5.7 Deflection vs. time curves for composite pavement models at 600 mm offset.

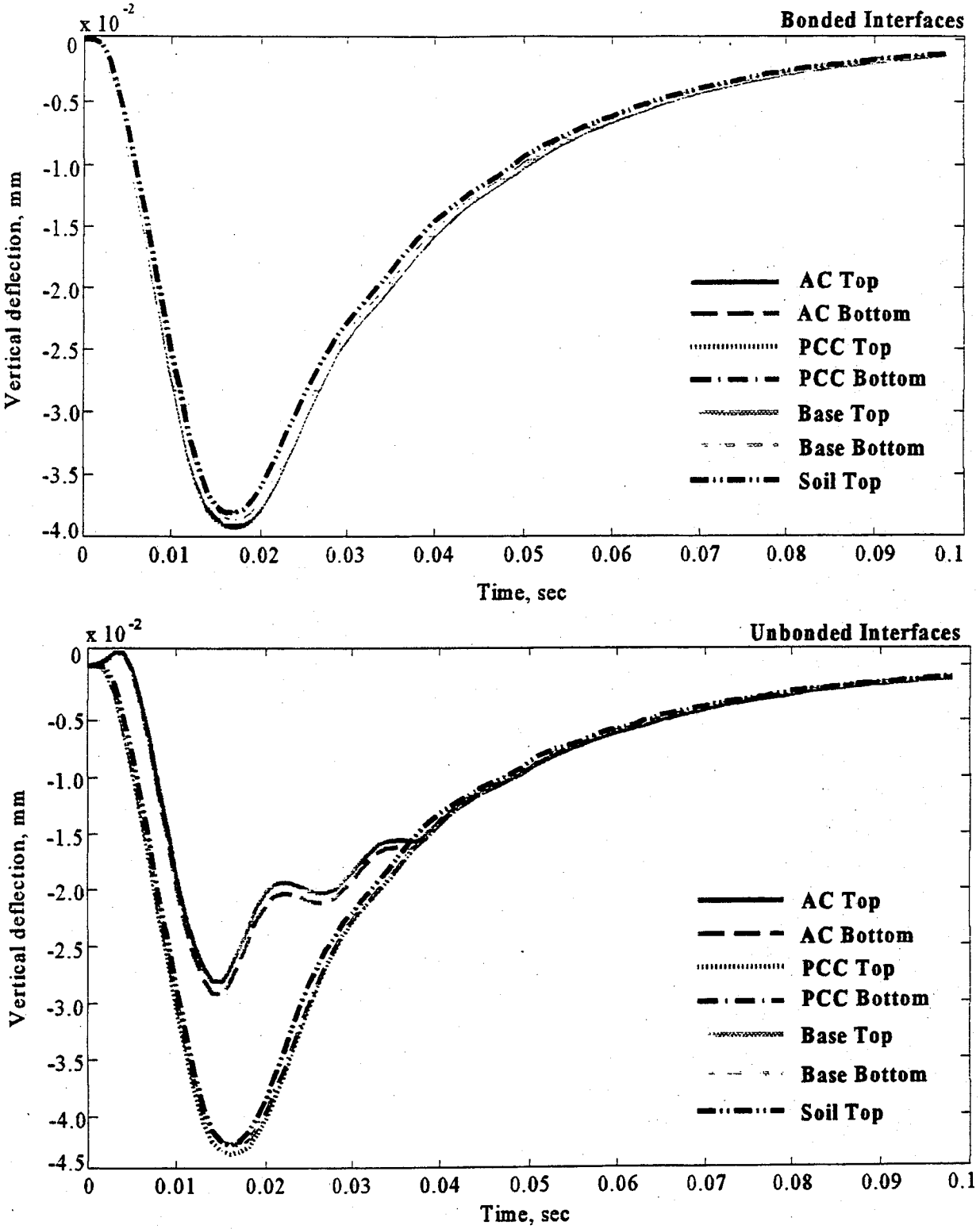

FIGURE 5.8 Deflection vs. time curves for composite pavement models at 900 mm offset.

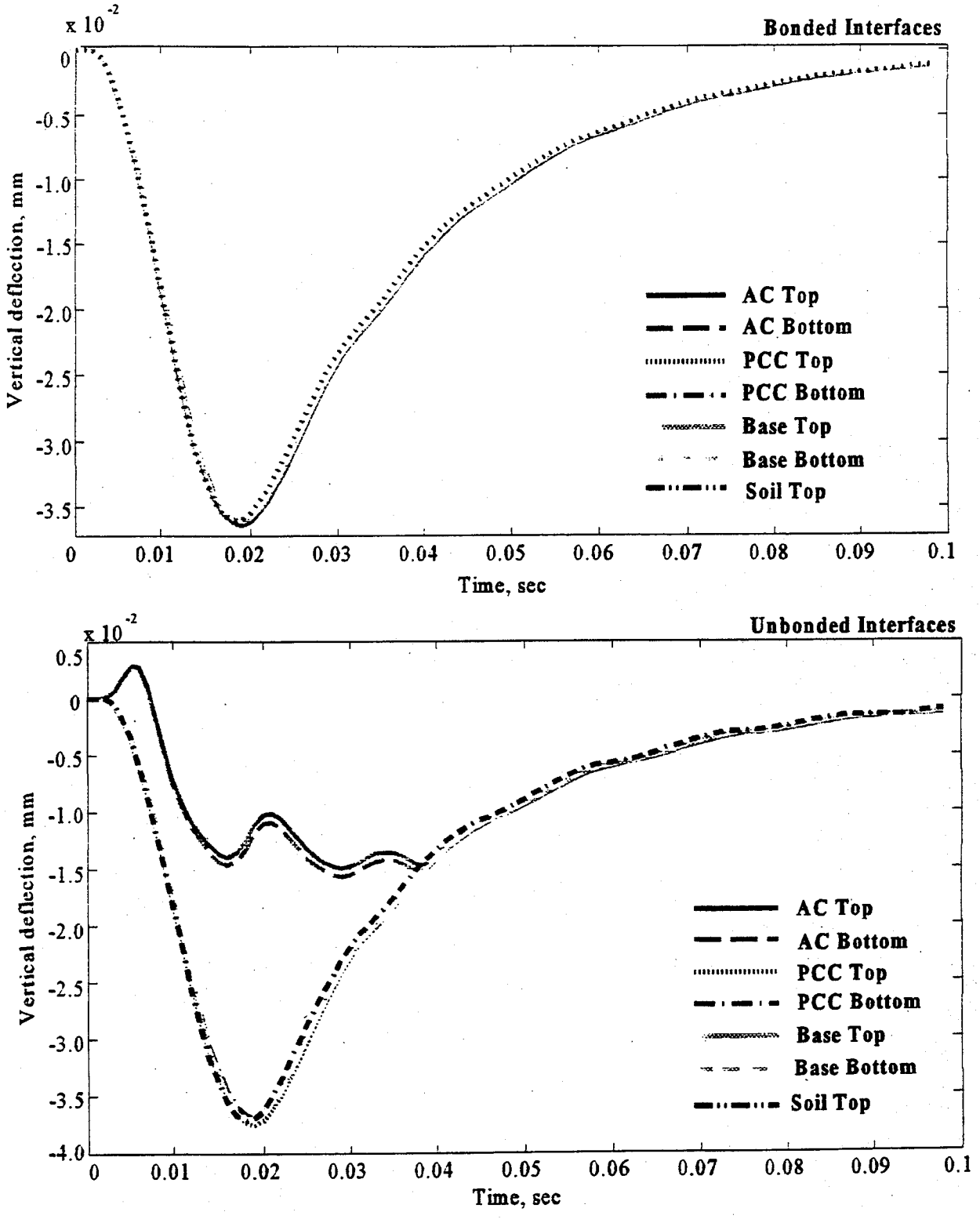

FIGUR 5.9 Deflection vs. time curves for composite pavement models at 1200 mm offset.

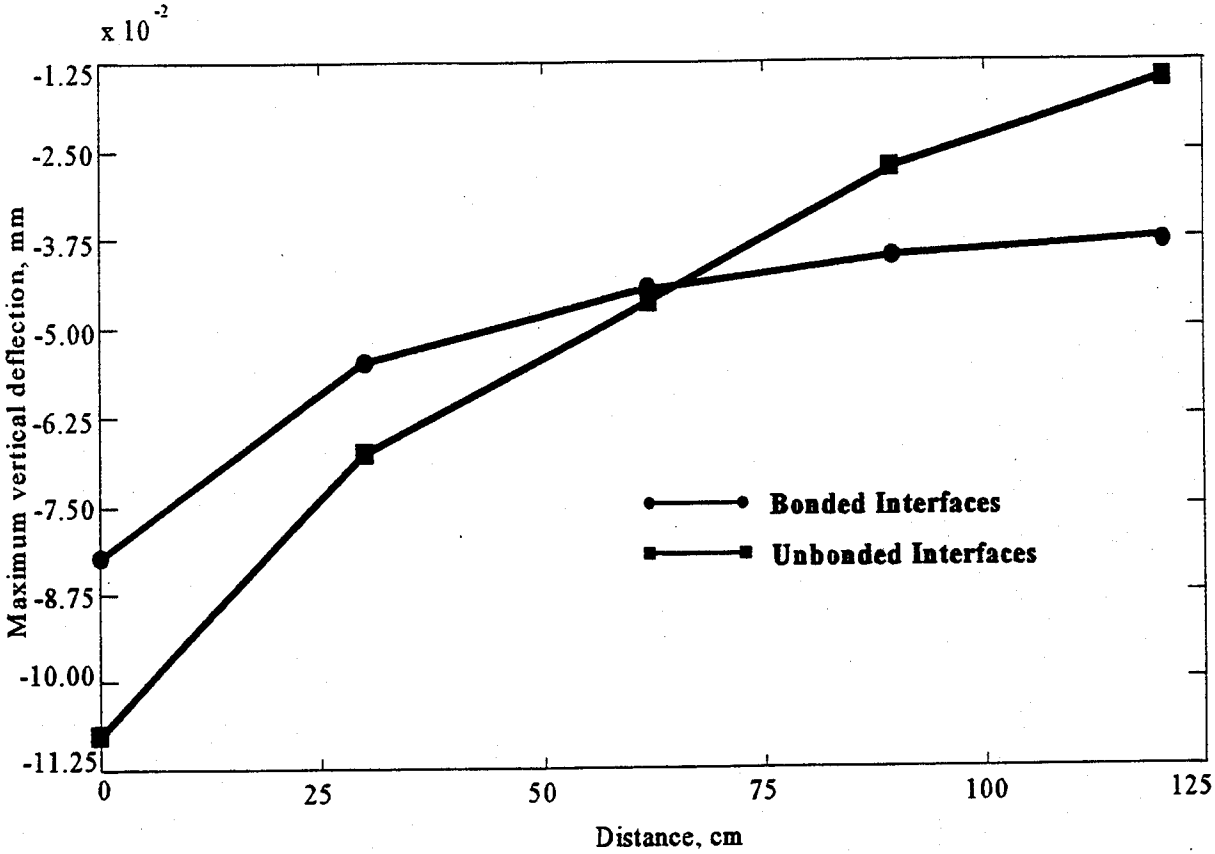

FIGURE 5.10 Deflection basins for the composite pavement models.

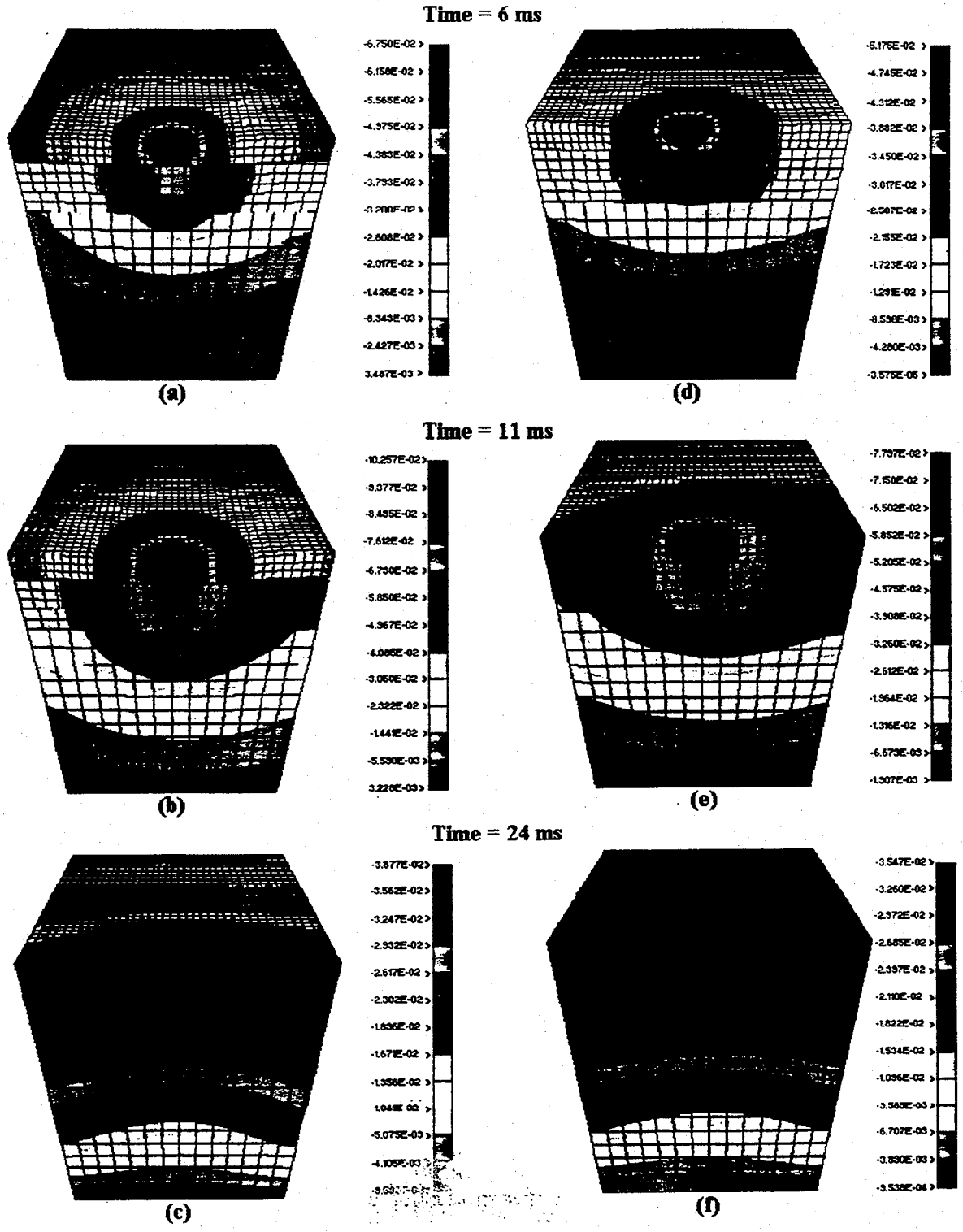

FIGURE 5.11 Fringes of vertical deformation for a composite pavement (mm)
(a - c) unbonded interfaces, (d - f) bonded interfaces.
displacement magnification factor = 600

CHAPTER 6

THEORETICAL ANALYSIS OF RIGID PAVEMENTS UNDER FWD LOAD

6.1. INTRODUCTION

To investigate the dynamics of rigid pavements under the action of FWD, the SHRP section 285803 was modeled for the two cases of fully bonded and fully unbonded interfaces. The material data and the layer thicknesses were obtained from the data published by Mallela and George *(47)*. The pavement cross section is presented in Figure 6.1. The finite element model size and boundary conditions are shown in Figure 6.2. The SHRP 285803 section consists of a concrete slab resting on a strong stabilized base layer and fairly strong subgrade. The material properties and layer thicknesses for this section are listed in Table 2.1. The impact pressure-time relation applied on the model is shown in Figure 6.3.

6.2. VERTICAL DEFORMATION VERSUS TIME

The deflection versus time graphs for the rigid pavement section with a strong stabilized base are shown in Figures 6.4 to 6.8. The patterns of deformation of all pavement layers are the same at any vertical section in the pavement along the direction of traffic. The type of bond between layers has little effect on the pattern of deformation. However, it does effect the magnitude of the response of the rigid pavement to the impact load. The unbonded pavement model shows more flexibility (higher vertical deformation) than the model with fully bonded interfaces. The behavior of the whole pavement structure is governed by the response of the most rigid top layer that is the concrete slab. The study of the vertical deflections propagation through the rigid pavement model leads to the conclusion that surface deflections represent well the deflections within the pavement layers.

A slight time delay between the response of the base top and bottom is observed in the case

of unbonded interfaces. This time delay exists only at the section through the center of the loading plate, as shown in Figure 6.4. The absence of significant time shifts in the model can be explained by similarity between the elastic properties of the slab and stabilized base layer and by the relatively small layer thicknesses.

6.3. EFFECT OF LAYERS BONDING ON DEFLECTION BASIN

The deflection basins of rigid pavements obtained from the finite element models are shown in Figure 6.9. In each case, the deflection basins were constructed using the maximum downward vertical deflections obtained from the deflection versus time records for the specified surface locations. The deflection basins for the bonded and unbonded interfaces show a 30 percent maximum absolute difference in the amount of maximum surface deflections. Deflection basin value under the center of the loading plate is significantly higher for the unbonded model. At distances away from the loading plate, the difference in the values of the deflection basins is reduced to less than 10 percent.

6.4. DYNAMIC DISPLACEMENT DISTRIBUTIONS

The deflection versus time graphs indicate that at any instance of time all pavement layers at any vertical section have the same amount of deformation. The exceptions to this rule are the deformations recorded at the vertical section through the center of the loading plate. Figure 6.10 shows the fringes of vertical deflection distribution obtained at the time of the maximum surface deformation at the zero offset position. To get a better insight on the displacement propagation, the displacement distributions are shown on the quarter of the pavement model. Case (a) represents the model with unbonded interfaces and case (b) represents the model with fully bonded interfaces. In both cases, the concrete slab deforms in a characteristic saucer shape forcing the underlying layers to follow the same pattern of deformation. The interface bond strength does not appear to affect the

form of deformation. However, it does effect the magnitude of the model response to the impact load. The maximum vertical deformations of the model with unbonded interfaces are 30 percent higher than deformations of the model with bonded interfaces.

6.5. CONCLUSIONS

The dynamic behavior of rigid pavements is governed by the deformation of the stiffest top layer. The surface deflections are well representative of the deflections through the depth of pavement structure. The maximum vertical deflection under the center of the loading plate is much higher for the unbonded model. At distances away from the loading plate, the difference in the maximum deflection values, for the two types of interface bonds, is smaller.

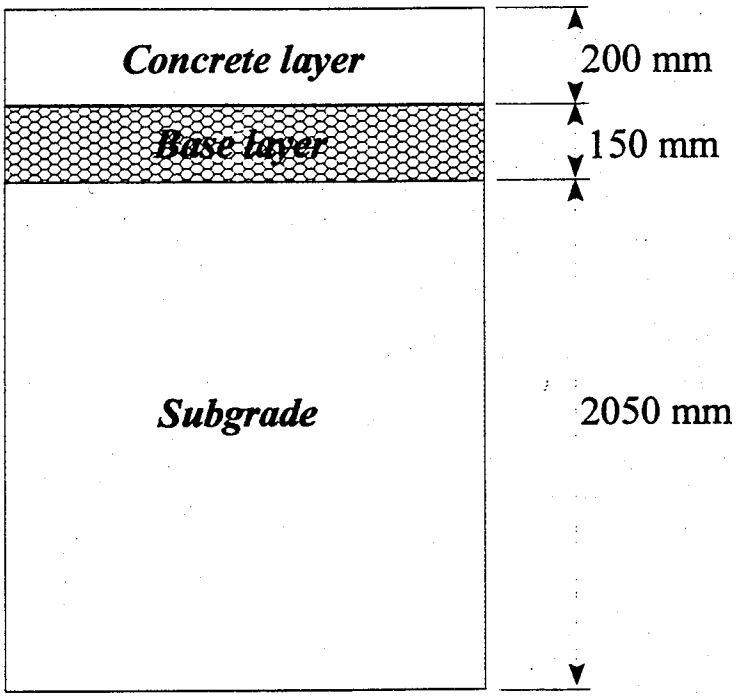

FIGURE 6.1 **Rigid pavement section used in the finite element models.**

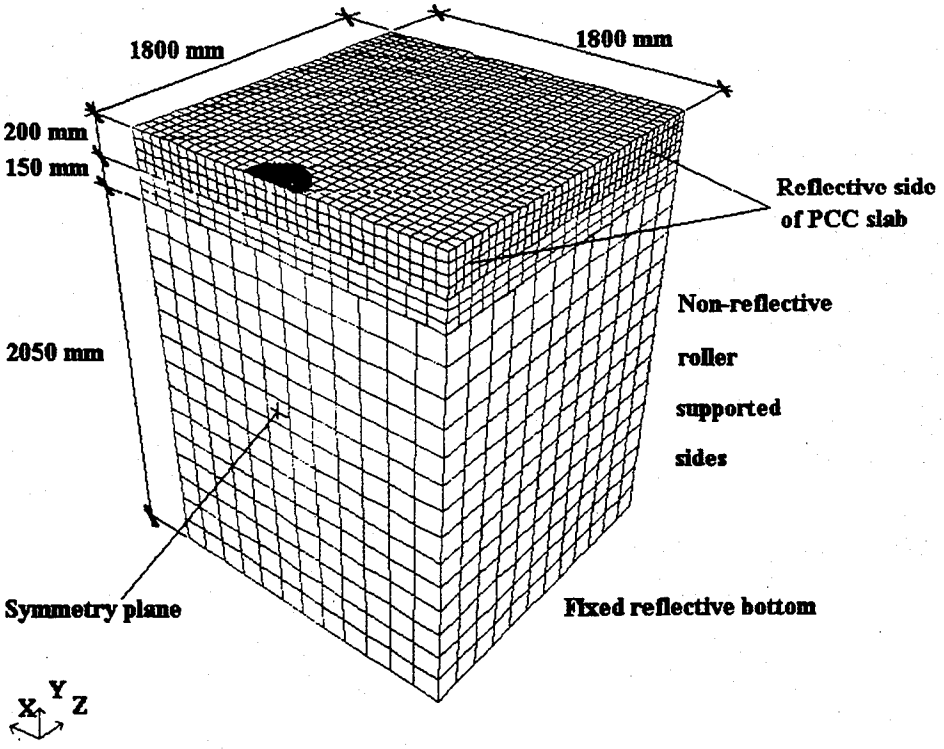

FIGURE 6.2 Finite element mesh and boundary conditions for rigid pavement model.

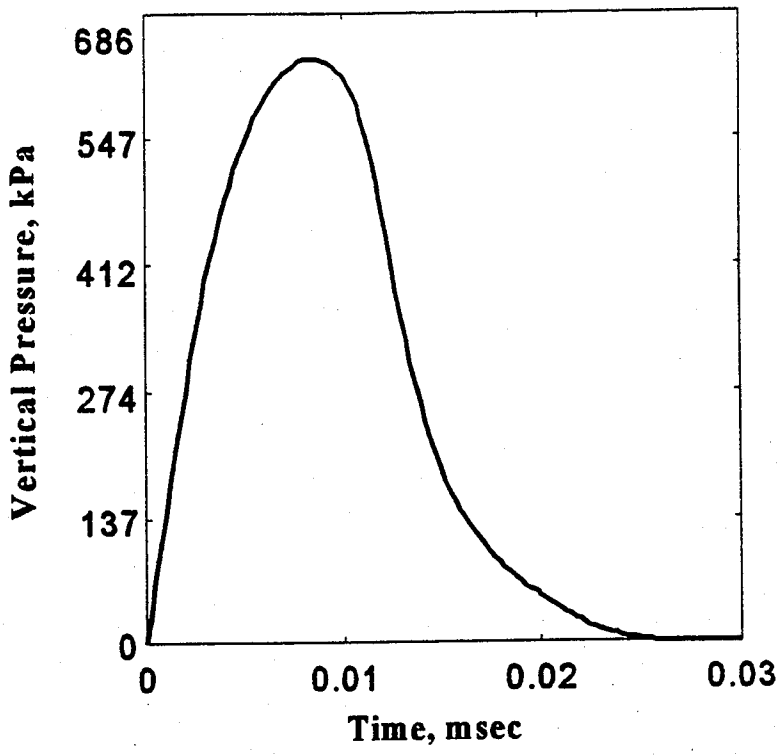

FIGURE 6.3 Loading curve used with the rigid pavement model.

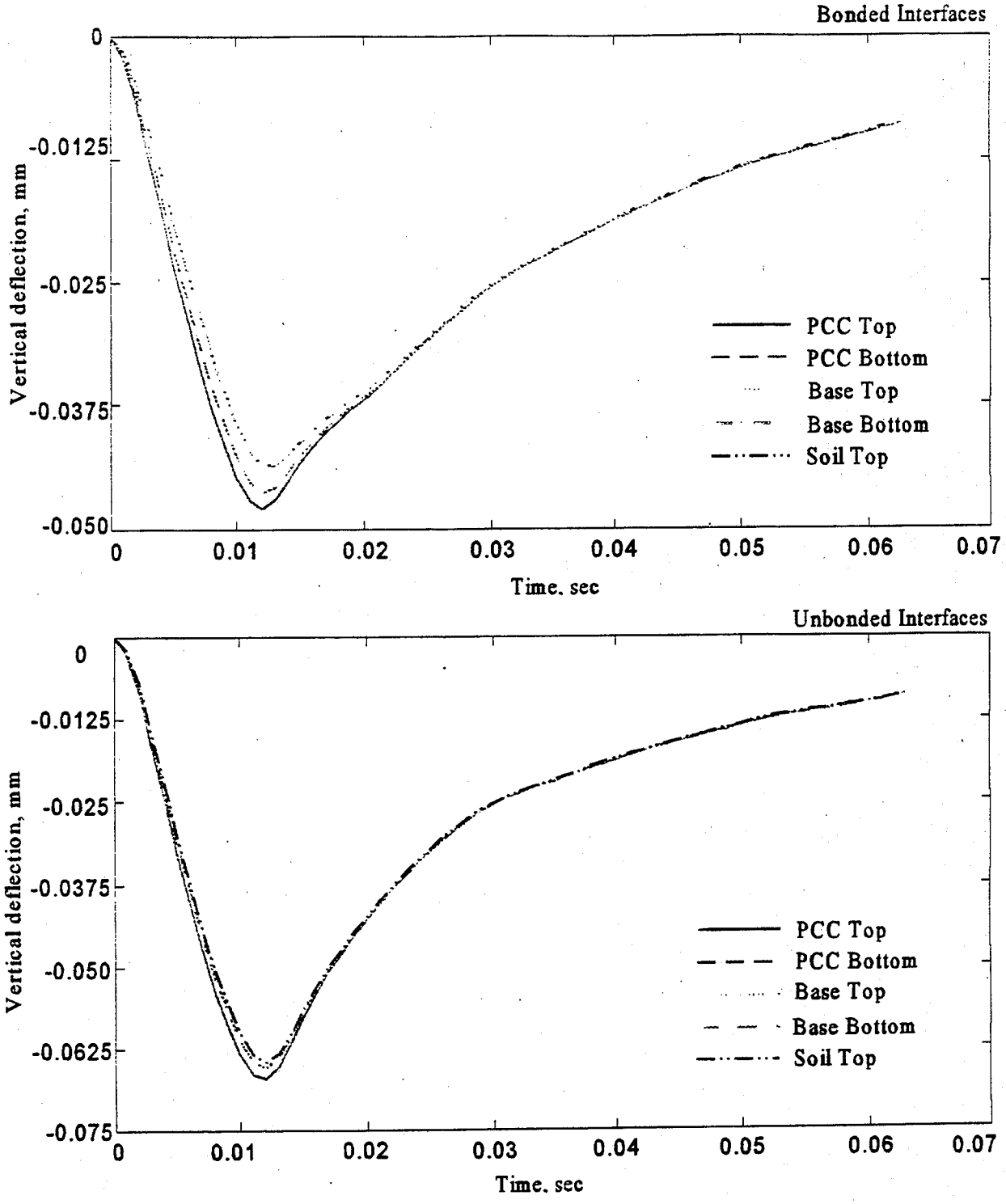

FIGURE 6.4 Deflection vs. time curves for the rigid pavement section at 0 mm offset.

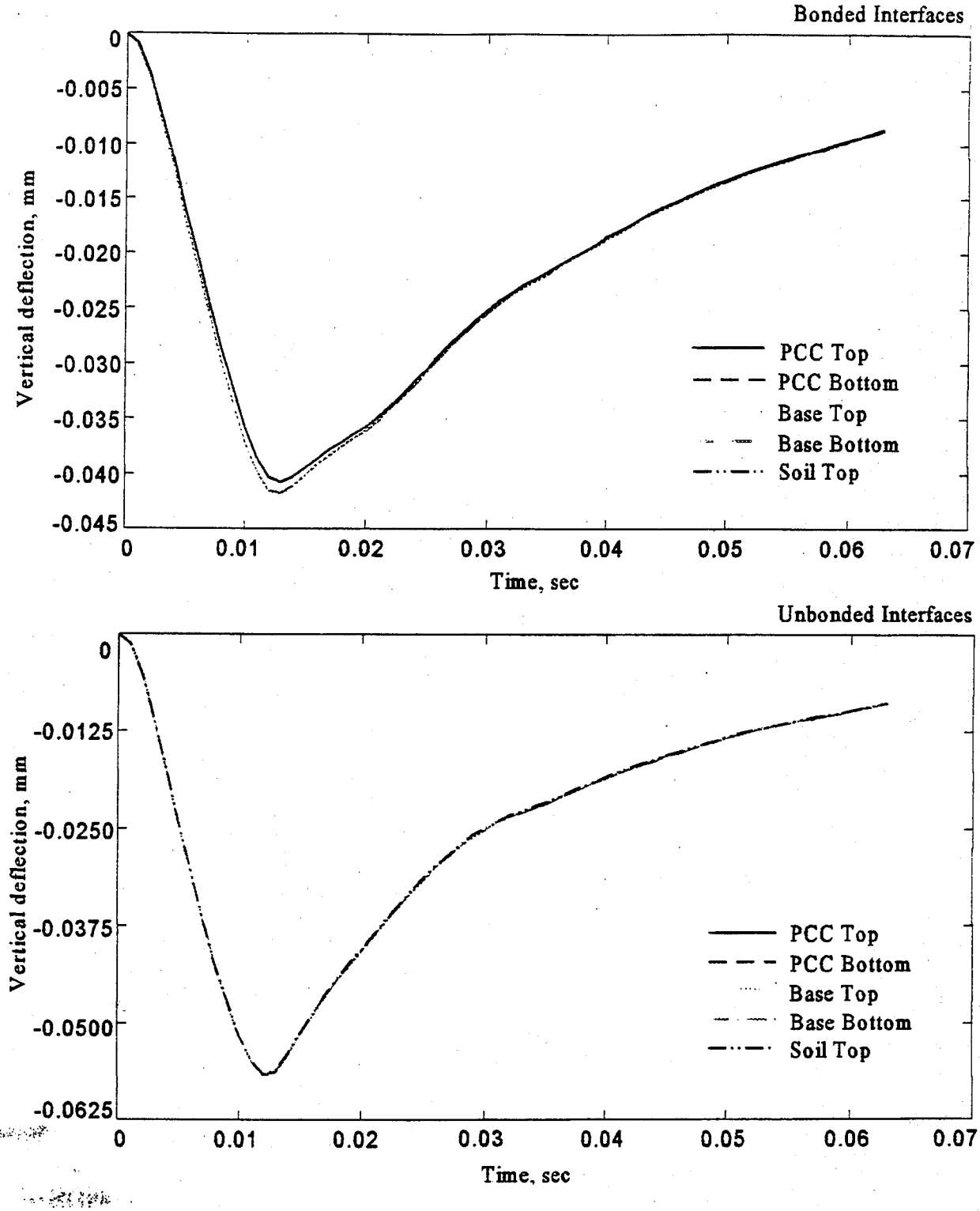

FIGURE 6.5 Deflection vs. time curves for the rigid pavement section at 300 mm offset.

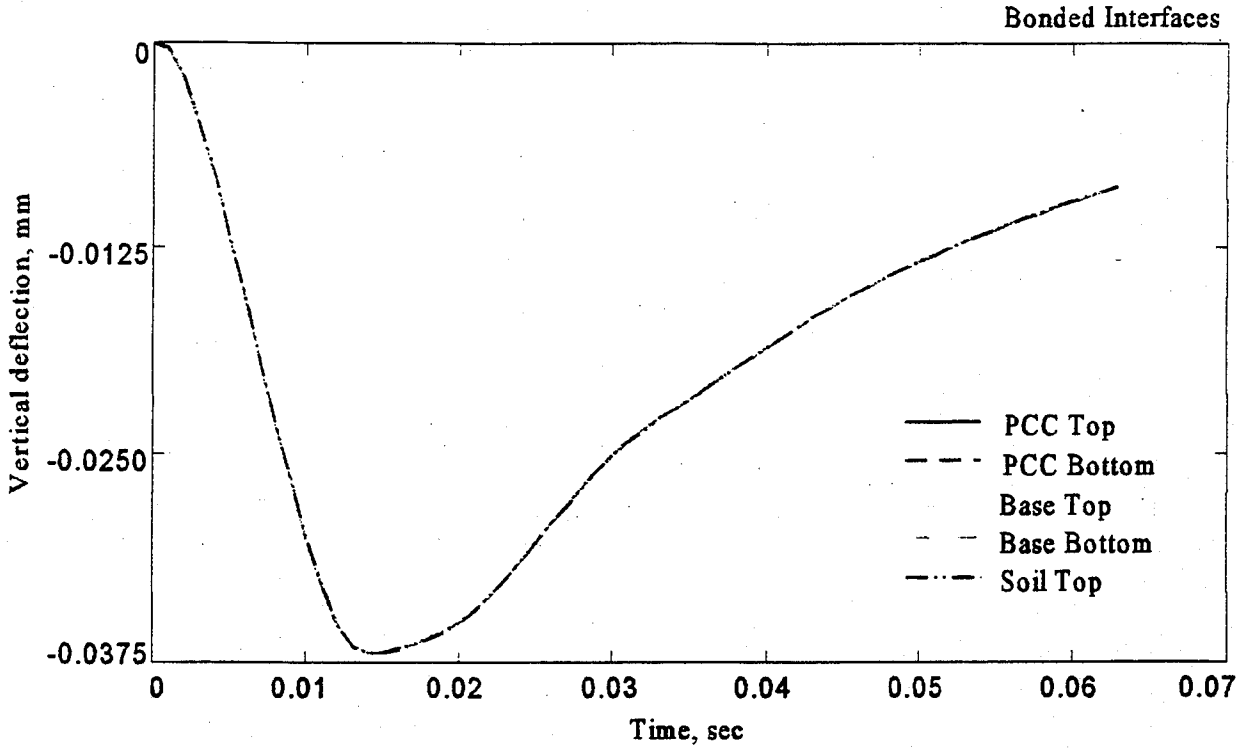

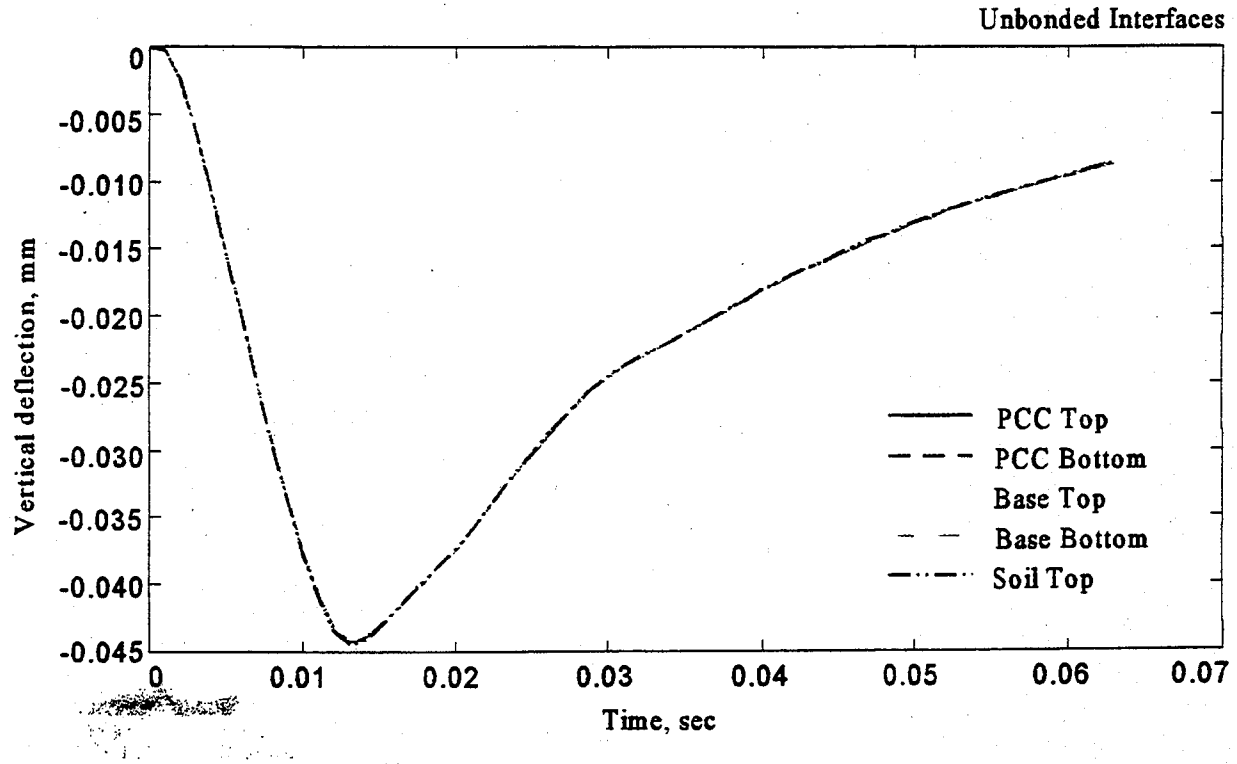

FIGURE 6.6 Deflection vs. time curves for the rigid pavement section at 600 mm offset.

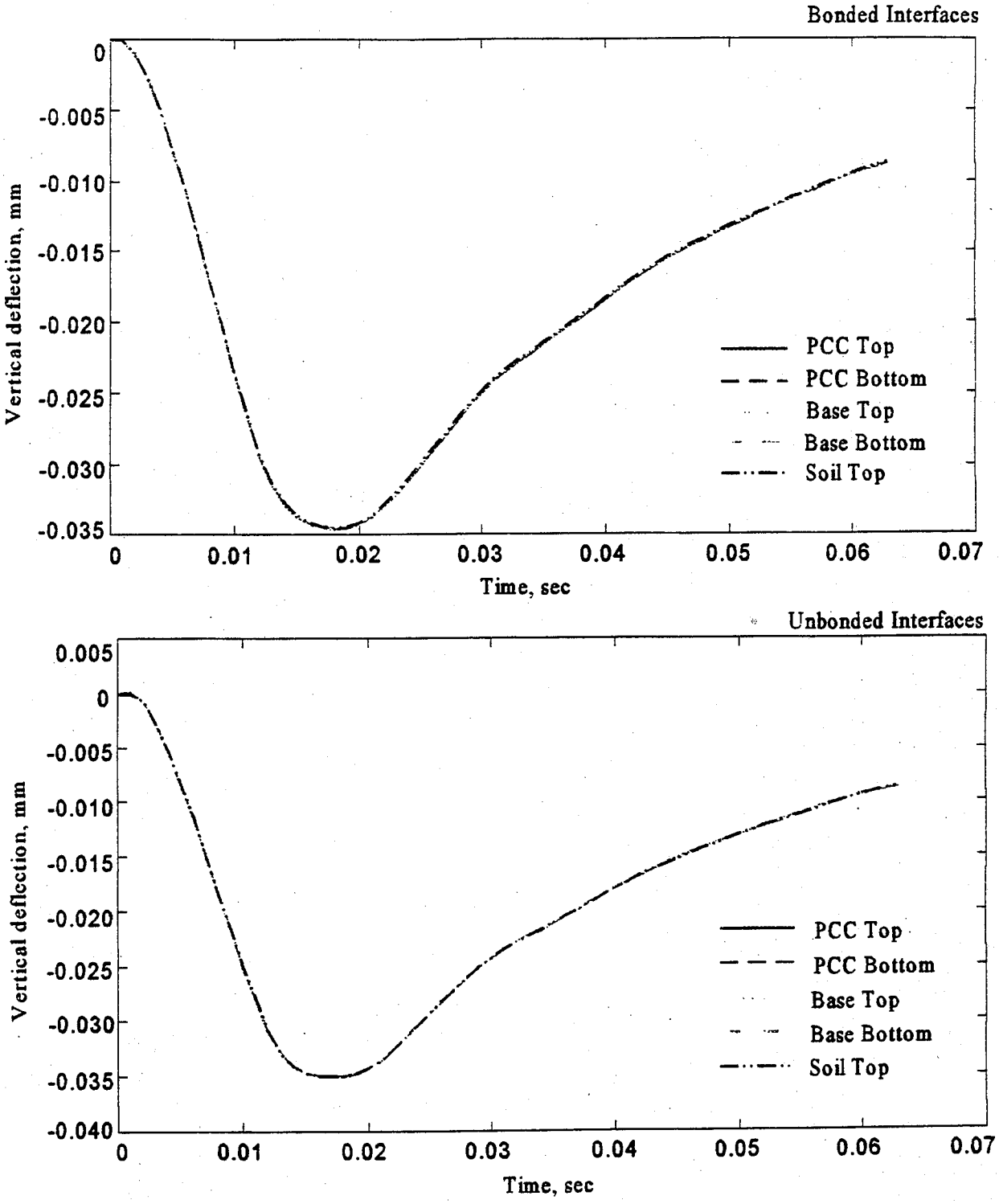

FIGURE 6.7 Deflection vs. time curves for the rigid pavement section at 900 mm offset.

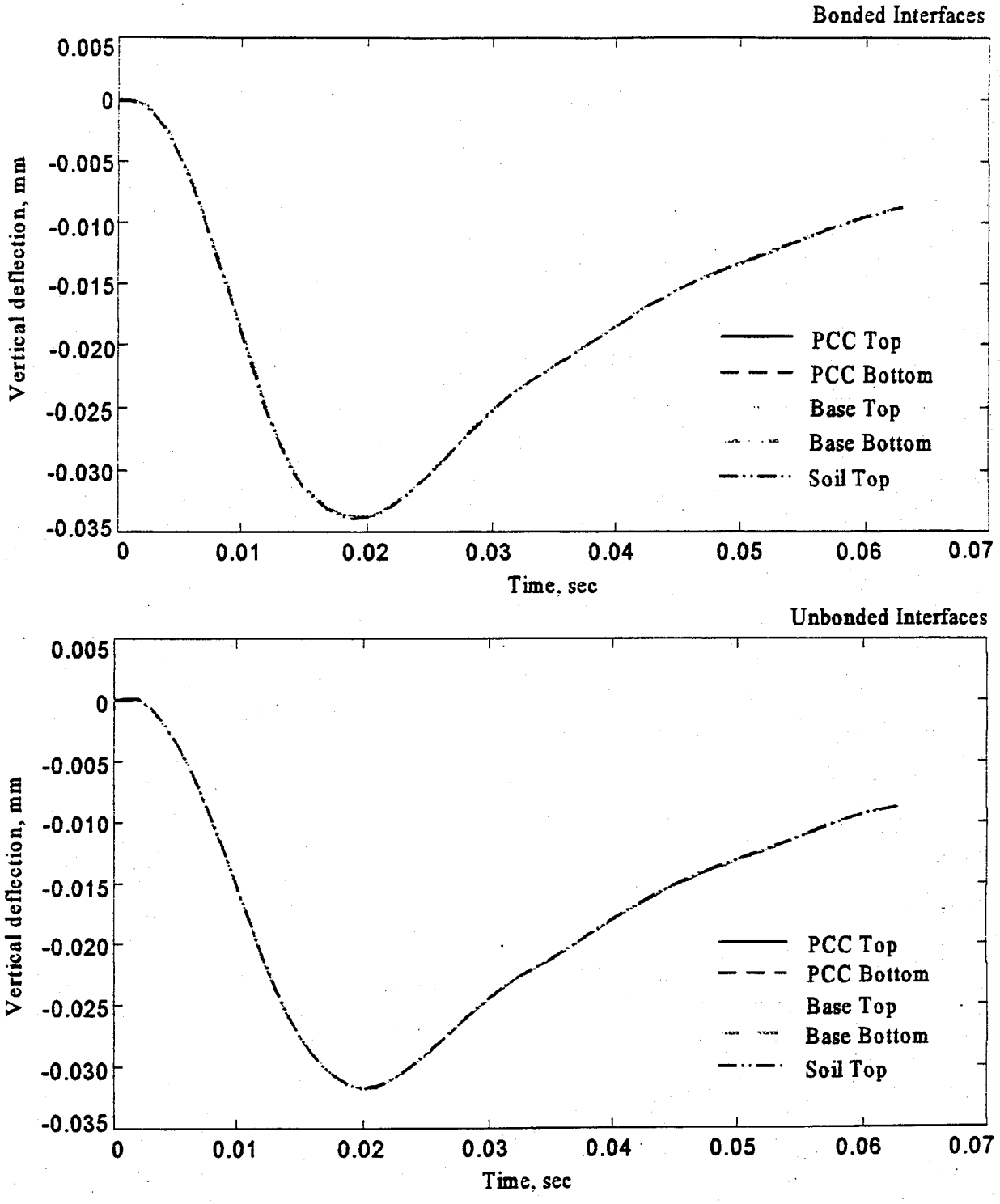

FIGURE 6.8 Deflection vs. time curves for the rigid pavement section at 1200 mm offset.

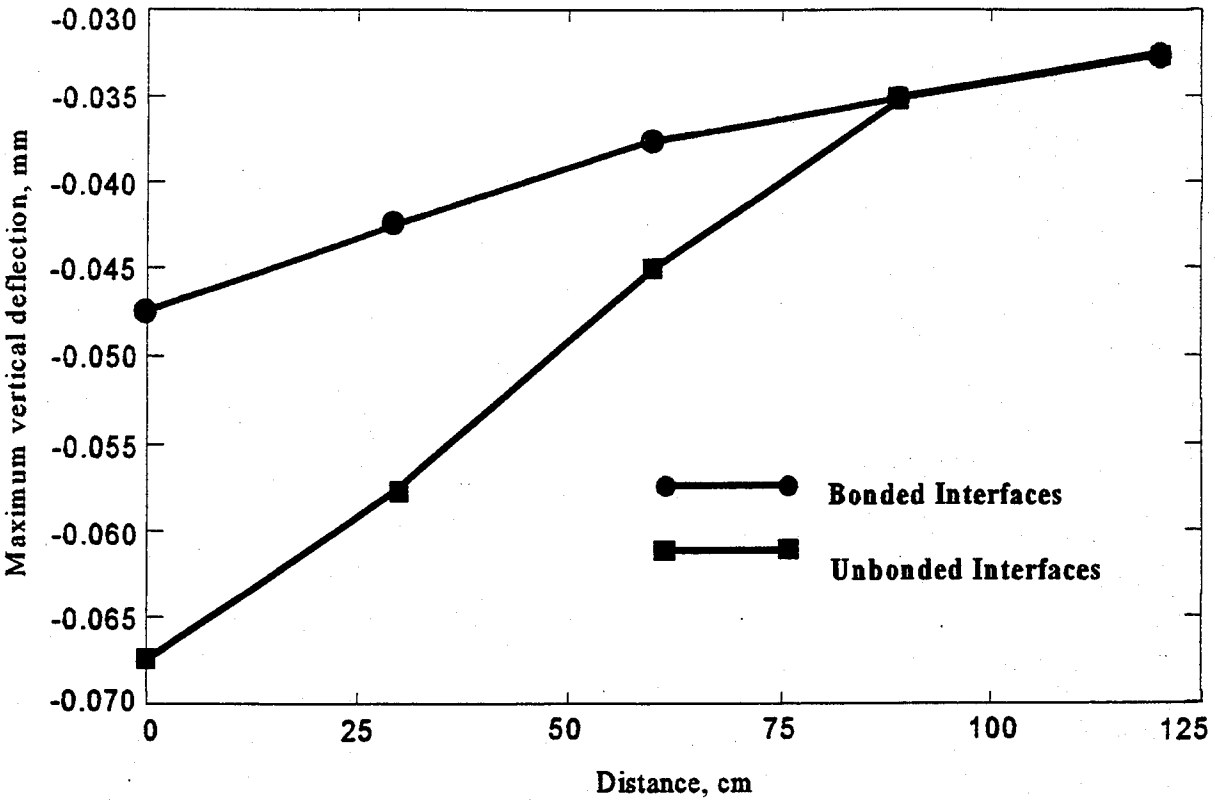

FIGURE 6.9 Deflection basins for rigid pavement models with bonded and unbonded interfaces.

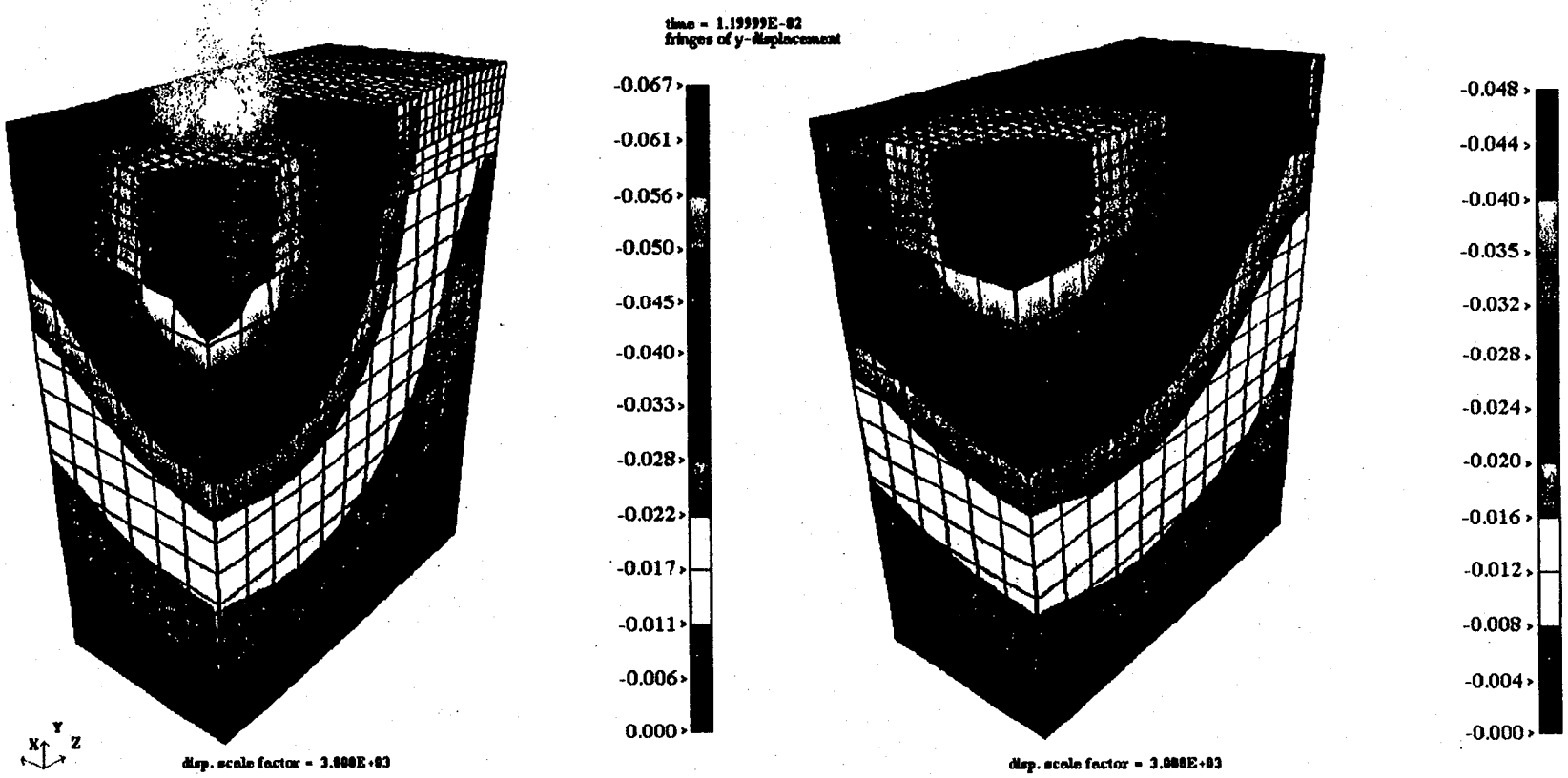

(a) Unbonded Interfaces

(b) Bonded Interfaces

FIGURE 6.10 Fringes of maximum vertical deformation in rigid pavement models (mm).

CHAPTER 7

CONCLUSIONS

The significance of a strong bond between pavement layers has been emphasized in this work. Care should be taken to assure the existence of an interface bond when testing pavements using FWD. Analysis of the mechanism of dynamic deflection in different pavement structures led to the following important considerations:

1. For pavements with an asphalt-concrete top layer, the dynamic deflection patterns are significantly different in the cases of bonded and unbonded interfaces between pavement layers. Once the bonds between layers are broken, the top layer has more freedom of vibration and the pavement structure no longer behaves as a solid, but rather as a set of plates of different stiffness.

2. An unbonded asphalt-concrete layer may show higher upward deformation at different FWD sensor locations. These upward deflections may be used for the detection of the asphalt-concrete layer delamination.

3. The rate of rebound from the maximum surface deflection is dependent on the layers interface bond strength. Therefore, study of the whole deformation vs. time curve instead of only maximum values permits extraction of more information about existing pavement condition.

4. The results for the flexible pavement models with bonded and unbonded interfaces indicate that the main backcalculation assumption that surface deformations represent the deformations in subsequent layers is valid for pavements with well bonded interfaces. The FWD serves in this case as a reliable tool for the evaluation of pavements structural capacity. However, for the case of unbonded interfaces, the pattern of surface deformation deviates significantly from the pattern of deformation on the top of the subgrade. In this case,

correlation of the surface deflections to the deflections in the subsequent layers should be carefully considered. Backcalculation procedures that account for the condition of the bond between pavement layers should be used for the evaluation of flexible pavement layers moduli.

5. Models with an unbonded asphalt-concrete top layer indicate that the asphalt-concrete layer may separate from the rest of pavement structure when subjected to impact loading.

6. Bonded pavement models show consistently smaller deformation than the unbonded models. Therefore, the pavements with bonded interfaces appear to be stiffer and capable of carrying higher structural capacity.

7. An FWD test may result in the incorrect evaluation of the overlaid pavements that suffered delamination or, in general, pavements whose layer interfaces have deteriorated. In this case, it may be necessary to lower the applied dynamic load to a level that would not cause separation at the interfaces. This may be achieved by using a stress wave propagation technique, such as spectral analysis of surface waves (if the interfaces are free from voids).

8. Due to upward deformation of an asphalt layer at distant geophone locations, DC coupling of the transducers should be used to differentiate between negative and positive deformations.

9. Deflection records obtained from the FWD test of shallow pavement sections may be affected by reflective wave interference.

10. The dynamic behavior of rigid pavements is governed by the deformation of the stiffest top layer. The surface deflections are well representative of the deflections through the depth of pavement structure.

11. Inclusion of a visco-elastic material model to characterize asphalt-concrete response has little

effect on the deflection results obtained from the finite element model. This can be explained by the short transient nature of loading. Therefore, linear elastic characterization of the asphalt-concrete is appropriate for modeling of an asphalt-concrete materials response to impact loads.

12. The present practice of evaluation of the pavement moduli profile using an FWD test should be modified to account for the dynamic behavior of pavement layers with unbonded interfaces.

13. Theoretical deflections predicted by DYNA3D models are in good agreement with the measured deflections. The use of dynamic finite element analysis in the backcalculation of pavement moduli may lead to higher accuracy of the FWD results compared with the conventional multi-layer elasto-static approach.

14. The dynamic finite element analysis approach used in this work offers the opportunity to experiment and modify the normal design configurations in order to prolong the service life of pavement structures. Interesting explanations of many failure modes could be reached and cures could be suggested.

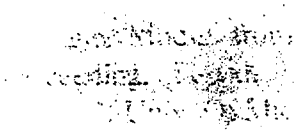

REFERENCES

1. Hoffman, M. S. And Thompson, M.R, "Comparative Study of Selected Nondestructive Testing Devices", Transportation Research Board, Record 852, 1982

2. "Standard Test Method for Deflections with a Falling-Weight-Type Impulse Load Device", 1995 Annual Book of ASTM Standards, Section 4, Construction, Volume 04.03 Road and Paving Materials; Pavement Management Technologies, ASTM, Philadelphia, PA, 1995

3. Sebaaly, B.E., "Dynamic Models for Pavement Analysis," Ph.D. Dissertation, Arizona State University, 1987

4. Meier, R.W., G. J. Rix Backcalculation of Flexible Pavement Moduli Using Artificial Neural Networks, Transportation Research Board, Record 1448, Washington, D.C., 1994, pp. 75 - 82

5. Meier, R.W., G. J. Rix Backcalculation of Flexible Pavement Moduli from Dynamic Deflection Basins Using Artificial Neural Networks, Transportation Research Board, Record 1482, Washington, D.C., 1995, pp. 72 - 81.

6. R. W. May, H. L. Von Quintus, "The Quest For a Standard Guide to NDT Backcalculation", *Nondestructive Testing of Pavements and Backcalculation of Moduli* (Second Volume), pp. 505-520, ASTM STP 1198, Philadelphia, 1994.

7. Y. H. Huang, *Pavement Analysis and Design*, pp. 451-453, Prentice Hall, Englewood Cliffs, New Jersey, 1993.

8. AASHTO Guide for Design of Pavement Structures, Chapter 3, Guides for Field Data Collection, American Association of State Highway and Transportation Officials, 1993, pp. 32-37, 96-97.

9. SHRP's Layer Moduli Backcalculation Procedure: Software Selection, Contract No. SHRP-90-P-001B, Prepared by PCS/Law Engineering for SHRP, 1991

10. Stubstad, R. N., Connor, B., "Use of the FWD to predict Damage Potential to Alascan Highways during Spring Thaw", Transportation Research Board, Record 930, 1983

11. Irwin, L.N., "Detrmination of Pavement Lay[illegible]om Surface Deflection Data for Pavement Performance Evaluation,"Proce[illegible] International Conference on Structural Design of Asphalt Pavements, No. 1, Univ. Of Michigan, Aug. 1977

12. McCullough, B.F., Taute, A., "Use of Deflection Measurements for Determining Pavement Material Properties,"Transportation Research Board, Record 852, 1982

13. Seaman, L., J. W. Simons, D. A. Shockey, R. F. Carmichael, and B. F. McCullough, " Unified Airport Pavement Design Procedure," Unified Airport Pavement Design and Analysis Concepts Workshops, July 16-17, 1991, Federal Aviation Administration, Washington, D.C., pp. 447-537

14. Chou, Y.J., J. Uzzan, and R.L. Lytton, "Backcalculation of Layer Moduli from Nondestructive Pavement Deflection Data Using Expert System", *Nondestructive Testing of Pavements and Backcalculation of Moduli*, ASTM STP 1026, Philadelphia, 1994, pp. 341-354

15. Irwin, L.H., W.S. Yang, and R.N. Stubstad,"Deflection Reading Accuracy and Layer Thickness Accuracy in Backcalculation of Pavement Layer Moduli," *Nondestructive Testing of Pavements and Backcalculation of Moduli*, ASTM STP 1026, Philadelphia, 1994, pp. 229-244

16. Huang, Y.H. Pavement Analysis and Design. 1993, Prentice Hall, Inc., Englewood Cliffs, NJ, pp. 7, 208

17. Foster, C.L. and Fergus, J.N., "Stress Distribution in Homogeneous Soil," Highway Research Board Special Report 12F, Washington, D. C., 1951

18. Young, M.J. "Analytical and Experimental Studies of Borehole Seismic Methods," Ph.D. Dissiertation, the University of Texas at Austin, 1987.

19. Nazarian, S., "In Situ Determination of Elastic Moduli of Soil Deposits and Pavement Systems by Spectral-analysis-of-surface-waves Method," Ph. D. dissertation, the University of Texas at Austin, 1984.

20. Nazarian, S. And K.H. Stokoe II, "In Situ Determination of Elastic Moduli of Pavement Systems by Spectral Analysis of Surface Waves Method," Research Report 368-1f, Center for Transportatio Research, the University of Texas at Austin, 1985.

21. Rix, G.J., K.H. Stokoe, II, and J.M. Rosset, "Experimental Study of Factors Affecting the Spectral-Analysis-of-Surface-Waves Method," Research Report 1123-5, Center for Transportatio Research, the University of Texas at Austin, 1991.

22. J. S. Heisey, K.H. Stokoe II, and A. H. Meyer, "Moduli Pavement Systems from Spectral Analysis of Surface Waves," Transportation Research Record 852, 1982.

23. Nazarian, S., K.H. Stokoe II, and W.R Hudson (1983), "Use of Spectral Analysis of Surface Waves Method for Determination of Moduli and Thickness of Pavement Systems," Transportation Research Record 930, 1983.

24. Nazarian, S., and K. Stokoe II, "Non Destructive Testing of Pavement Usingsurface Waves," Transportation Research Record 993, 1984.

25. Nazarian, S., and K. Stokoe II, " Use of Surface Waves in Pavement Evaluation," Transportation Research Record 1070, 1986.

26. Foinquinos R., J.M. Roesset, and K.H. Stokoe II, "Response of Pavement Systems to Dynamic Loads Imposed by Nondestructive Tests," Transportation Research Record 1504, 1995.

27. Haskell, N.A., "The Dispersion of Surface Waves in Multilayered Media," Bulletin of the Seismological Society of America, Vol. 43, 1953.

28. Dunkin, J.W., "Computation of Modal Solutions in Layered, Elastic Media at High Frequencies," Bulletin of the Seismological Society of America, Vol. 55, 1965.

29. Thrower, E.N., "The Computation of the Dispersion of Elastic Waves in Layered Media," Journal of Sound and Vibration (1965), 210-226.

30. Nazarian S., K. Stokoe II, R.C. Briggs, and R. Rogers, "Determination of Pavement Layer Thickness and Moduli by Sasw Method," Transportation Research Record 1196, 1988.

31. Rix, G., "Experimental Study of Factors Affecting the Spectral Analysis of Surface Waves Method," Ph.D. Dissiertation, the University of Texas at Austin, 1988.

32. Hiltunen, D.R. and R.D. Woods, "Influence of Source and Receiver Geometry on theTesting of Pavements by the Surface Wave Method", ASTM STP-1026, 1989.

33. Huang, Y.H., and S.T. Wang,. Finite-Element Analysis of Rigid Pavements with Partial Subgrade Contact. *Highway Research Record No.485*, National Research Council, Washington, D. C., 1974, pp. 39-54.

34. Huang, Y.H., and S.T. Wang, Finite-Element Analysis of Concrete Slabs and Its Implications for Rigid Pavement Design. *Highway Research Record No.466*, National Research Council, Washington, D. C., 1973, pp. 55-69

35. Ong, C. L., D. E. Newcomb, and R. Siddharthan, Comparison of Dynamic and Static Backcalculation Moduli for Three-Layer Pavements. *Transportation Research Record 1293*, TRB, National Research Council, Washington, D. C., 1991, pp. 86-92.

36. Chatti, K., Lysmer, J., and Monismith C. L., "Dynamic Finite-Element Analysis of Jointed Concrete Pavements," Transportation Research Record 1449, TRB, National Research Council, Washington, D. C., 1994, pp.79-90

37. Kukreti, A. R., Taheri, M. R., and Ledesma, R. H., "Dynamic Analysis of Rigid Airport Pavements with Discontinuities," Journal of Transportation Engineering, Vol. 118, No. 3, ASCE, 1992, pp.341-360

38. Zagloul, S.M., and T.D. White, Use of a Three-Dimensional, Dynamic Finite Element Program for Analysis of Flexible Pavement. *Transportation Research Record 1388*, TRB, National Research Council, Washington, D.C., 1993, pp. 60-69.

39. Zagloul, S.M., T.D. White, V.P. Drenevich, and B. Coree, Dynamic Analysis of FWD Loading and Pavement Response using a Three-Dimensional Dynamic Finite Element Program. *Nondestructive Testing of Pavements and Backcalculation of Moduli (Second Volume), ASTM STP 1198*, American Society for Testing and Materials, Philadelphia, 1994, pp. 105-138.

40. Uddin, W., D. Zhang, and F. Fernandez, Finite Element Simulation of Pavement Discontinuities and Dynamic Load Response. *Transportation Research Record 1448*, TRB, National Research Council, Washington, D.C., 1994, pp. 100-106.

41. Mallela, J., and K.P. George, Three-Dimensional Dynamic Response Model for Rigid Pavements. *Transportation Research Record 1448*, TRB, National Research Council, Washington, D.C., 1994, pp. 92-99.

42. Forte, T., k. Majizadeh, J. Kennedy, J. Hadden, T. White, "Federal Aviation Administration Modeling," Unified Airport Pavement Design and Analysis Consepts Workshops, July 16-17, 1991, Federal Aviation Administration, Washington, D.C., pp. 233-313

43. Zagloul, S. M., White, T. D., and Kuczek, T., "Use of Three-Dimensional, Dynamic, Nonlinear Analysis to Develop Load Equivalency Factors for Composite Pavements," Transportation Research Record 1449, TRB, National Research Council, Washington, D. C., 1994, pp. 199-208

44. Zagloul, S. M., White, T. D., and Kuczek, T., "Evaluation of Heavy Load Damage Effect on Concrete Pavements Using Three-Dimensional, Nonlinear Dynamic Analysis," Transportation Research Record 1449, TRB, National Research Council, Washington, D. C., 1994, pp. 123-133

45. Zagloul, S. M., White, T. D., Ramirez, J. A., and NBR Prasad, "Computerized Overload Permitting Procedure for Indiana," Transportation Research Record 1448, TRB, National Research Council, Washington, D. C., 1994, pp. 40-52

46. Jooste, F. J. And Fernando, E. G., "Modeling of Pavement Response Under Superheavy Loads," Transportation Research Record 1448, TRB, National Research Council, Washington, D. C., 1994, pp. 69-74

47. Kirkner, D. J., Caulfield, P. N., and McCann, D. M., "Three-Dimensional Finite Element Simulation of Permanent Deformations in Flexible Pavement Systems," Transportation Research Record 1448, TRB, National Research Council, Washington, D. C., 1994, pp.34-39

48. Hopman, P.C., Pronk, A.C., Kunst, P.A.J.C., Molenaar, A.A.A., Molenaar, J.M.M., "Appliction of the Visco-Elastic Properties of Asphalt Concrete," Proceedings, Seventh International Conference on Asphalt Pavements, Volume 1, The International Society of Aspalt Pavements, Nottingham, England, 1992, pp. 73-88

49. Key, S.W., "HONDO - A Finite Element Computer Program for the Large Deformation Dynamic Response of Axisymmetric Solids," Sandia National Laboratories, Albuquerque, N.M., Rept. 74-0039, 1974

50. Chang, D.W. "Nonlinear Effects on Dynamic Response of Pavements Using the Nondestructive Testing Techniques", Ph.D. Dissertation, the University of Texas at Austin, TX, 1991, pp. 67-73

51. Seaman, L., J.W. Simons, D.A. Shokey, "Unified Airport Pavement Design Procedure," "Federal Aviation Administration Modeling," Unified Airport Pavement Design and Analysis Consepts Workshops, July 16-17, 1991, Federal Aviation Administration, Washington, D.C., pp. 460-461

32. Hoffman, M.S. and Thompson, M.R., "Nondestructive Testing of Flexible Pavements - Field Testing Program Summary," University of Illinois at Urbana Champaign, Transportation Engineering Series 31, Illinois Cooperative Highway and Transportation Research Program, Series 188, June 1981

53. Traylor, M.L., "Nondestructive Testing of Flexible Pavements," Department of Civil Engineering, University of Illinois at Urbana Champaign, Ph. D. Thesis, 1979

54. Mikhail, M. Y., "Three Dimensional Mechanistic Analysis of Vehicle-Pavement Interaction," Department of Civil and Environmental Engineering, Arizona State University, Ph. D. Thesis, 1996

55. Hoffman, M.S. and Thompson, M.R., "Nondestructive Testing of Flexible Pavements - Field Testing Program Summary," University of Illinois at Urbana Champaign, Transportation Engineering Series 31, Illinois Cooperative Highway and Transportation Research Program, Series 188, June 1981